Analog epigenetic cell memory by graded DNA methylation

Sebastian Palacios[1,2,3†], Simone Bruno[1,4†], Ron Weiss[2], Elia Salibi[1], Andrew Kane[2], Katherine Ilia[2,3], and Domitilla Del Vecchio[1,2*]

[1] Department of Mechanical Engineering, Massachusetts Institute of Technology, Cambridge, MA, 02139, USA.

[2] Department of Biological Engineering, Massachusetts Institute of Technology, Cambridge, MA, 02139, USA.

[3] Institute for Medical Engineering and Science, Massachusetts Institute of Technology, Cambridge, MA, 02139, USA.

[4] Department of Data Science, Dana-Farber Cancer Institute, Boston, MA, 02115, USA.

[†] These authors contributed equally to this work

[*] Corresponding author: ddv@mit.edu

Summary. DNA methylation and histone modifications mediate the long-term maintenance of gene expression states and are believed to be established in an all-or-none manner, allowing cells to maintain memory of silenced and active gene states. Here, we investigate whether these modifications can also enable memory of any gene expression level, and thus can equip cells with "analog memory". Surprisingly, we find that cells can maintain intermediate gene expression levels by grades of DNA methylation that remain stable over time. Our nucleosome modification model recapitulates this result when H3K9me3 does not catalyze the recruitment of DNA methylation and the remaining DNA methylation kinetics are slow. The observation that long-term memory is possible for any gene expression level deepens our understanding of epigenetic cell memory and potentially broadens our view of what constitutes a cell type.

Introduction

Epigenetic cell memory allows the cells of multi-cellular organisms to maintain different phenotypes despite a common genetic code. These phenotypes are encoded in distinct gene expression patterns, which are maintained long-term by the concerted action of gene regulatory networks [1] and epigenetic modifications to DNA and histones [2–4]. In particular, DNA methylation and covalent modifications to histones have appeared as key mediators of the long-term maintenance of gene expression states [5, 6]. Modifications such as histone 3 lysine tail (H3K9 and H3K4) and DNA (CpG) methylation, control the extent to which DNA is compacted and accessible to transcriptional machinery [7, 8]. In particular, H3K9 tri-methylation (H3K9me3) and DNA

methylation are associated with a highly compact chromatin structure characterized by a lack of transcription [9, 10], while H3K4 thri-methylation (H3K4me3) at promoters is associated with actively transcribed genes [11]. Histone modifications H3K9me3 and H3K4me3 can propagate to nearby unmodified histones because they each recruit writers of the same modification [12, 13], leading to a positive feedback mechanism that mediates the maintenance of the modification [14].

DNA methylation has been regarded as the embodiment of inheritance since it can propagate through subsequent cell divisions by the action of maintenance enzymes that copy the methylation pattern of the parental DNA strand on the newly synthesized DNA strand upon DNA replication [7]. In recent years, however, DNA methylation is emerging as a more dynamic process than originally thought [15, 16]. Evidence suggests that DNA methylation might be in a dynamic equilibrium under the continuous and competitive action of writer and "eraser" enzymes [17]. At the same time, DNA methylation is not an isolated process, but rather it operates in orchestration with histone modifications [18]. Specifically, DNA methylation dynamically interacts with H3K4me3 through mutual inhibition [19, 20], and with H3K9me3 through mutual catalysis [21, 22]. When this cross-catalysis is sufficiently strong, it is theoretically possible that only fully methylated and completely unmethylated patterns are propagated stably through cell division, leading to long-term maintenance of silenced and active gene states only [23]. This possibility is consistent with recent genome-wide studies showing that DNA methylation pattern is not faithfully maintained, and that fully methylated and completely unmethylated sites have higher maintenance fidelity than intermediately methylated sites [24]. These findings are consistent with early experiments that found an "all or none" distribution of DNA methylation across the genome [25], and that although intermediate levels of DNA methylation are possible, they have low frequency [26, 27].

Gene silencing and reactivation dynamics, following sequence-specific recruitment of chromatin regulators to DNA, have been recently investigated in chromosomally integrated semi-synthetic reporter systems [28–31] and at endogenous gene loci [32, 33]. In particular, single cell dynamic analysis revealed that gene silencing and reactivation occur in an "all or none" fashion, wherein transient recruitment of a chromatin regulator to a gene modulates the fraction of cells that become permanently silenced rather than modulating the level of gene expression [28]. Independent studies performed on endogenous gene loci in plants had also found that memory is encoded in "on" or "off" gene states, with the fraction of silenced cells dependent on the duration of stimulation [34]. Experiments on knock-in reporters in *S. Cerevisiae* at HML/HMR loci recapitulated this finding by showing that the dosage of the chromatin regulator controls the fraction of silenced cells but not gene expression level [35]. Taken together, these findings, along with previous evidence, support the hypothesis that epigenetic cell memory may be an exclusive attribute of active and silenced gene states, suggesting that cellular memory is digital. Here, we investigate whether memory of intermediate gene expression states is also possible.

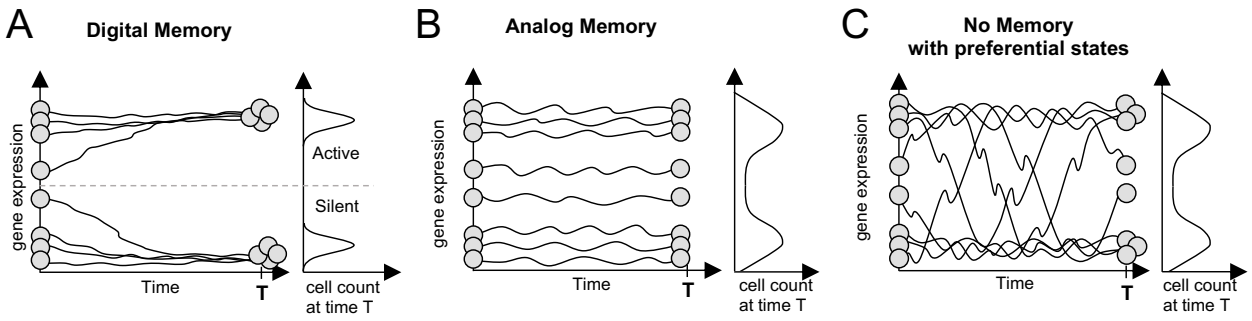

Fig. 1. Digital versus analog memory of gene expression. A Memory is digital when the cell can maintain in time either silenced or fully active gene expression states, but no other states. **B** Memory is analog when the cell can maintain any initial gene expression level. **C** Lack of memory with preferential states result in long-term gene expression trajectories that are independent of the initial state. However, preferential states are visited more often. The stationary distribution of gene expression across the cell population depicts on the x-axis the number of cells that express at the level indicated on the y-axis.

Models of digital epigenetic memory posit that cells can stably keep only silenced or fully active gene states (Fig. 1A). By contrast, cells have analog memory when they can stably maintain any gene expression level (Fig. 1B). Although single cell trajectories determine the type of memory, the stationary distribution of gene expression levels across the cell population is informative. Specifically, the presence of cells with gene expression at intermediate levels is incompatible with digital memory. Nevertheless, this feature is, alone, insufficient to claim analog memory since also a case of no memory with preferential states can result in the same stationary distribution (Fig. 1C). In this case, however, the cells with intermediate gene expression levels are *en route* to one of the two preferential states, which are visited more often. So, whether the intermediate states are stable or transient distinguishes analog memory from a case of no memory with preferential states.

Here, we investigate whether DNA methylation and histone modifications enable cells to maintain stably intermediate gene expression states. To this end, we utilize a semi-synthetic genetic reporter system integrated in the mammalian chromosome coupled with targeted recruitment of epigenetic effectors. We discovered that cells can maintain any gene expression level and that this level, in clonal populations, inversely correlates with the grade of DNA methylation within the promoter and operator sites. In turn, the grade of DNA methylation, as determined by the mean number of CpGs methylated, remains approximately stable in time in the absence of any input epigenetic effector. Yet, we can permanently repress or activate a partially active gene that has an intermediate DNA methylation grade, by transiently recruiting to the gene DNA methylation writer or “eraser” enzymes, respectively. These findings place DNA methylation as a causal determinant of persistent gene expression level. Our nucleosome modification model, which includes the interactions between DNA methylation, H3K4me3, and H3K9me3, recapitulates these results when H3K9me3 does not catalyze DNA methylation and the basal establishment and erasure of DNA methylation are negligible.

Results

A genetic reporter system to study gene expression dynamics at an endogenous mammalian locus

We first set out to develop an experimental system to systematically probe and analyze the role that histone and DNA methylation play in the establishment and maintenance of gene expression states. To this end, we constructed a genetic reporter in an endogenous mammalian locus [36] in Chinese hamster ovary cells (CHO-K1) and engineered a set of epigenetic effectors to modulate histone and DNA methylation at the genomic reporter. The genetic reporter is comprised of the constitutive mammalian elongation factor 1a promoter (EF1a) driving the expression of fluorescent protein EBFP2. We also flanked the genetic reporter with cHS4 chromatin insulators [37]. Furthermore, the reporter comprises binding sites upstream of the promoter for DNA-binding proteins PhlF and rTetR [38] (Fig. 2A). The binding of PhlF and rTetR to DNA can be modulated using 2,4-diacetylphloroglucinol (DAPG) and doxycycline (dox), respectively. This experimental approach enabled us to precisely control the recruitment of epigenetic effectors to the genetic reporter by fusing them to PhlF or rTetR. Moreover, the region upstream of the promoter comprises guide RNA (gRNA) target sites, which enables the targeted recruitment of epigenetic effectors fused to dCas9. The general experimental approach involves expressing the epigenetic effectors using transient transfection in the cells bearing the genetic reporter, followed by fluorescence-activated cell sorting to obtain cells that have been transfected for analysis at various time points (Fig. 2B).

Gene expression stationary distribution across DNMT3A-treated cells has intermediate levels

We first investigated the gene expression dynamics, following recruitment of H3K9me3 to the promoter. To this end, we fused DNA-binding protein PhlF to KRAB [39], an epigenetic effector that modulates the incorporation of H3K9me3 into chromatin [40]. We then expressed PhlF-KRAB via transient transfection in the cells bearing the genetic reporter. Subsequently, we performed fluorescent-activated cell sorting to obtain cell populations across different levels of transfection and then performed time-course flow cytometry measurements. We observed rapid repression of gene expression for cells that expressed PhlF-KRAB, while no repression for cells transfected with PhlF. To evaluate the establishment of memory, we utilized DAPG to inhibit the binding of PhlF-KRAB and PhlF to DNA beginning 144 hours (6 days) after transfection. Irrespective of the dosages of PhlF-KRAB, gene

expression reverted to the active gene state within 4 days after reaching maximal repression (Fig. 2C). We then performed chromatin immunoprecipitation (ChIP) and methylated DNA immunoprecipitation (MeDIP) followed by qPCR, and observed a reduction in H3K4me3, an increase in H3K9me3, and no increase in DNA methylation at the genetic reporter (Fig. 2D), consistent with prior reports [28]. Taken together, these data show that a temporal pulse of PhlF-KRAB, along with a corresponding increase in H3K9me3 and reduction in H3K4me3, is unable to permanently silence gene expression. This is consistent with previous reports in mammalian cells, where KRAB-based epigenetic editing resulted in temporary repression while failing to enable long-term silencing [33, 41]. A two-state nucleosome modification model that includes H3K9me3 and H3K4me3 only is sufficient to describe these observations (see SI Section S.3 and Fig. S.4A,B). This model includes autocatalysis of H3K9me3 and H3K4me3 and mutual inhibition, consistent with previous models [14, 23]. The model can reproduce the cell distribution temporal dynamics of Fig. 2C (SI Fig. S.4B). In particular, the observed transient bimodality of the distribution (Fig. 2C, high KRAB, days 7 and 8) requires that the basal erasure of each modification is sufficiently slower than the rate of their own autocatalysis and that the mutual inhibition is balanced [23].

Next, we investigated the gene expression dynamics following the recruitment of DNA methylation to the promoter. To this end, we first expressed DNMT3A-dCas9 [41], a fusion of dCas9 and the catalytic domain of DNMT3A, and a gRNA in the cells bearing the genetic reporter via transient transfection. Subsequently, we utilized fluorescent-activated cell sorting to obtain cell populations for various levels of transfection and proceeded with time-course flow cytometry measurements (Fig. 2E). The gRNA was designed to recruit DNMT3A-dCas9 to five target sites upstream of the promoter. We observed in the flow cytometry measurements that gene expression was repressed, reaching maximal repression consistent with a silenced state approximately 10 days after transfection. No repression was observed for cells where a gRNA with a scrambled target sequence was utilized with DNMT3A-dCas9. After reaching maximal repression, the cell distributions remained stationary. ChIP and MeDIP followed by qPCR showed an increase in H3K9me3 and DNA methylation of the reporter for cells where DNMT3A-dCas9 was targeted to it (Fig. 2F), consistent with prior reports [28]. Moreover, as reported before [28], we also observed an increase in the number of cells in the silenced state for increasing levels of the epigenetic effector. Nevertheless, for all DNMT3A-dCas9 dosages, the stationary distribution of gene expression across the cell population exhibited intermediate levels of gene expression (Fig. 2E), compatible with analog but not with digital memory (Fig. 1).

A nucleosome modification model predicts analog memory in the absence of H3K9me3-mediated catalysis of DNA methylation

Consequently, we interrogated our nucleosome modification model (SI Figs. S.1A,C and [23]) to determine conditions that could allow cells with intermediate levels of gene expression to stably maintain this level. First, we determined conditions under which the model could reproduce the observed DNMT3A-dCas9 dose-dependent stationary distributions of Fig. 2D. We found that, in addition to basal erasure of histone modifications being sufficiently slower than autocatalysis, already required to reproduce the data of Fig. 2C, the model could recapitulate the data (SI Fig. S.4C) under the following additional conditions. First, DNA methylation decay is negligible on the time scales of our experiments ($\mu' \approx 0$), which is consistent with the reported high efficiency of DNMT1-mediated maintenance of methylated CpGs [42]. Second, H3K9me3 does not catalyze DNA methylation establishment ($\alpha' = 0$, SI Section S.3), which is consistent with the ChIP and MeDIP data (Fig. 2D). Third, mutual inhibition between repressive (H3K9me3 and DNA methylation) and activating (H3K4me3) modifications is sufficiently strong (ε' sufficiently large, SI Section S.4). With these assumptions, the model simplifies to that illustrated in Fig. 2G, and recapitulates the data of both Fig. 2C and Fig. 2E (SI Fig. S.4).

We therefore used this simplified model to investigate the temporal dynamics of cells with intermediate levels of gene expression in the stationary distribution. In this model, in the absence of epigenetic effectors, DNA methylation grade, defined by the mean fraction of the number of CpGs methylated in the gene, remains constant in time since DNA methylation decay is negligible and DNA methylation establishment is absent (no epigenetic effector and no catalysis by H3K9me3). Because DNA methylation grade inversely modulates H3K4me3 level (Fig. 2H, top), and H3K4me3 is proportional to gene expression (SI Section S.2), then also gene expression level persists in time (Fig. 2I). That is, the model predicts analog epigenetic memory. Despite this graded dosage-dependence, however, the model also predicts a bimodal dose-response of gene expression to DNMT3A-dCas9 temporal pulses (Fig. 2J), consistent with the experimental data (Fig. 2D). The model reveals that this arises from an ultrasensitive response of DNA methylation grade to DNMT3A-dCas9 transient dosage (Fig. 2H, bottom). Further parameter investigation indicates that this dose response curve becomes more graded when the mutual inhibition between activating and repressing histone modifcations is weakened (ε' smaller), leading to a unimodal probability distribution (SI Fig. S.1D, E). This provides an explanation for the observed bimodal distribution of gene expression in response to recruitment of DNMT3A-dCas9, despite the persistence of intermediate gene expression levels.

This model is a simplification of our originally published model [23], which included the possibility of having

H3K9me3 catalyze DNA methylation ($\alpha' \neq 0$). Indeed, when this catalysis is present and is sufficiently strong, then the model predicts that only active and silenced gene expression states can be stably maintained (SI Section S.3 and Fig. S.1B), consistent with digital memory (Fig. 1A).

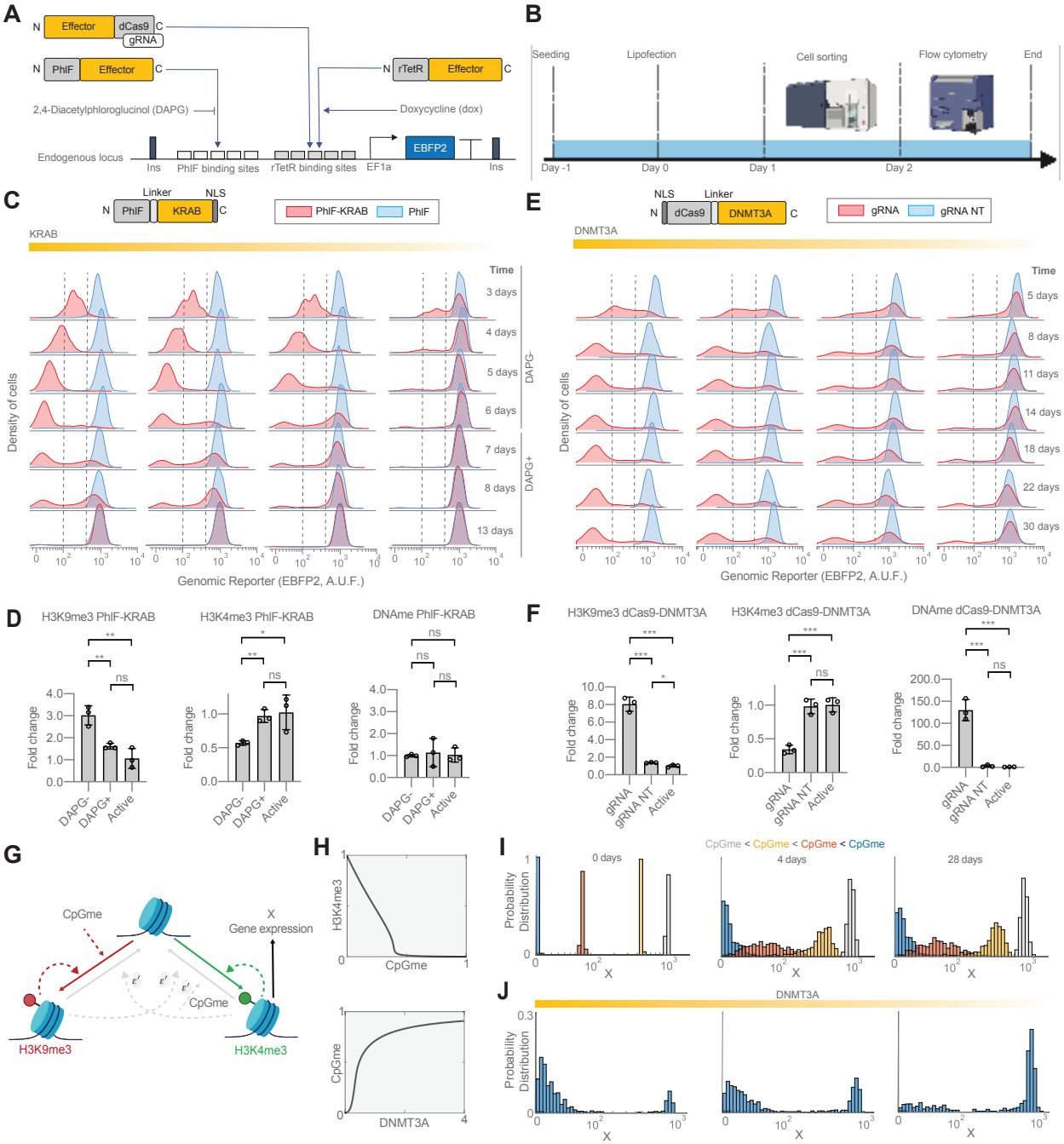

Fig. 2. Continued on the following page.

Fig. 2. **Gene expression stationary distribution across DNMT3A-treated cells is consistent with analog but not with digital memory.** **A** Schematic of the genetic reporter system chromosomally integrated into an endogenous locus. A mammalian constitutive promoter EF1a drives the expression of EBFP2. Upstream binding sites enable the targeted recruitment of epigenetic modulators, which can be fused to rTetR, PhlF or dCas9. The genetic reporter is flanked by chromatin insulators. **B** Experimental overview describing transient transfection of cells bearing the genetic reporter, fluorescence-activated cell sorting of transfected cells, and sequential flow cytometry measurements. **C** Experimental analysis of gene expression dynamics after epigenetic modulation via PhlF-KRAB or PhlF for various levels of transfection according to the experimental timeline shown in panel B. Shown are distributions from flow cytometry measurements of EBFP2 for 4 different levels of transfection. Cell culture media was supplemented with DAPG (30 μM) during 6 days after transfection. Dashed lines indicate the region of intermediate levels of gene expression. Data shown are from 3 independent replicates. **D** ChIP-qPCR and MeDIP-qPCR analysis after PhlF-KRAB epigenetic modulation 6 days after transfection and cell sorting for the highest levels of transfection. The promoter in the genetic reporter was amplified. Data is from three independent replicates. Reported are fold changes and their mean as determined by the $\Delta\Delta C_t$ method with respect to the active state. Error bars are SD. **E** Experimental analysis of gene expression dynamics by epigenetic modulation via DNMT3A-dCas9 for various levels of transfection according to the experimental timeline shown in panel B. A gRNA designed for 5 target sequences upstream of the promoter was used. A scrambled gRNA (gRNA NT) was utilized as a control. Shown are distributions from flow cytometry measurements of EBFP2 for 4 different levels of transfection. Dashed lines indicate the region of intermediate levels of gene expression. Data shown are from a representative replicates from 3 independent replicates. **F** ChIP-qPCR and MeDIP-qPCR analysis of epigenetic modulation using DNMT3A-dCas9 14 days after transfection and cell sorting for the highest levels of transfection. The promoter in the genetic reporter was amplified. Shown are data from 3 independent transfections. Reported are fold changes and their mean from three independent replicates using the $\Delta\Delta C_t$ method with respect to the active state. Error bars are SD. **G** Simplified chromatin modification circuit diagram obtained when KRAB = 0, DNMT3A = 0, TET1 = 0, and H3K9me3 does not catalyze *de novo* DNA methylation. We use solid arrows to represent the nucleosome modifications and gene expression. We use dashed arrows to represent the recruitment process and the consequent effect on establishment or erasing. For each arrow, we use red for processes involved in the H3K9me3 establishment, green for processes involved in the H3K4me3 establishment, gray for processes involved in the erasure of histone modifications, and black for gene expression. **H** Top plot: dose-response curve for the (CpGme,H3K4me3) pair for different values of ε' obtained from simulations of system (S.11) with (CpGme, H3K9me3, H3K4me3) $= (k, 0, 1-k)$ as initial conditions, with $0 \leq k \leq 1$. Bottom plot: dose-response curve for the (DNMT3A,CpGme) pair obtained from simulations of system (S.16) with (CpGme,H3K9me3,H3K4me3) $= (0, 0, 1)$ as initial conditions. The parameter values used for these simulations are listed in SI Section S.9 (See SI Fig. S.1D and S.3 for how different values of ε and ε' influence the deterministic behavior of the system). Here, the DNMT3A dynamics is modeled as a pulse that exponentially decreases over time. The value on the x-axis corresponds to the DNMT3A value at time 0. **I** Probability distributions of the system represented by reactions listed in SI Tables S.1 and S.3. The distributions are obtained computationally using the Stochastic Simulation Algorithm (SSA) [43] and we indicate with X the gene expression level (logicle scale). The parameter values used for these simulations are listed in SI Section S.9. See SI Figs. S.1B and S.2 for how different values of α' and μ' influence the probability distribution of the system. **J** Probability distributions of the system after t = 28 days, obtained as described in panel I. The parameter values used for these simulations are listed in SI Section S.9 (see SI Fig. S.1E and S.3 for how different values of ε and ε' influence the probability distribution of the system). Here, the DNMT3A dynamics is modeled as a pulse that exponentially decreases over time. In our model, α' is the normalized rate of DNA methylation establishment through repressive histone modifications, μ' is ratio between the DNA methylation erasure rate and the activating histone modification erasure rate, and ε (ε') is the parameter that scales the ratio between the basal (recruited) erasure rate and the auto-catalysis rate of each modification.

Silenced, active, and intermediate gene expression states are stably maintained and inversely correlate with DNA methylation grade

Based on the experimental and modeling results, we therefore hypothesized that epigenetic memory could be analog, thus enabling cells to maintain memory of any gene expression level. To test this hypothesis, we

first sought to investigate whether the cells within DNMT3A-silenced populations expressing intermediate gene expression levels exhibit long-term stability of gene expression. To this end, we performed fluorescence-activated cell sorting of the DNMT3A-silenced cells from low, intermediate, and high gene expression levels (Fig. 3A). We then performed time-course flow cytometry measurements to analyze the long-term gene expression dynamics. The cells at low and high levels of gene expression maintained an approximately stable gene expression level, consistent with digital memory. However, the cells with intermediate levels of expression (Fig. 3B), after an initial widening of the fluorescence distribution, also remained at a stable intermediate gene expression level. To characterize the epigenetic state of these cells, we performed targeted bisulfite sequencing and ChIP-qPCR to assess DNA methylation, H3K9me3, and H3K4me3. Cell populations with low gene expression levels exhibited higher H3K9me3 and lower H3K4me3 in the genetic reporter as compared to cells in the active gene expression state (Fig. 3D). These results are consistent with the known role of H3K9me3 as chromatin modification associated with repression and H3K4me3 as a chromatin modification associated with active transcription at promoters [44].

Bisulfite sequencing data of the genomic reporter showed that cells with intermediate levels of gene expression bear an intermediate DNA methylation grade (Fig. 3E). Specifically, the mean number of methylated CpGs (DNA methylation grade) in the region comprising the promoter and rTetR binding sites is the highest for cells with low expression, intermediate for the intermediate expression, and low for high expression (Fig. 3F). Furthermore, there is a linear negative correlation (p-value <0.05) between median gene expression level and DNA methylation grade (Fig. 3G). Under weak, but not under strong, cross-catalysis of DNA methylation by H3K9me3 our model recapitulates these experimental findings (SI Figs. S.1B and S.2).

Next, we further tested the hypothesis that epigenetic memory could be analog by subdividing according to gene expression level a population of cells that had been previously sorted from intermediate gene expression levels (Fig. 3H, I, L). If epigenetic memory were analog, cells sorted from different gene expression levels would maintain these distinct levels over time. Accordingly, we used fluorescence-activated cell sorting to obtain cells from a cell population with stable intermediate gene expression distribution according to four different gene expression levels (Fig. 3H). Each of the four cell populations maintained distinct gene expression levels according to the initial gene expression level on the day of sorting (Fig. 3I, L). This experimental observation supports the hypothesis that epigenetic memory is analog and is in agreement with the model (SI Fig. S.5).

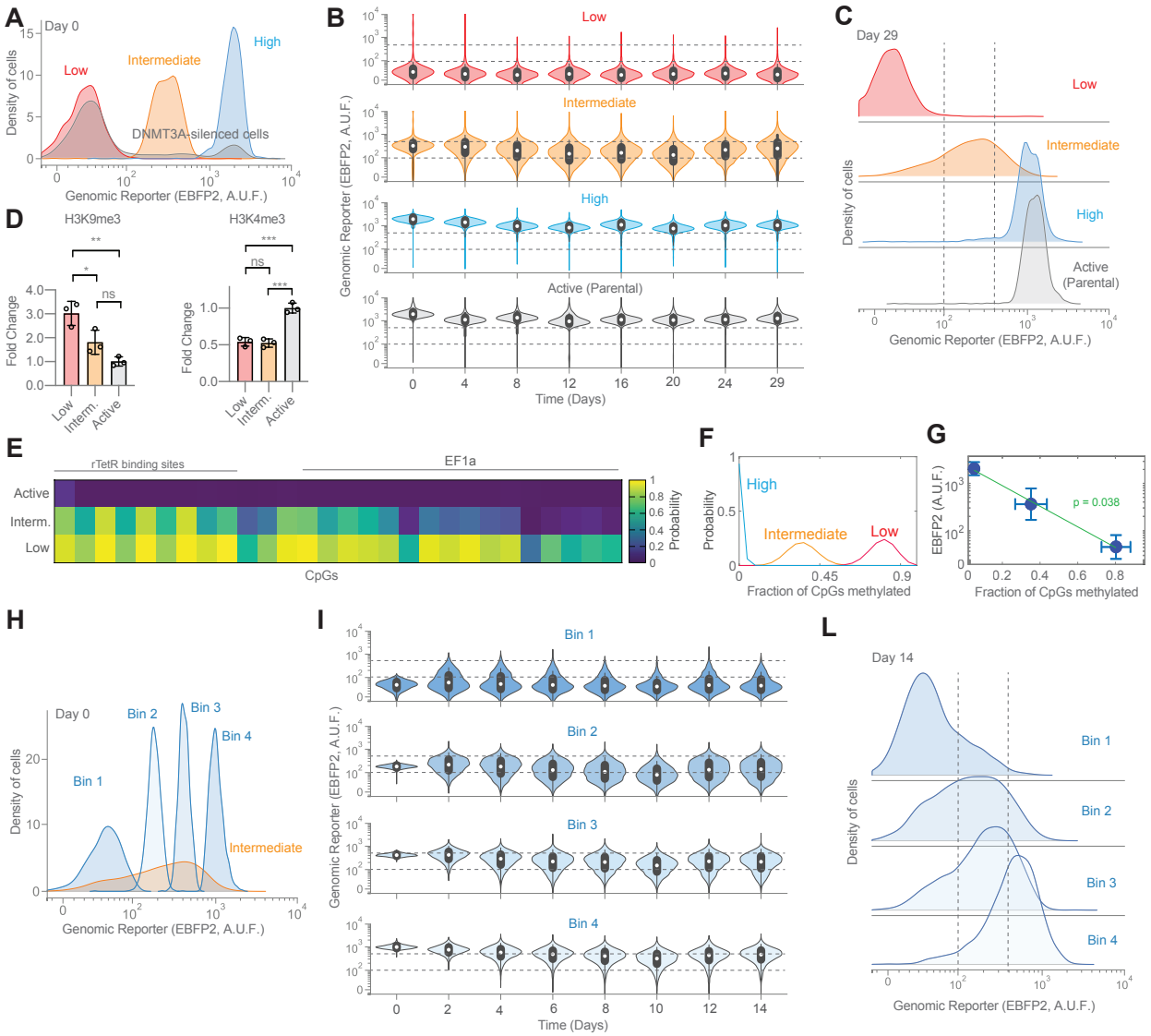

Fig. 3. Continued on the following page.

Fig. 3. **Intermediate levels of gene expression are stable in DNMT3A-silenced cell populations and exhibit intermediate DNA methylation grades** **A** Distributions from flow cytometry measurements of cells with low, intermediate, and high levels of gene expression obtained using fluorescence-activated cell sorting from a cell population stably silenced with DNMT3A-dCas9. Shown is a representative replicate from three independent transfections (DNMT3A-dCas9) followed by three independent fluorescence-activated cell sorts. **B** Flow cytometry-based time-course analysis of the dynamics of gene expression exhibited by cells obtained in panel A. Distributions shown for one representative replicate. **C** Distributions from flow cytometry measurements obtained on the last time point in panel B. Distributions are for one representative replicate. **D** ChIP-qPCR for H3K9me3 and H3K4me3 of the promoter in the genetic reporter for cells with low and intermediate levels of gene expression as compared to cells in the active state. Shown are fold changes and corresponding mean from three independent replicates as determined by the $\Delta\Delta C_t$ method with respect to the active state. Error bars are SD. **E** Heatmap of bisulfite sequencing of the genetic reporter exhibiting an inverse correlation between DNA methylation grade and gene expression. Shown is the mean percentage of methylation for each CpG from three independent replicates. **F** Probability distribution of the fraction of CpGs methylated (See "Methods" section for details on deriving these plots from data in panel E). **G** Correlation plot. The green line represents the best-fit linear regression line $y = -0.5059x + 0.5497$. The p-value associated with the slope coefficient is p $= 0.038 < 0.05$ (See "Methods" section for details on deriving the linear regression line). **H** Distributions from flow cytometry of cells (blue) sorted from a population of cells that has maintained intermediate levels of gene expression (orange). Data shows a representative replicate from three independent replicates. **I** Time-course analysis of cells obtained in panel H. Data shows a representative replicate from three independent replicates. **L** Distributions of gene expression 14 days after the cell sorting shown in panel H corresponding to the last time point in panel I. Data shows a representative replicate from three independent replicates.

Gene expression levels are stably maintained in an analog manner as dictated by DNA methylation grade

To further test the hypothesis that epigenetic memory operates on an analog basis as determined by DNA methylation grade, we set out to characterize the long-term dynamics of gene expression with extensive sampling of single cells from DNMT3A-silenced cell populations followed by monoclonal expansion and analysis. This approach provides a high-resolution evaluation of gene expression trajectories generated exclusively from one initial DNA methylation grade. We therefore performed fluorescence-activated single-cell sorting from the three distinct cell populations that had been previously sorted from a DNMT3A-silenced population (Fig. 4A). Specifically, we selected eight different regions of gene expression levels spanning across the low, intermediate, and high gene expression levels. We sampled single cells from each of those regions and performed monoclonal expansion, which resulted in >10 monoclonal populations for each of the eight gene expression regions and a total of 93 monoclonal populations (Fig. 4A, B). Flow cytometry was then performed for each of the monoclonal populations 14 days after the initial single-cell sort (Fig. 4B). These data showed a continuum of gene expression levels across the 93 populations ranging from background expression level to active gene expression level. We observed that the coefficient of variation, defined as the standard deviation divided by the mean, was larger for monoclonal populations with intermediate gene expression levels. This is consistent with the model, where intermediate DNA methylation grades drive the two-state nucleosome modification system into a bistable regime, in which H3K4me3

(and hence gene expression level) fluctuate between the two stable states under the influence of noise (SI Section S.4, Figs. S.2 and S.3A). To further test whether the gene expression levels from the monoclonal populations could be maintained in time, we selected 8 monoclonal populations (highlighted in Fig. 4B), spanning the EBFP2 expression range from the 93 clones and performed time-course flow cytometry measurements up to 161 days after the initial single-cell sort (Fig. 4C). In these measurements, we observed that the EBFP2 distributions remained stable, validating the starting hypothesis that cells can maintain memory of any gene expression level.

We next investigated DNA methylation grade as a determinant of persistent gene expression level. To this end, we characterized the DNA methylation grade of the eight monoclonal populations at different time points. Specifically, we performed targeted bisulfite sequencing of the genetic reporter in each of the eight populations at two different time points (Fig. 4D,E). These data indicate that ranging from maximal gene expression to no gene expression, an increased number of CpGs in the promoter and upstream region are methylated. To acquire a quantitative understanding of the graded nature of this variation, we computed from the bisulfite sequencing data the probability distribution of the number of methylated CpGs (see Methods) in the gene's promoter and its upstream region for each of the eight clones (Fig. 4F,G). This plot confirmed that the mean number of methylated CpGs increases monotonically in a graded manner through the eight populations. Remarkably, the correlation between the median EBFP2 expression level of each population and the median number of methylated CpGs is close to linear (p $= 5.34 \cdot 10^{-5} < 0.05$, Fig. 4H,I), confirming an inverse correlation between DNA methylation and gene expression level.

The data of Fig. 4F further show that the variability of the number of methylated CpGs about their mean value is larger for intermediate DNA methylation grades when compared to low and high methylation grades. The mathematical model recapitulates this property (Fig. 4G) when it includes also the two following possible molecular interactions: (a) H3K9me3 helps recruit DNA methylation maintenance enzyme (DNMT1) to the gene [45] and (b) DNMT1 can cause de novo DNA methylation, although at very low rate [46, 47] (see SI Section S.5 for model derivation). With these assumptions, the errors made by DNMT1 in maintaining some of the CpGs are less probable for a fully methylated gene and the errors in *de novo* methylating additional CpGs are less probable for a gene with no methylation. These facts result in tighter distributions for highly or lowly methylated gene states (see SI Section S.5 and Fig. S.6 for model analysis.).

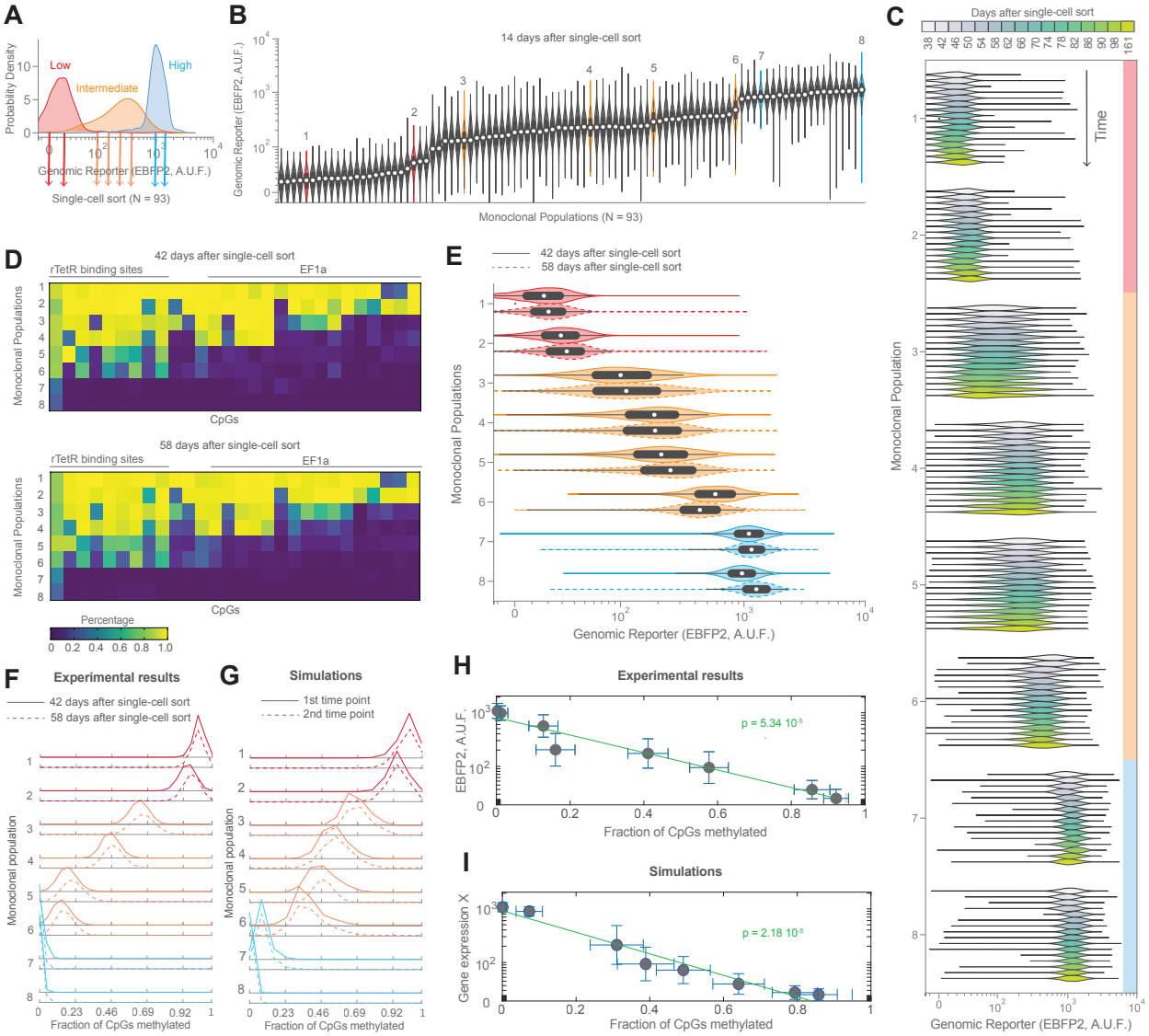

Fig. 4. Continued on the following page.

Fig. 4. **Epigenetic memory exhibits analog behavior and inversely correlates with grades of DNA methylation. A** Distributions of gene expression of cells that have stably maintained low, intermediate, and high levels of gene expression. Arrows indicate the levels of gene expression from where single-cell sorting was performed to obtain monoclonal populations. The total number of monoclonal populations obtained was at least 10 for each of the eight levels of gene expression. **B** Monoclonal populations (N = 93) measured 14 days after single-cell sort using flow cytometry. Clones indicated with numbers 1-8 were selected for further analysis. Colors represent the distribution of origin in panel A. **C** Flow cytometry-based time course analysis of gene expression dynamics of the eight monoclonal populations selected in panel B. **D** Bisulfite sequencing of the genetic reporter in the eight monoclonal population at two different time points. **E** Flow cytometry measurements of the genetic reporter in the eight monoclonal population at two different time points corresponding to those shown on panel D. **F** Probability distribution of the fraction of CpGs methylated (See "Methods" section for details on deriving these plots from data in panel E). **G** Probability distributions of the system represented by reactions listed in SI Tables S.5 and S.3. The distributions are obtained computationally using SSA [43] and, on the x we have the fraction of CpGs methylated. The parameter values used for these simulations are listed in SI Section S.9. **H** Correlation plot between the mean fraction of CpGs methylated and its mean gene expression level at 42 days after single-cell sort. The green line represents the best-fit linear regression $y = -0.3756x + 0.4358$. The p-value associated with the slope coefficient is p $= 5.34 \cdot 10^{-5} < 0.05$ (See "Methods" section for details on deriving the linear regression parameters). **I** Correlation plot between the mean fraction of CpGs methylated and its mean gene expression level, X, obtained via simulations. The green line represents the best-fit linear regression $y = -0.4673x + 0.4580$. The p-value associated with the slope coefficient is p $= 2.18 \cdot 10^{-5} < 0.05$ (See "Methods" section for details on deriving the linear regression parameters).

Finally, we sought to investigate whether overriding the DNA methylation grade in cells with intermediate levels of gene expression cause changes to gene expression level. To enhance DNA methylation we therefore utilized DNMT3A-dCas9 as we have shown before that it adds DNA methylation to the gene (Fig. 2F), also consistent with prior reports [41]. To remove DNA methylation, we engineered fusion proteins comprising rTetR fused to the catalytic domains of TET1 [48] to construct rTetR-TET1. Moreover, we fused rTeR to KRAB to construct rTetR-KRAB in order to evaluate changes to gene expression when enhancing H3K9me3. We therefore transiently transfected these epigenetic effectors in cells that had been previously sorted for intermediate levels of gene expression from the DNMT3A-dCas9-silenced cells (Fig. 3A) and exhibited intermediate DNA methylation grades (Fig. 3E,F). As before, we utilized fluorescence-activated cell sorting to obtain highly transfected cells and performed time-course flow cytometry measurements (Fig. 5). By 10 days after transfection with DNMT3A-dCas9, the EBFP2 distribution was silenced, overlapping cells with low levels of gene expression, and remained stable (Fig. 5A). Transient transfection with rTetR-TET1 resulted in nearly complete and permanent reactivation of gene expression (Fig. 5B). By contrast, in transient transfection experiments with rTetR-KRAB, we observed levels of repression consistent with the silenced state 6 days after transfection but then expression reverted to the initial intermediate level and remained stable afterwards (Fig. 5C). These data indicate that transient recruitment of DNA methylation writer or eraser enzymes to an intermediadely methylated, and partially active gene, silences or reactivates the gene, permanently, thereby pinpointing DNA methylation grade as a causal determinant of gene expression level, in accordance with the model predictions (SI Fig. S.7).

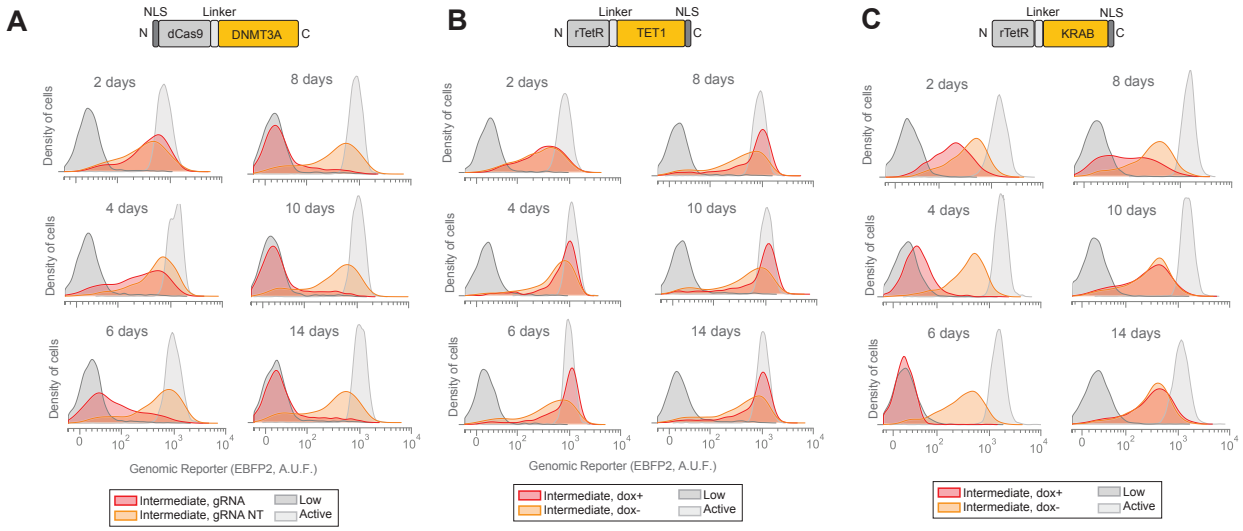

Fig. 5. DNA methylation grade as a causal determinant of gene expression level. **A** Time-course of flow cytometry measurements after expression of DNMT3A-dCas9 via transient transfection in cells that have stably maintained intermediate levels of gene expression. **B** Time-course of flow cytometry measurements after transfection of rTetR–TET1 in cells that have stably maintained intermediate levels of gene expression. **C** Time-course of flow cytometry measurements after transfection of rTetR-KRAB in cells that have stably maintained intermediate levels of gene expression.

Editing DNA methylation at the genetic reporter to achieve a reversible switch with long-term states

Engineered genetic switches are highly desirable for future therapeutic applications, and a number of such systems have been engineered in mammalian cells [49–51]. Long-term maintenance of each of the stable gene expression states is a critical design requirement for these systems, along with the ability to efficiently switch the state by transient stimulation. Therefore, we investigated whether we could exploit the long-term maintenance of gene expression levels in our genetic reporter (Fig. 4C) along with the ability to modulate it with DNMT3A and TET1 (Fig. 5) to achieve a reversible switch with long-term stable states. To this end, we first sought to determine the extent to which we could optimize the dosage of the epigenetic effectors in order to achieve high switching efficiency in the presence of the small molecule (Dox).

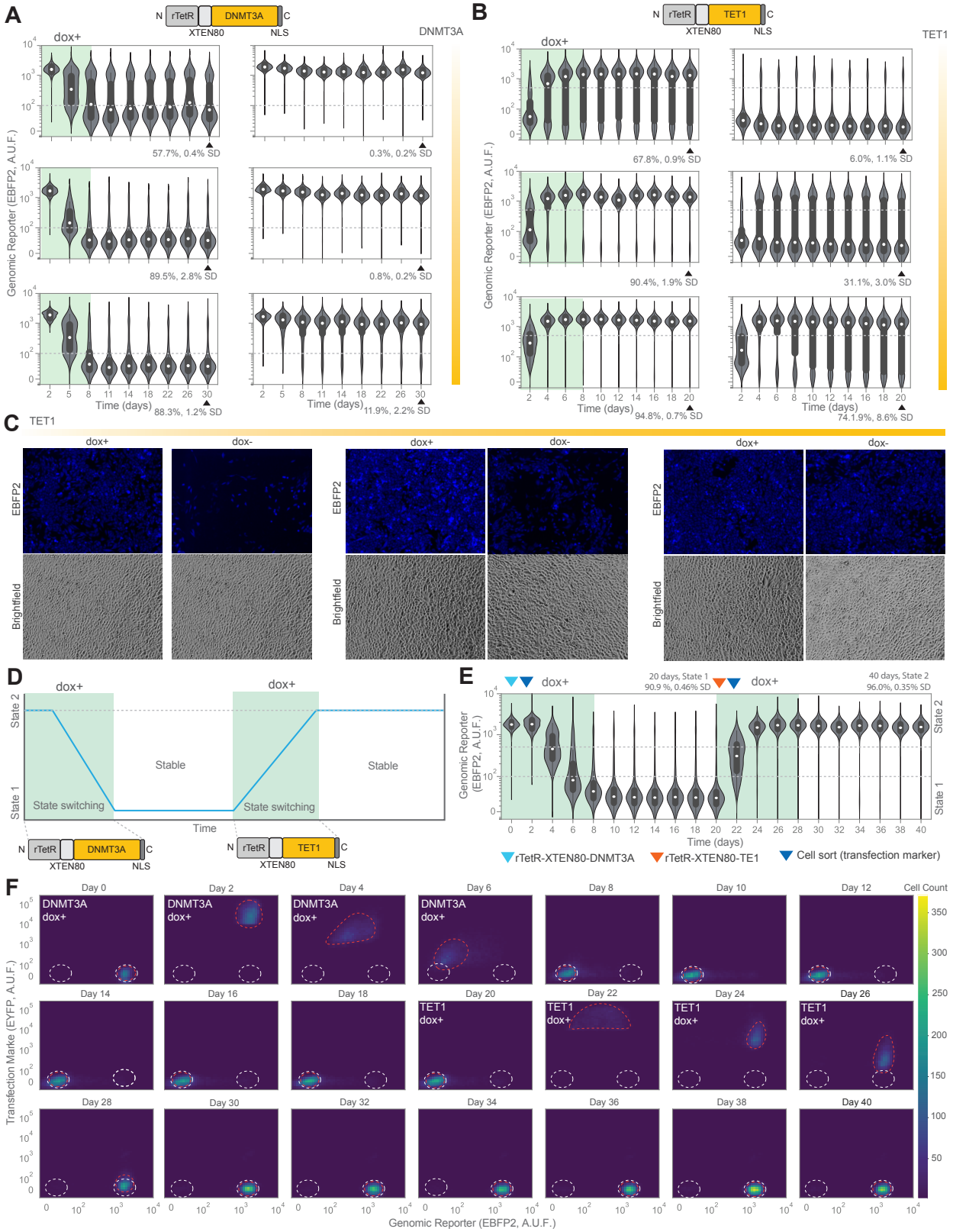

Fig. 6. Continued on the following page.

Fig. 6. **DNA methylation-based two-state reversible switch. A** Experimental analysis of DNMT3A-mediate silencing. The dashed line indicates the threshold for the silenced state. Shown is a representative replicate from 3 independent replicates. The percentage shown is mean percentage in the silenced state from 3 independent replicates. **B** Experimental analysis of TET1-mediate activation. Reactivation from DNMT3A-silenced cells. The dashed line shows the threshold for the active state. Shown is a representative replicate from 3 independent replicates. The percentage shown is mean percentage in the active state from 3 independent replicates. **C** Microscopy of TET1-mediated activation from panel B. Shown is 20 days after transfection with rTetR-XTEN80-TET1. Data is a representative replicate from three independent replicates. **D** Experimental overview of demonstration of reversible switching between the two stable states. **E** Demonstration of reversible switching between the two stable states. Data shown is from a representative replicate from 3 independent replicates. **F** 2D histograms of reversible switching between the two stable states. White dashed lines indicate the stable states without input. Red dashed lines indicate the current location of the cells.

To this end, we first engineered rTetR-XTEN80-DNMT3A and rTetR-XTEN80-TET1 by fusing rTetR to either catalytic domains of DNMT3A or TET1 using an XTEN80 linker. We then expressed rTetR-XTEN80-DNMT3A in cells bearing the genetic reporter in the active state using transient transfection (Fig. 6A). Subsequently, we performed fluorescence-activated cell sorting of the cells into three levels of transfection followed by time-course flow cytometry measurements. For both the medium and high dosages of rTetR-XTEN80-DNMT3A, more than 88% of the cells switched to the silenced state in the presence of dox, but only less than 12% switched in the absence of Dox (Fig. 6A). We then expressed rTetR-XTEN80-TET1 in cells in the silenced state and correspondingly performed fluorescence-activated cell sorting into three levels of transfection followed by time-course flow cytometry measurements. Already for the lowest dosage of rTetR-XTEN80-TET1, we observed 67.8% of the cells switching to the active state in the presence of dox with only 6% switching in the absence of dox (Fig. 6B, top panel). On the other hand, with the high dosage of the epigenetic effector, 94.8% of cells switched in the presence of dox but with high leakiness in the absence of dox (Fig. 6B, bottom panel). Medium dosage of the epigenetic effector resulted in 90.4% of the cells switching with dox and 31.1% switching in the absence of dox (Fig. 6B, bottom panel). Microscopy data shows the dynamics of switching to the active state after transfection (Fig. 6C).

We then set out to demonstrate the two-state switching dynamics in a single experiment. Specifically, we first expressed rTetR-XTEN80-DNMT3A via transient transfection in cells bearing our genetic reporter in the active state, and then utilized a fluorescence-activated cell sorter to obtain cells with high levels of transfection (Fig. 6C, D, E). The cells stably silenced and we observed that 90.9% of the cells were in the silenced state 20 days after transfection with rTetR-XTEN80-DNMT3A (Fig. 6D, E). We then expressed rTetR-XTEN80-TET1 via transient transfection 20 days after transfection with rTetR-XTEN80-DNMT3A. Cells transitioned from the silenced state to the active state within only 4 days after transfection, and remained stable afterwards (Fig. 6D, E). These data show that the TET1/DNMT3A epigenetic effector pair and reporter system may be used as a building block for future engineered switches in which the stable states can be maintained long-term, while at the same time can be efficiently switched.

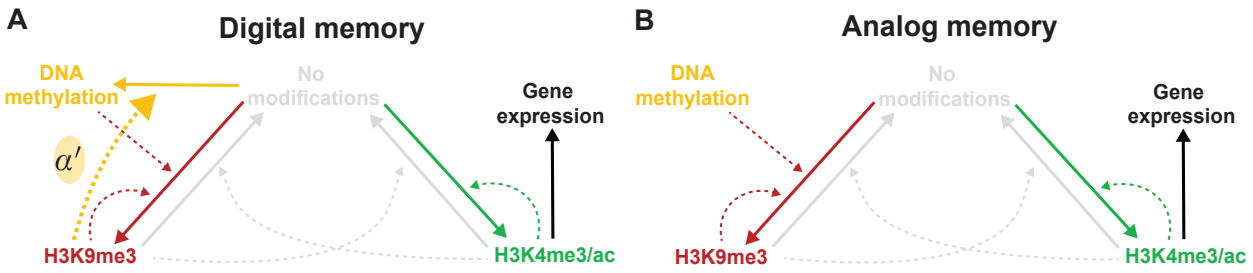

Fig. 7. The interactions between DNA methylation and histone modifications explain the difference between digital and analog epigenetic memory. (A) H3K9me3 recruits writer enzymes for DNA methylation (catalysis of DNA methylation by H3K9me3, yellow dashed arrow). (B) H3K9me3 does not recruit writer enzymes for DNA methylation. In the diagrams, we have assumed that no external epigenetic effectors (such as KRAB, DNMT3A, and TET1) are present. The rate of DNA methylation catalysis by H3K9me3 is represented by α'. Refer to SI Fig. S.1A and C for the complete diagram and model.

Discussion

The extent to which long-term epigenetic memory is an exclusive attribute of silenced and active gene states or it is possible for any gene expression level is the question addressed by this paper. Unexpectedly, we found that cells can stably maintain any gene expression level (Fig. 3B and I and Fig. 4C) and that this level inversely correlates with grades of DNA methylation in the gene's promoter and upstream operator sites (Fig. 3E-G and Fig. 4E,I,M). Each DNA methylation grade, in turn, measured by the mean number of methylated CpGs, also persists in time (Fig. 4F). In turn, recruitment of DNA methylation writer or eraser enzymes to an intermediately methylated, and partially active, gene leads to silencing or full activation, respectively (Fig. 5). Taken together, these results indicate that long-term analog memory of gene expression is possible and that the persistence of DNA methylation grade enables it. Our nucleosome modification model, which includes DNA methylation and its interactions with histone modifications H3K9me3 and H3K4me3, recapitulates analog epigenetic cell memory under the critical conditions: (i) DNMT1-enabled DNA methylation maintenance error rate is very low, leading to an approximately stable DNA methylation grade, and (ii) H3K9me3 does not catalyze *de novo* DNA methylation, although the latter can catalyze the former (see SI Section S.3). In particular, failure of (ii), that is, a strong catalysis of DNA methylation by H3K9me3, even when (i) holds, leads to digital memory (SI Figs. S.1B and S.2). Therefore, a model emerges that can explain the molecular determinants of digital versus analog epigenetic cell memory (Fig. 7).

Although DNA methylation patterns can, in principle, propagate through cell division by the copy-paste action of DNA methylation maintenance enzyme DNMT1 [7], the extent to which DNA methylation patters are actually maintained in cells has been more recently questioned [16]. DNA methylation is a more dynamic epigenetic mark than originally thought, due to the continuous write-erase actions of DNMT3A and TET1 [17], and to interactions

with histone modifications [18].These, not only include mutual catalysis with H3K9me3 [21, 22] and inhibition with H3K4me3 [19, 20], but also the influence of these histone modifications on the maintenance activity mediated by DNMT1 [45]. These reciprocal actions, taken together, influence the fidelity at which DNA methylation can be inherited through cell division. In fact, the positive feedback loop where DNA methylation catalyzes H3K9me3 and this, in turn, catalyzes *de novo* DNA methylation, can push an initially partially methylated gene to be fully methylated. The competitive interaction of DNA methylation with H3K4me3, in turn, can cause H3K4me3 to win over an initially low DNA methylation state and to revert this to unmethylated. When these interactions are sufficiently strong, then digital memory can emerge (SI Section S.3, Fig. S.2), and fully methylated and completely unmethylated sites can achieve higher maintenance fidelity when compared to sites where not all the CpGs are methylated [24].

The MeDIP and ChIP data have shown that H3K9me3 does not catalyze DNA methylation in our system (Fig. 3E), consistent also with the data of Bintu *et al.* [28]. With this, our nucleosome modification model allows for the possibility that also intermediate DNA methylation grades can be stably maintained (SI Fig. S.1), which is confirmed by our bisulfite sequencing data (Fig. 4F). These data also show that the variability of the number of methylated GpGs about its mean level is larger for intermediate DNA methylation grades (Fig. 4F). The nucleosome modification model would not be able to recapitulate this if we had regarded the DNA methylation process as isolated from H3K9me3 and H3K4me3 (SI Section S.5 and Fig. S.6). Specifically, the model recapitulates this feature when it includes the known facts that DNMT1 is recruited by H3K9me3 [45] and that DNMT1 can make mistakes, although at a very low rate [46, 47] (see Fig. 4G and SI Section S.5, Fig. S.6.

Our data generated by recruitment of DNMT3A to the reporter system is consistent with that of Bintu *et al.* [28] as the authors also observed that, despite the all or none silencing dynamics, cells existed at intermediate gene expression levels. We analyzed these intermediately expressing cells in this paper and revealed a stable epigenetic state. While it is well established that DNA methylation has a repressive effect on gene expression [32], the extent to which DNA methylation grade is a modulator of gene expression level has not been fully characterized. Here, we have shown that the DNA methylation grade in the promoter and its immediate upstream operator sites inversely correlates with gene expression level via an approximately linear relationship (Fig. 4M). This, and the fact that recruitment of DNA methylation eraser or writer enzymes to an intermediately methylated, and partially active, gene fully activates or silences expression (Fig. 5), respectively, indicate DNA methylation grade as a causal modulator of gene expression level.

More broadly, analog epigenetic cell memory questions the concept of cell type as a discrete entity emerging from a sequence of binary decisions that either silence or activate genes, as captured by the Waddington

epigenetic landscape metaphore [52]. With analog memory, cell fate may become a fluid entity that instead arises from a continuum spectrum of choices of gene expression levels. Such a broadened view of cell fate opens the possibility for the existence of uncharacterized “graded cell types”, with functions that have not been appreciated yet due to the lower frequency of these “continuous” types when compared to the majority of discrete cell types, which are also more clearly identified. Consistent with this broader notion of a cell type is the recent discovery of gradients of cell types in the hippocampus [53], with which DNA methylation grades may be associated [54]. These findings suggest that graded cell types are biologically plausible, thereby leading to revisiting the notion of cell fate as a discrete entity all together [55].

Methods

Cell conditions

Cells were cultured in growth media comprised of Dulbecco’s Modified Eagle Medium (DMEM) supplemented with 10% FBS, 1X non-essential amino acids, and 1X penicillin/streptomycin at 37℃ in a 5% CO2 incubator. The growth media was changed every 2-4 days. For routine passaging, the growth media was aspirated, followed by the addition of 0.25% trypsin. After incubation at 37℃ in a 5% CO2 incubator for 7 minutes, trypsin was neutralized with an equal or excess volume of growth media at room temperature. The cells were then centrifuged for 3 minutes at 200g, the supernatant discarded, and the pellet was resuspended in fresh growth media. The resuspended cells were then diluted (ratio between 1 and 20) and reseeded into new culture plates for subsequent cell culture.

Transfections

Cells were cultured in growth media at 37℃ in a 5% CO2 incubator. The cells were then treated with 0.25% trypsin and incubated for 7 minutes at 37℃ in a 5% CO2 incubator. The cell suspension was subsequently neutralized with an equal or excess volume of growth media at room temperature. The cells were centrifuged for 3 min at 200g. The supernatant was discarded, and the cell pellet was resuspended in the growth media. Cells were then seeded in 12-well tissue culture plates at 300,000 cells/well and incubated for 24 hours at 37℃ in a 5% CO2 incubator. Transfection complexes were prepared using Lipofectamine LTX (Invitrogen) according to the manufacturer’s instructions. Briefly, one tube contained DNA and PLUS reagent in Opti-MEM, and another tube contained Lipofectamine LTX in Opti-MEM. The tubes were combined and incubated at room temperature for 5 minutes to form the transfection complexes. The growth media was removed from the cells and replaced with

growth media without antibiotics. The transfection complexes was added dropwise, and the plates were gently swirled for even distribution. After 24 hours of incubation at 37℃ in a 5% CO2 incubator, replacement for routine growth media supplemented with 1X penicillin/streptomycin was performed.

Cell line construction

The genetic reporter was integrated using BxB1-mediated site-specific chromosomal integration into a landing pad in the LP20 locus in CHO-K1 cells [36]. This locus had been previously found by a homology-based computational search (BLAST) using the Rosa26 locus as a reference. The landing pad expresses EYFP exclusively before chromosomal integration. For integration, 500ng of the chromosomal integration vector and 500ng of the BxB1 expression vector were transfected into the cells. After 24 hours, routine cell culture was commenced with the supplementation of growth media with 8μg/ml for 2 weeks. Subsequently, a fluorescence-activated cell sorter (BD Aria) was utilized to obtain cells that were positive for EBFP2 expression and negative for EYFP.

Cell sorting

Cells were trypsinized using 0.25% trypsin. The cells were then incubated at 37℃ in a 5% CO2 incubator for 7 minutes. Subsequently, trypsin was neutralized with an equal or excess volume of growth media at room temperature. The cells were then centrifuged at 200g for 3 minutes. The supernatant was discarded and the cell pellet was resuspended in growth media supplemented with 2.5g/ml BSA. The cell suspension was then filtered through a filter cap into flow cytometry tubes. Cell sorting was then performed using a fluorescence-activated cell sorter (BD Aria). EBFP2 was measured using a 405nm laser and a 450/50 filter. EYFP was measured using a 488nm laser and 515/20 filter.

Flow cytometry

Cells were trypsinized using 0.25% trypsin. The cells were then incubated at 37℃ in a 5% CO2 incubator for 7 minutes. Next, trypsin was neutralized with an equal or excess volume of growth meda at room temperature. The cells were subsequently centrifuged at 200g for 3 minutes. The supernatant was discarded and the cell pellet was resuspended in growth media. The cell suspension was filtered through a filter cap into flow cytometry tubes. Flow cytometry data was then collected using a flow cytometer (BD LSRFortessa). EBFP2 was measured using a 405nm laser and a 450/50 filter. EYFP was measured using a 488nm laser and 530/30 filter.

Time-course flow cytometry

Following transfection, a fluorescence-activated cell sorter was used to obtain cells with specific levels of a

transfection marker (EYFP). Cell sorting was performed between 42-48 hours after transfection. When flow cytometry was performed on the day of cell sorting, a fraction of the cells that were sorted was utilized for flow cytometry measurements, and the rest of the cells were reseeded on tissue culture plates. For subsequent flow cytometry measurements, the cells were trypsinized using 0.25% trypsin and incubated at 37℃ in a 5% CO2 incubator. Trypsin was neutralized with an equal or excess volume of growth media at room temperature. The cells were then centrifuged for 3 min at 200g. The supernatant was discarded, and the cells were resuspended in growth media. A fraction of the cells were utilized for the acquisition of flow cytometry measurements. The rest of the cells were diluted (ratio between 1 and 20) and reseeded into new tissue culture plates for subsequent measurements.

ChIP-qPCR and MeDIP-qPCR

ChIP-qPCR was performed using the True MicroChIP-seq kit (Diogenode) according to the manufacturer's instructions. MeDIP-qPCR was performed using the MagMeDIP-qPCR kit (Diogenode) according to the manufacturer's instructions. All sonication was performed using a Bioruptor Pico (Diogenode). We utilized antibodies for H3K4me3 (C15410003, Diogenode), H3K9me3 (C15410056, Diogenode), and anti-5mC for DNA methylation from the MagMeDIP-qPCR (Diogenode). The qPCRs were performed using Power SYBR Green PCR Master Mix (Applied Biosystems) in a LightCycler 96 (Roche). Folds reported refer to the standard $\Delta\Delta C_t$ method. For the genetic reporter, the promoter region was amplified. Actin was used as a reference gene for H3K4me3. IgF2 as used as a reference gene for H3K9me3 and DNA methylation.

Cloning

Expression vectors for the epigenetic effectors were cloned using Golden Gate Assembly. The cloning was performed in a single reaction with the plasmids comprising the destination vector, cHS4 chromatin insulator, EF1a promoter, 5' UTR, gene sequence, 3' UTR, and polyadenylation signal. Gene sequences for rTetR-TET1, rTetR-XTEN80-TET1, rTeTR-DNMT3A, rTeTR-XTEN80-DNMT3A, PhlF-KRAB, rTetR-KRAB, and PhlF were synthesized and cloned into a plasmid with compatible overhangs for Golden Gate Assembly (Azenta). For the genetic reporter, the region comprising the PhlF and rTetR binding sites was synthesized (Azenta) and subsequently cloned upstream of a vector containing the EF1a promoter using restriction cloning. Golden Gate Assembly was then performed in a reaction comprising a destination vector, upstream cHS4 chromatin insulator, EF1a promoter with upstream DNA-binding sites, 5' UTR, EBFP2, 3' UTR, and polyadenylation signal. The expression vector was then digested and cloned along with the downstream cHS4 chromatin insulator into a chromosomal integration vector using Gibson Assembly.

Microscopy

Microscopy images were acquired using a Zeiss Axio Observed Z1.

Quantification and statistical analysis

To determine the probability of a specific fraction of CpGs being methylated based on bisulfite sequencing data, which offers the probability of a specific CpG being methylated for the cell population, we employ the following method. This approach is applied to both bisulfite sequencing datasets presented in Figs. 3E and 4D, resulting in the corresponding plots in Figs. 3F and 4F, respectively.

Let us assume that the gene of interest has a total of N CpGs. Then, for any $0 \leq j \leq N$, having j CpGs methylated corresponds to the event where precisely j CpGs are methylated, and all other CpGs (i.e., $N - j$) are unmethylated. Noe, let us define the probability of the described event as P_j, where $0 \leq j \leq N$. Additionally, let the probability of CpG i being methylated be p_i, and the probability of CpG i being unmethylated be q_i, where $1 \leq i \leq N$. The bisulfite sequencing data provide us with p_i, and since the event "CpG unmethylated" is the complement of "CpG methylated", q_i is known and can be expressed as $q_i = 1 - p_i$. Then, the probability that exactly j CpGs are methylated out of a total of N CpGs, where each CpG has its own probability of being methylated (p_i) or not being methylated (q_i), can be calculated by using the following formula:

$$P(\text{Exactly } j \text{ CpGs are methylated}) = \sum_{\substack{S \subseteq \{1,2,\ldots,N\} \\ |S|=j}} \left(\prod_{i \in S} p_i \cdot \prod_{k \in \{1,2,\ldots,N\} \setminus S} q_k \right). \tag{1}$$

More precisely, the sum ($\sum$) is taken over all possible subsets S of events with exactly j elements. For each subset S, we calculate the product of the probabilities of the events in S occurring ($\prod_{i \in S} p_i$). We then calculate the product of the probabilities of the events not in S occurring ($\prod_{k \in \{1,2,\ldots,N\} \setminus S} q_k$). The overall probability is the sum of these products for all subsets S. In simpler terms, the formula considers all possible combinations of j events occurring out of N events, multiplying the probabilities of those events occurring and the probabilities of the remaining events not occurring in each combination. The sum aggregates these probabilities for all valid combinations, providing the probability that exactly j events happen.

As illustrative example, let us consider the case in which the total number of CpG in the gene of interest are $N = 3$. Then, defining the probability of CpG i to be and not to be methylated as p_i and $q_i = 1 - p_i$, with $i = 1, 2, 3$, we then can calculate the probability of having j CpGs methylated, i.e., P_j, with $j = 0, 1, 2, 3$, using (1), obtaining $P_0 = q_1 q_2 q_3$, $P_1 = p_1 q_2 q_3 + q_1 p_2 q_3 + q_1 q_2 p_3$, $P_2 = p_1 p_2 q_3 + p_1 q_2 p_3 + q_1 p_2 p_3$, and $P_3 = p_1 p_2 p_3$. The probability distribution of the fraction of CpGs methyalated is then obtained by plotting (j, P_j) for $j = 0, 2, ..., N$.

Concerning the best-fit linear regression lines shown in Figs. 3G and 4H and I, they were obtained using MATLAB's polyfit function. Furthermore, the p-value associated with the slope coefficient was determined through the fitlm function.

Computational analysis

All simulations conducted in this paper were done using Gillespie's Stochastic Simulation Algorithm (SSA) [43].

Acknowledgements

We would like to thank Dr. Lacramioara Bintu for helping us optimize the conditions for chromatin and DNA shearing, Dr. James J. Collins for providing scientific comments and suggestions on the link between the model predictions and the experimental data, Kalon Overholt for providing useful references on DNA methylation and providing feedback on some of the figures, and the Biological Engineering Comm Lab for helping us refine some of the diagrams. Furthermore, we would like to thank our funding: NSF-MODULUS, Award number 2027949.

References

1. Graf, T. & Enver, T. Forcing cells to change lineages. *Nature* **462,** 587–94. https://doi.org/10.1038/nature08533 (2009).
2. Kouzarides, T. Chromatin modifications and their function. *Cell* **128,** 693–705. https://doi.org/10.1016/j.cell.2007.02.005 (2007).
3. Allis, C. D., Caparros, M.-L., Jenuwein, T. & Reinberg, D. *Epigenetics* (Cold Spring Harbor Laboratory Press, Second Edition, 2015).
4. Huang, S., Litt, M. & Blakey, C. A. *Epigenetic Gene Expression and Regulation* (Academic Press, 2015).
5. Heard, E. & Martienssen, R. A. Transgenerational epigenetic inheritance: myths and mechanisms. *Cell* **157,** 95–109. https://doi.org/10.1016/j.cell.2014.02.045 (2014).
6. Allis, C. D. & Jenuwein, T. The molecular hallmarks of epigenetic control. *Nat Rev Genet* **17,** 487–500. https://doi.org/10.1038/nrg.2016.59 (2016).
7. Li, E. & Zhang, Y. DNA methylation in mammals. *Cold Spring Harb Perspect Biol* **6.** https://doi.org/10.1101/cshperspect.a019133 (2014).
8. Cheng, X. Structural and functional coordination of DNA and histone methylation. *Cold Spring Harb Perspect Biol.* **6,** 693–705. https://doi.org/10.1101/cshperspect.a018747 (2014).
9. Bannister, A. J. *et al.* Selective recognition of methylated lysine 9 on histone H3 by the HP1 chromo domain. *Nature* **410,** 120–4. https://doi.org/10.1038/35065138 (2001).
10. Jones, P. L. *et al.* Methylated DNA and MeCP2 recruit histone deacetylase to repress transcription. *Nat Genet* **19,** 187–191. https://doi.org/10.1038/561 (1998).
11. Schneider, R. *et al.* Histone H3 lysine 4 methylation patterns in higher eukaryotic genes. *Nat Cell Biol* **6,** 73–7. https://doi.org/10.1038/ncb1076 (2003).
12. Hathaway, N. A. *et al.* Dynamics and memory of heterochromatin in living cells. *Cell* **149,** 1447–1460. https://doi.org/10.1016/j.cell.2012.03.052 (2012).
13. Zhang, T., Cooper, S. & Brockdorff, N. The interplay of histone modifications - writers that read. *EMBO Rep* **16,** 1467–1481. https://doi.org/10.15252/embr.201540945 (2015).
14. Dodd, I. B., Micheelsen, M. A., Sneppen, K. & Thon, G. Theoretical Analysis of Epigenetic Cell Memory by Nucleosome Modification. *Cell* **129,** 813–822. https://doi.org/10.1016/j.cell.2007.02.053 (2007).

15. Stelzer, Y., Shivalila, C. S., Soldner, F., Markoulaki, S. & Jaenisch, R. Tracing dynamic changes of DNA methylation at single-cell resolution. *Cell* **163,** 218–29. https://doi.org/10.1016/j.cell.2015.08.046 (2015).

16. Mattei, A. L., Bailly, N. & Meissner, A. DNA methylation: a historical perspective. *Trends Genet* **38,** 676–707. https://doi.org/10.1016/j.tig.2022.03.010 (2022).

17. Charlton, J. *et al.* TETs compete with DNMT3 activity in pluripotent cells at thousands of methylated somatic enhancers. *Nature genetics* **52,** 819–827. https://doi.org/10.1038/s41588-020-0639-9 (2020).

18. Du, J., Johnson, L. M., Jacobsen, S. E. & Patel, D. J. DNA methylation pathways and their crosstalk with histone methylation. *Nat Rev Mol Cell Biol* **16,** 519–32. https://doi.org/10.1038/nrm4043 (2015).

19. Ooi, S. K. *et al.* DNMT3L connects unmethylated lysine 4 of histone H3 to de novo methylation of DNA. *Nature* **448,** 714–717. https://doi.org/10.1038/nature05987 (2007).

20. Nan, X. *et al.* Transcriptional repression by the methyl-CpG-binding protein MeCP2 involves a histone deacetylase complex. *Nature* **393,** 383–389. https://doi.org/10.1038/30764 (1998).

21. Lopez-Serra, L. & Esteller, M. Proteins that bind methylated DNA and human cancer: reading the wrong words. *Br J Cancer* **98,** 1881–1885. https://doi.org/10.1038/sj.bjc.6604374 (2008).

22. Fuks, F. *et al.* The methyl-CpG-binding protein MeCP2 links DNA methylation to histone methylation. *J Biol Chem* **278,** 4035–4040. https://doi.org/10.1074/jbc.M210256200 (2003).

23. Bruno, S., Williams, R. J. & Del Vecchio, D. Epigenetic cell memory: The gene's inner chromatin modification circuit. *PLOS Computational Biology* **18,** 1–27. https://doi.org/10.1371/journal.pcbi.1009961 (2022).

24. Hay, A. D. *et al.* Epigenetic inheritance is unfaithful at intermediately methylated CpG sites. *Nat Commun* **14,** 5336. https://doi.org/10.1038/nrm4043 (2023).

25. Bird, A. P. & Taggart, M. H. Variable patterns of total DNA and rDNA methylation in animals. *Nucleic Acids Res* **8,** 1485–1497. https://doi.org/10.1093/nar/8.7.1485 (1980).

26. Hodges, E. *et al.* DNA methylation changes and complex intermediate states accompany lineage specificity in the adult hematopoietic compartment. *Molecular cell* **44,** 17–28. https://doi.org/10.1016/j.molcel.2011.08.026 (2011).

27. Stadler, M. B. *et al.* DNA-binding factors shape the mouse methylome at distal regulatory regions. *Nature* **480,** 490–495. https://doi.org/10.1038/nature10716 (2011).

28. Bintu, L. *et al.* Dynamics of epigenetic regulation at the single-cell level. *Science.* https://doi.org/10.1126/science.aab2956 (2016).

29. Ma, Y., Budde, M. W., Zhu, J. & Elowitz, M. B. Tuning methylation-dependent silencing dynamics by synthetic modulation of CpG density. *ACS Synthetic Biology* **12,** 2536–2545 (2023).

30. Lensch, S. *et al.* Dynamic spreading of chromatin-mediated gene silencing and reactivation between neighboring genes in single cells. *Elife* **11,** e75115 (2022).

31. Van, M. V., Fujimori, T. & Bintu, L. Nanobody-mediated control of gene expression and epigenetic memory. *Nature Communications* **12.1,** 537 (2021).

32. Liu, X. S. *et al.* Rescue of fragile X syndrome neurons by DNA methylation editing of the FMR1 gene. *Cell* **172,** 979–992 (2018).

33. Nuñez, J. K. *et al.* Genome-wide programmable transcriptional memory by CRISPR-based epigenome editing. *Cell* **184,** 2503–2519 (2021).

34. Angel, A., Song, J., Dean, C. & Howard, M. A Polycomb-based switch underlying quantitative epigenetic memory. *Nature* **476,** 105–108. https://doi.org/10.1038/nature10241 (2011).

35. Saxton, D. S. & Rine, J. Distinct silencer states generate epigenetic states of heterochromatin. *Mol Cell* **82,** 3566–3579. https://doi.org/10.1016/j.molcel.2022.08.002 (2022).

36. Gaidukov, L. *et al.* A multi-landing pad DNA integration platform for mammalian cell engineering. *Nucleic Acids Res.* **46,** 4072–4086 (May 2018).

37. Recillas-Targa, F. *et al.* Position-effect protection and enhancer blocking by the chicken beta-globin insulator are separable activities. *Proc. Natl. Acad. Sci. U. S. A.* **99,** 6883–6888 (May 2002).

38. Stanton, B. C. *et al.* Systematic transfer of prokaryotic sensors and circuits to mammalian cells. *ACS Synth. Biol.* **3,** 880–891 (Dec. 2014).

39. Margolin, J. F. *et al.* Krüppel-associated boxes are potent transcriptional repression domains. *Proc. Natl. Acad. Sci.* **91,** 4509–4513. 10.1073/pnas.91.10.4509 (1994).

40. Schultz, D. C., Ayyanathan, K., Negorev, D., Maul, G. G. & Rauscher, F. J. SETDB1: a novel KAP-1-associated histone H3, lysine 9-specific methyltransferase that contributes to HP1-mediated silencing of euchromatic genes by KRAB zinc-finger proteins. *Annual Review of Physical Chemistry* **16,** 919–32. https://doi.org/10.1101/gad.973302 (2002).

41. O'Geen, H. *et al.* dCas9-based epigenome editing suggests acquisition of histone methylation is not sufficient for target gene repression. *Nucleic Acids Res.* **45,** 9901–9916 (Sept. 2017).

42. Jackson, M. *et al.* Severe global DNA hypomethylation blocks differentiation and induces histone hyperacetylation in embryonic stem cells. *Mol Cell Biol* **24.** https://doi.org/10.1128/MCB.24.20.8862-8871 (2004).

43. Gillespie, D. T. Stochastic Simulation of Chemical Kinetics. *Annual Review of Physical Chemistry* **58,** 35–55. https://doi.org/10.1146/annurev.physchem.58.032806.104637 (2007).

44. Bannister, A. J. & Kouzarides, T. Regulation of chromatin by histone modifications. *Cell Res.* **21,** 381–395.

45. Ren, W. *et al.* Direct readout of heterochromatic H3K9me3 regulates DNMT1-mediated maintenance DNA methylation. *Proceedings of the National Academy of Sciences of the United States of America* **117,** 18439–18447. https://doi.org/10.1073/pnas.2009316117 (2020).

46. Laird, C. D. *et al.* Hairpin-bisulfite PCR: assessing epigenetic methylation patterns on complementary strands of individual DNA molecules. *Proceedings of the National Academy of Sciences of the United States of America* **101,** 204–209. https://doi.org/10.1073/pnas.2536758100 (2004).

47. Riggs, A. & Xiong, Z. Methylation and epigenetic fidelity. *Proceedings of the National Academy of Sciences of the United States of America* **101,** 4–5. https://doi.org/10.1073/pnas.2536758100 (2004).

48. Liu, X. S. *et al.* Editing DNA methylation in the mammalian genome. *Cell* **167,** 233–247 (Sept. 2016).

49. Kramer, B. P. & Fussenegger, M. Hysteresis in a synthetic mammalian gene network. *Proc Natl Acad Sci U S A* **102,** 9517–22. https://doi.org/10.1073/pnas.0500345102 (2005).

50. Lebar, T. *et al.* A bistable genetic switch based on designable DNA-binding domains. *Nat Commun* **5.** https://doi.org/10.1038/ncomms6007 (2014).

51. Zhu, R., Del Rio-Salgado, J. M., Garcia-Ojalvo, J. & Elowitz, M. B. Synthetic multistability in mammalian cells. *Science* **375.** https://doi.org/10.1126/science.abg9765 (2022).

52. Waddington, C. H. *The strategy of the genes* (Routledge, 1957).

53. Yao, Z. *et al.* A taxonomy of transcriptomic cell types across the isocortex and hippocampal formation. *Cell* **184,** 3222–3241. https://doi.org/10.1016/j.cell.2021.04.021 (2021).

54. Liu, H. *et al.* DNA methylation atlas of the mouse brain at single-cell resolution. *Nature* **598,** 120–128. https://doi.org/10.1038/s41586-020-03182-8 (2021).

55. Zeng, H. What is a cell type and how to define it? *Cell* **185,** 2739–2755. https://doi.org/10.1016/j.cell.2022.06.031 (2022).

Supplementary Information (SI)

S.1 Model of chromatin modification circuit

The chromatin modification circuit reaction model considered in our study, shown in Fig. S.1A, was constructed starting from the one in [23] and it is based on known molecular interactions from the literature. Here, we give a brief description of the reaction model (see [23] for additional details). The chromatin modifications considered in the circuit are H3K9 methylation (H3K9me3), H3K4 methylation (H3K4me3) and DNA methylation. The basic unit of the model is the nucleosome with DNA wrapped around it, D, that can be modified with H3K4me3, $\mathrm{D^A}$, DNA methylation, $\mathrm{D_1^R}$, H3K9me3, $\mathrm{D_2^R}$, or both H3K9me3 and DNA methylation, $\mathrm{D_{12}^R}$. The reaction model can be graphically represented by the circuit of Fig. S.1A, whose associated reactions are given in SI Section S.6. More precisely, writer enzymes have the ability to *de novo establish* chromatin marks. Additionally, histone modifications recruit writer enzymes for the same modification to nearby modifiable nucleosomes (*auto-catalysis*), and DNA methylation and repressive histone modification cooperate by recruiting each other's writer enzymes (*cross-catalysis*). Ultimately, these modifications can be passively removed through dilution during DNA replication or by the action of eraser enzymes (*basal erasure*). Both activating and repressive modifications are involved in the recruitement of each other's eraser enzymes (*recruited erasure*).

Now, defining the number of $\mathrm{D^A}, \mathrm{D_1^R}, \mathrm{D_2^R}, \mathrm{D_{12}^R}, \mathrm{D}$ as n^A, n_1^R, n_2^R, n_{12}^R, and n^D, let us derive the related ordinary differential equation (ODE) model in terms of the fractions $\bar{D}^A = n^A/\mathrm{D_{tot}}$, $\bar{D}_1^R = n_{D_1^R}/\mathrm{D_{tot}}$, $\bar{D}_2^R = n_{D_2^R}/\mathrm{D_{tot}}$, $\bar{D}_{12}^R = n_{D_{12}^R}/\mathrm{D_{tot}}$ and $\bar{D} = n_D/\mathrm{D_{tot}}$, with $\mathrm{D_{tot}}$ the total number of nucleosomes on a gene of interest. This can be done by assuming that $\mathrm{D_{tot}}$ is sufficiently large so that $\bar{D}^A$, $\bar{D}_1^R$, $\bar{D}_2^R$, $\bar{D}_{12}^R$ and $\bar{D}$ can be treated as real number. Now, let us introduce $D_{tot} = \mathrm{D_{tot}}/\Omega$ where Ω is the reaction volume, and define the normalized inputs: $u_{10}^R = k_{W0}^1/k_M^A D_{tot}$, $u_1^R = k_W^1/(k_M^A D_{tot})$, $u_{20}^R = k_{W0}^2/(k_M^A D_{tot})$, $u_2^R = k_W^2/(k_M^A D_{tot})$, $u_0^A = k_{W0}^A/(k_M^A D_{tot})$, and $u^A = k_W^A/(k_M^A D_{tot})$. Furthermore, let us introduce the following dimensionless parameters:

$$\alpha = \frac{k_M}{k_M^A} \quad \bar{\alpha} = \frac{\bar{k}_M}{k_M^A}, \quad \alpha' = \frac{k'_M}{k_M^A}, \tag{S.1}$$

in which α ($\bar{\alpha}$, α') is the non-dimensional rate constant associated with auto-catalysis (cross-catalysis). We consider α, $\bar{\alpha}$, and α' to have the same order. This will not affect the qualitative predictions obtained in this work. Let

$$\varepsilon = \frac{\delta + \bar{k}_E^A}{k_M^A D_{tot}}, \quad \varepsilon' = \frac{k_E^A}{k_M^A}, \quad \mu = \frac{k_E^R}{k_E^A}, \quad \mu' = \frac{k_T'^*}{k_E^A}, \tag{S.2}$$

with $b = O(1)$ such that $(\delta + \bar{k}_E^R)/(\delta + \bar{k}_E^A) = b\mu$ and $\beta = O(1)$ such that $(\delta' + k_T')/(\delta + \bar{k}_E^A) = \beta\mu'$. Then, μ (μ') encapsulates the asymmetry between the erasure rates of repressive histone modifications (DNA methylation) and activating marks. Furthermore, given that $(\delta + \bar{k}_E^R)/(k_M^A D_{tot}) = b\varepsilon\mu$, $(\delta' + k_T')/(k_M^A D_{tot}) = \beta\varepsilon\mu'$, $k_E^R/k_M^A = \mu\varepsilon'$ and $k_T'^*/k_M^A = \mu'\varepsilon'$, ε (ε') is a parameter that scales the ratio between the basal (recruited) erasure rate and the auto-catalysis rate of each modification. Considering the normalized time $\tau = tk_M^A D_{tot}$, the ODEs associated with the chromatin modification circuit are

$$
\begin{aligned}
\frac{d\bar{D}_1^R}{d\tau} &= (u_{10}^R + u_1^R + \alpha'(\bar{D}_2^R + \bar{D}_{12}^R))\bar{D} + \mu(b\varepsilon + \varepsilon'\bar{D}^A)\bar{D}_{12}^R - (u_{20}^R + \alpha(\bar{D}_2^R + \bar{D}_{12}^R) + \bar{\alpha}(\bar{D}_1^R + \bar{D}_{12}^R))\bar{D}_1^R \\
&\quad - \mu'(\beta\varepsilon + \varepsilon'\bar{D}^A))\bar{D}_1^R \\
\frac{d\bar{D}_{12}^R}{d\tau} &= (u_{10}^R + \alpha'(\bar{D}_2^R + \bar{D}_{12}^R))\bar{D}_2^R + (u_{20}^R + \alpha(\bar{D}_2^R + \bar{D}_{12}^R) + \bar{\alpha}(\bar{D}_1^R + \bar{D}_{12}^R))\bar{D}_1^R \\
&\quad - (\mu'(\beta\varepsilon + \varepsilon'\bar{D}^A) + \mu(b\varepsilon + \varepsilon'\bar{D}^A))\bar{D}_{12}^R \\
\frac{d\bar{D}_2^R}{d\tau} &= (u_{20}^R + u_2^R + \alpha(\bar{D}_2^R + \bar{D}_{12}^R) + \bar{\alpha}(\bar{D}_1^R + \bar{D}_{12}^R))\bar{D} + \mu'(\beta\varepsilon + \varepsilon'\bar{D}^A)\bar{D}_{12}^R - (u_{10}^R + \alpha'(\bar{D}_2^R + \bar{D}_{12}^R))\bar{D}_2^R \\
&\quad - \mu(b\varepsilon + \varepsilon'\bar{D}^A))\bar{D}_2^R \\
\frac{d\bar{D}^A}{d\tau} &= (u_0^A + u^A + \bar{D}^A)\bar{D} - (\varepsilon + \varepsilon'(\bar{D}_2^R + \bar{D}_{12}^R) + \varepsilon'(\bar{D}_1^R + \bar{D}_{12}^R))\bar{D}^A,
\end{aligned}
\tag{S.3}
$$

with $\bar{D} = 1 - \bar{D}_1^R - \bar{D}_{12}^R - \bar{D}_2^R - \bar{D}^A$ (see [23] for full derivation).

S.1.1 Expressions for k_W^1, k_W^2, k_T', $k_T^{'*}$ and u_1^R, u_2^R, μ'

In our study, we exploit KRAB, DNMT3A and TET1 to modulate the DNA compaction and then gene expression. KRAB is a well-known epigenetic effector that mediates the recruitment of H3K9me3. As we introduce KRAB through transient transfection, it will gradually decrease due to dilution until it eventually dies out. Furthermore, KRAB is fused to the DNA binding domain (DBD) PhlF. This fusion not only allows us to obtain sequence-specific recruitment, but also to regulate the binding and unbinding of KRAB through DAPG, as DAPG inhibits the ability of PhlF-KRAB to bind to DNA. To incorporate these aspects into our model, we can modify the expression for k_W^2 derived in [23] as follows:

$$
k_W^2 = \tilde{k}_W^2 \frac{1}{1 + \frac{DAPG}{K_2}} W_2 e^{-\delta t}, \tag{S.4}
$$

in which W_2 is PhlF-KRAB, $\tilde{k}_W^2$ is a function independent of PhlF-KRAB, whose expression can be found in [23], and K_2 is the dissociation constant related to the binding - unbinding reactions between DAPG and PhlF-KRAB.

Then, the normalized input u_2^R can be written as

$$u_2^R = \frac{k_W^2}{k_M^A D_{tot}} = \frac{\tilde{k}_W^2}{k_M^A} \frac{1}{1+\frac{DAPG}{K_2}} \frac{W_2}{D_{tot}} e^{-\frac{\delta}{k_M^A D_{tot}} t k_M^A D_{tot}} = \tilde{u}_2^R \frac{1}{1+\frac{DAPG}{K_2}} \bar{W}_2 e^{-\varepsilon\tau}, \tag{S.5}$$

in which we define $\tilde{u}_2^R = \tilde{k}_W^2 / k_M^A$ and $\bar{W}_2 = W_2/D_{tot}$.

The enzyme DNMT3A is a DNA methyltransferase that catalyzes *de novo* DNA methylation. As for KRAB, we introduce DNMT3 through transient transfection, and then its concentration will gradually decrease. To incorporate this aspect into our model, we can modify the expression for k_W^1 derived in [23] as follows:

$$k_W^1 = \tilde{k}_W^1 W_1 e^{-\delta t}, \tag{S.6}$$

in which W_1 is DNMT3A and $\tilde{k}_W^1$ is a function independent of DNMT3A, whose expression can be found in [23]. Then, the normalized input u_1^R can be written as

$$u_1^R = \frac{k_W^1}{k_M^A D_{tot}} = \frac{\tilde{k}_W^1}{k_M^A} \frac{W_1}{D_{tot}} e^{-\frac{\delta}{k_M^A D_{tot}} t k_M^A D_{tot}} = \tilde{u}_1^R \bar{W}_1 e^{-\varepsilon\tau}, \tag{S.7}$$

in which we define $\tilde{u}_1^R = \tilde{k}_W^1 / k_M^A$ and $\bar{W}_1 = W_1/D_{tot}$.

Finally, TET1 is an enzyme that catalyzes the removal of DNA methylation. As for KRAB, we introduce also TET1 through transient transfection and we fuse it to a DBD. More specifically, we employ rTetR, a DBD that binds DNA exclusively in the presence of doxycycline (DOX). To incorporate these aspects into our model, we can modify the expressions for k_T' derived in [23] as follows:

$$k_T' = k_{T1}' + \tilde{k}_T' \frac{\frac{DOX}{K_1}}{1+\frac{DOX}{K_1}} T e^{-\delta t}, \quad k_T'^* = k_{T1}'^* + \tilde{k}_T'^* \frac{\frac{DOX}{K_1}}{1+\frac{DOX}{K_1}} T e^{-\delta t}, \tag{S.8}$$

in which k_{T1}' ($k_{T1}'^*$) is the component of the rate coefficient that does not depend on the external rTetR-TET1 transiently transfected, whose expression can be found in [23], T is rTetR-TET1 transiently transfected, $\tilde{k}_T'$ and $\tilde{k}_T'^*$ are functions independent of rTetR-TET1, whose expressions can be found in [23], and K_1 is the dissociation constant related to the binding - unbinding reactions between DOX and rTetR-TET1. Then, the non-dimensional parameter μ' can be written as

$$\mu' = \frac{k_T'^*}{k_E^A} = \frac{k_{T1}'^*}{k_E^A} + \frac{\tilde{k}_T'^* D_{tot}}{k_E^A} \frac{\frac{DOX}{K_1}}{1+\frac{DOX}{K_1}} \frac{T}{D_{tot}} e^{-\frac{\delta}{k_M^A D_{tot}} t k_M^A D_{tot}} = \mu_1' + \tilde{\mu}' \frac{\frac{DOX}{K_1}}{1+\frac{DOX}{K_1}} \bar{T} e^{-\varepsilon\tau}, \tag{S.9}$$

in which we define $\mu_1' = \frac{k_{T1}'^*}{k_E^A}$, $\tilde{\mu}'$, and $\bar{T} = T/D_{tot}$.

S.2 Model of transcriptional regulation

Concerning the transcriptional regulation, chromatin state affects transcription by modulating nucleosome compaction and then gene expression. More precisely, we assume that transcription is predominantly allowed by $\mathrm{D^A}$. Additionally, a low level of transcription is attributed to D and to all the species characterized by repressive chromatin modifications. The inclusion of the latter in the model aims to reflect the experimental observation that gene expression levels are never entirely equal to zero. Furthermore, the gene product X is subject to dilution due to cell division and degradation. The reactions associated with the gene expression model can be found in SI Table S.3. Considering the normalized time $\tau = tk_M^A D_{tot}$ and introducing the non-dimensional parameters $\bar{\beta}_m^A = \beta_m^A/k_M^A D_{tot}$, $\bar{\beta}_m = \beta_m/k_M^A D_{tot}$, $\bar{\beta} = \beta/k_M^A D_{tot}$, $\bar{\gamma}_m = \gamma_m/k_M^A D_{tot}$, $\bar{\gamma} = \gamma/k_M^A D_{tot}$, the ordinary differential equation (ODE) model for X and m can be written as

$$\frac{d\bar{m}}{d\tau} = \bar{\beta}_m^A \bar{D}^A + \bar{\beta}_m(\bar{D} + \bar{D}_1^R + \bar{D}_2^R + \bar{D}_{12}^R) - \bar{\gamma}_m \bar{m}, \quad \frac{d\bar{X}}{d\tau} = \bar{\beta}\bar{m} - \bar{\gamma}\bar{X}. \tag{S.10}$$

In this paper, we will refer to the model that integrates the complete chromatin modification circuit model (Section S.1) along with the transcriptional regulation model outlined in this section as the "4D+X model."

S.3 Effect of α' and μ' on the stochastic behavior of the system

In this section, we analyze the stochastic behavior of the 4D+X model with a specific focus on understanding how the parameters α' (normalized rate of DNA methylation establishment through repressive histone modifications) and μ' (ratio between the DNA methylation erasure rate and the activating histone modification erasure rate) affect the probability distribution of gene expression levels and then the type of memory that can be achieved.

When the erasure rate of DNA methylation is 0 ($\mu' = 0$), achieving analog memory is possible only when there is no establishment of DNA methylation through repressive histone modifications ($\alpha' = 0$) (Fig. S.1B). For $\alpha' > 0$, the gene expression level shifts either to a low or high level. Furthermore, the higher α', the more the distribution tends to shift towards a low gene expression level (Fig. S.2 - top panel). When μ' is different from 0, only digital memory can be achieved (Fig. S.2 - intermediate and bottom panels). Moreover, the higher μ' is, the more the gene expression level shifts towards a high level (Fig. S.2 - bottom panel). Overall, these results suggest that analog memory can be achieved only when DNA methylation does not get erased (or it is erased so slowly compared to histone modification dynamics that μ' can be considered equal to 0) and does not get established by repressive histone modifications ($\alpha' = 0$).

If these conditions are verified, and external inputs (KRAB, DNMT3A, and TET1) are not applied or are applied transiently (transient transfection), then the number of nucleosomes with methylated DNA stabilizes at a constant value. Introducing the variable $\bar{Y}_1 = \bar{D}_1^R + \bar{D}_{12}^R$, that is, the fraction of nucleosomes with methylated DNA in the gene, the behavior of the original model (S.3) can be captured by a reduced 2D ordinary differential equation (ODE) model below:

$$\frac{d\bar{D}_2^R}{d\tau} = (\alpha\bar{D}_2^R + \bar{\alpha}\bar{Y}_1)\bar{D} - \mu(b\varepsilon + \varepsilon'\bar{D}^A)\bar{D}_2^R, \qquad \frac{d\bar{D}^A}{d\tau} = (u^A + \bar{D}^A)\bar{D} - (\varepsilon + \varepsilon'(\bar{D}_2^R + \bar{Y}_1))\bar{D}^A, \tag{S.11}$$

with $\bar{D} = 1 - \bar{D}^A - \bar{D}_2^R - \bar{Y}_1$ and $\bar{Y}_1 = constant$ (full derivation below). The reduced system can be associated with the chemical reaction system whose reaction list and diagram are shown in Fig. S.1C and D, respectively. It is important to point out that in the original model of chromatin modification circuit, it is assumed that the basic unit is a nucleosome with DNA wrapped around can have only one modifiable CpG [23]. There are cases in which this assumption is not verified. However, it is possible to demonstrate that removing this assumption yields a similar reduced model. This indicates that the assumption does not impact the qualitative results regarding the influence of the parameters α' and μ' on the probability distribution of gene expression levels (see SI Section S.7).

Derivation of model (S.11)

Let us first merge the rates linked to the enhancement of H3K9me3 establishment by $\bar{D}_{12}^R$ into a single rate. We will assume that this rate is identical to the one associated with the enhancement of H3K9me3 establishment by $\bar{D}_1^R$. Similarly, let us merge the rates linked to the recruited erasure of H3K4me3 by $\bar{D}_{12}^R$ into a single rate and assume that this rate is identical to the one associated with the recruited erasure of H3K4me3 by $\bar{D}_1^R$. These simplifying assumptions are not affecting the qualitatively results related to the effect of the cooperative and competitive interactions among chromatin modifications on the epigenetic cell memory. The ODE system (S.3) can then be rewritten as

$$
\begin{aligned}
\frac{d\bar{D}_1^R}{d\tau} &= (u_{10}^R + u_1^R + \alpha'(\bar{D}_2^R + \bar{D}_{12}^R))\bar{D} + \mu(b\varepsilon + \varepsilon'\bar{D}^A)\bar{D}_{12}^R - (u_{20}^R + \alpha(\bar{D}_2^R + \bar{D}_{12}^R) + \bar{\alpha}(\bar{D}_1^R + \bar{D}_{12}^R))\bar{D}_1^R \\
&\quad - \mu'(\beta\varepsilon + \varepsilon'\bar{D}^A))\bar{D}_1^R \\
\frac{d\bar{D}_{12}^R}{d\tau} &= (u_{10}^R + \alpha'(\bar{D}_2^R + \bar{D}_{12}^R))\bar{D}_2^R + (u_{20}^R + \alpha\bar{D}_2^R + \bar{\alpha}(\bar{D}_1^R + \bar{D}_{12}^R))\bar{D}_1^R \\
&\quad - (\mu'(\beta\varepsilon + \varepsilon'\bar{D}^A) + \mu(b\varepsilon + \varepsilon'\bar{D}^A))\bar{D}_{12}^R \\
\frac{d\bar{D}_2^R}{d\tau} &= (u_{20}^R + u_2^R + \alpha\bar{D}_2^R + \bar{\alpha}(\bar{D}_1^R + \bar{D}_{12}^R))\bar{D} + \mu'(\beta\varepsilon + \varepsilon'\bar{D}^A)\bar{D}_{12}^R - (u_{10}^R + \alpha'(\bar{D}_2^R + \bar{D}_{12}^R))\bar{D}_2^R \\
&\quad - \mu(b\varepsilon + \varepsilon'\bar{D}^A))\bar{D}_2^R \\
\frac{d\bar{D}^A}{d\tau} &= (u_0^A + u^A + \bar{D}^A)\bar{D} - (\varepsilon + \varepsilon'(\bar{D}_2^R) + \varepsilon'(\bar{D}_1^R + \bar{D}_{12}^R))\bar{D}^A,
\end{aligned}
\tag{S.12}
$$

Now, let us rewrite system (S.12) by assuming negligible basal *de novo* establishment ($u_{10}^R = u_{20}^R = u_0^A = 0$) and introducing the variable $\bar{Y}_1 = \bar{D}_1^R + \bar{D}_{12}^R$, that corresponds to the fraction of nucleosomes with methylated DNA. We then obtain

$$
\begin{aligned}
\frac{d\bar{Y}_1}{d\tau} &= (u_1^R)\bar{D} + (\alpha'(\bar{D}_2^R + \bar{D}_{12}^R))(\bar{D} + \bar{D}_2^R) - \mu'(\beta\varepsilon + \varepsilon'\bar{D}^A)\bar{Y}_1 \\
\frac{d\bar{D}_{12}^R}{d\tau} &= (\alpha'(\bar{D}_2^R + \bar{D}_{12}^R))\bar{D}_2^R + (\alpha\bar{D}_2^R + \bar{\alpha}\bar{Y}_1)\bar{D}_1^R - (\mu'(\beta\varepsilon + \varepsilon'\bar{D}^A) + \mu(b\varepsilon + \varepsilon'\bar{D}^A))\bar{D}_{12}^R \\
\frac{d\bar{D}_2^R}{d\tau} &= (u_2^R + \alpha\bar{D}_2^R + \bar{\alpha}\bar{Y}_1)\bar{D} + \mu'(\beta\varepsilon + \varepsilon'\bar{D}^A)\bar{D}_{12}^R - (\alpha'(\bar{D}_2^R + \bar{D}_{12}^R))\bar{D}_2^R - (\mu(b\varepsilon + \varepsilon'\bar{D}^A))\bar{D}_2^R \\
\frac{d\bar{D}^A}{d\tau} &= (u^A + \bar{D}^A)\bar{D} - (\varepsilon + \varepsilon'\bar{D}_2^R + \varepsilon'\bar{Y}_1)\bar{D}^A,
\end{aligned}
\tag{S.13}
$$

with $\bar{D} = 1 - \bar{Y}_1 - \bar{D}_2^R - \bar{D}^A$. Based on previous experimental results [28] and our experimental findings (see Fig. 2D), we can further simplify our model by assuming that the enhancement of DNA methylation establishment by H3K9me3 is negligible, i.e., $\alpha' = 0$. The ODE system (S.13) can then be rewritten as

$$
\begin{aligned}
\frac{d\bar{Y}_1}{d\tau} &= (u_1^R)\bar{D} - \mu'(\beta\varepsilon + \varepsilon'\bar{D}^A)\bar{Y}_1 \\
\frac{d\bar{D}_{12}^R}{d\tau} &= (\alpha\bar{D}_2^R + \bar{\alpha}\bar{Y}_1)\bar{D}_1^R - (\mu'(\beta\varepsilon + \varepsilon'\bar{D}^A) + \mu(b\varepsilon + \varepsilon'\bar{D}^A))\bar{D}_{12}^R \\
\frac{d\bar{D}_2^R}{d\tau} &= (u_2^R + \alpha\bar{D}_2^R + \bar{\alpha}\bar{Y}_1)\bar{D} + \mu'(\beta\varepsilon + \varepsilon'\bar{D}^A)\bar{D}_{12}^R - \mu(b\varepsilon + \varepsilon'\bar{D}^A)\bar{D}_2^R \\
\frac{d\bar{D}^A}{d\tau} &= (u^A + \bar{D}^A)\bar{D} - (\varepsilon + \varepsilon'\bar{D}_2^R + \varepsilon'\bar{Y}_1)\bar{D}^A,
\end{aligned}
\tag{S.14}
$$

with $\bar{D} = 1 - \bar{Y}_1 - \bar{D}_2^R - \bar{D}^A$. Now, let us rewrite the ODE system (S.14) introducing the expressions for u_2^R, u_1^R, and μ' derived in Section S.1.1 (Expressions (S.5), (S.7), and (S.9)):

$$
\begin{aligned}
\frac{d\bar{Y}_1}{d\tau} &= \tilde{u}_1^R \bar{W}_1 e^{-\varepsilon\tau}\bar{D} - (\mu_1' + \tilde{\mu}' \frac{\frac{DOX}{K_1}}{1+\frac{DOX}{K_1}}\bar{T}e^{-\varepsilon\tau})(\beta\varepsilon + \varepsilon'\bar{D}^A)\bar{Y}_1 \\
\frac{d\bar{D}_{12}^R}{d\tau} &= (\alpha\bar{D}_2^R + \bar{\alpha}\bar{Y}_1)\bar{D}_1^R - ((\mu_1' + \tilde{\mu}' \frac{\frac{DOX}{K_1}}{1+\frac{DOX}{K_1}}\bar{T}e^{-\varepsilon\tau})(\beta\varepsilon + \varepsilon'\bar{D}^A) + \mu(b\varepsilon + \varepsilon'\bar{D}^A))\bar{D}_{12}^R \\
\frac{d\bar{D}_2^R}{d\tau} &= (\tilde{u}_2^R \frac{1}{1+\frac{DAPG}{K_2}}\bar{W}_2 e^{-\varepsilon\tau} + \alpha\bar{D}_2^R + \bar{\alpha}\bar{Y}_1)\bar{D} + (\mu_1' + \tilde{\mu}' \frac{\frac{DOX}{K_1}}{1+\frac{DOX}{K_1}}\bar{T}e^{-\varepsilon\tau})(\beta\varepsilon + \varepsilon'\bar{D}^A)\bar{D}_{12}^R - \mu(b\varepsilon + \varepsilon'\bar{D}^A)\bar{D}_2^R \\
\frac{d\bar{D}^A}{d\tau} &= (u^A + \bar{D}^A)\bar{D} - (\varepsilon + \varepsilon'\bar{D}_2^R + \varepsilon'\bar{Y}_1)\bar{D}^A,
\end{aligned}
\tag{S.15}
$$

with $\bar{D} = 1 - \bar{Y}_1 - \bar{D}_2^R - \bar{D}^A$ and $\bar{D}_1^R = \bar{Y}_1 - \bar{D}_{12}^R$. Let us now consider the parameter regime in which the erasure rate of DNA methylation, without transfection of eTetR-TET1, is sufficiently low compared to histone modification dynamics,i.e., $\mu_1' \to 0$. This assumption is consistent with recent experimental data that suggest that the natural erasure of DNA methylation is a slow process [28]. The system (S.15) can then be rewritten as follows:

$$
\begin{aligned}
\frac{d\bar{Y}_1}{d\tau} &= \tilde{u}_1^R \bar{W}_1 e^{-\varepsilon\tau}\bar{D} - \tilde{\mu}' \frac{\frac{DOX}{K_1}}{1+\frac{DOX}{K_1}}\bar{T}e^{-\varepsilon\tau}(\beta\varepsilon + \varepsilon'\bar{D}^A)\bar{Y}_1 \\
\frac{d\bar{D}_{12}^R}{d\tau} &= (\alpha\bar{D}_2^R + \bar{\alpha}\bar{Y}_1)\bar{D}_1^R - (\tilde{\mu}' \frac{\frac{DOX}{K_1}}{1+\frac{DOX}{K_1}}\bar{T}e^{-\varepsilon\tau}(\beta\varepsilon + \varepsilon'\bar{D}^A) + \mu(b\varepsilon + \varepsilon'\bar{D}^A))\bar{D}_{12}^R \\
\frac{d\bar{D}_2^R}{d\tau} &= (\tilde{u}_2^R \frac{1}{1+\frac{DAPG}{K_2}}\bar{W}_2 e^{-\varepsilon\tau} + \alpha\bar{D}_2^R + \bar{\alpha}\bar{Y}_1)\bar{D} + \tilde{\mu}' \frac{\frac{DOX}{K_1}}{1+\frac{DOX}{K_1}}\bar{T}e^{-\varepsilon\tau}(\beta\varepsilon + \varepsilon'\bar{D}^A)\bar{D}_{12}^R - \mu(b\varepsilon + \varepsilon'\bar{D}^A)\bar{D}_2^R \\
\frac{d\bar{D}^A}{d\tau} &= (u^A + \bar{D}^A)\bar{D} - (\varepsilon + \varepsilon'\bar{D}_2^R + \varepsilon'\bar{Y}_1)\bar{D}^A,
\end{aligned}
\tag{S.16}
$$

with $\bar{D} = 1 - \bar{Y}_1 - \bar{D}_2^R - \bar{D}^A$ and $\bar{D}_1^R = \bar{Y}_1 - \bar{D}_{12}^R$. From the first equation in (S.16), it becomes evident that, following a temporary phase during which the externally transfected inputs decrease, $e^{-\varepsilon\tau} \approx 0$, and then $d\bar{Y}_1/d\tau \approx 0$. This implies that, once the transient phase concludes, $\bar{Y}_1$ stabilizes at a constant value and the behavior of the original model can be captured by the reduced 2D ODE model in (S.11).

S.4 Effect of ε and ε' on the deterministic and stochastic behavior of the system

In this section, we analyze the deterministic and stochastic behavior of our system, with a specific focus on understanding the effect of parameters ε (parameter that scales the ratio between the basal erasure rate and the auto-catalysis rate of each modification) and ε' (parameter that scales the ratio between the recruited erasure rate and the auto-catalysis rate of each modification) on the probability distribution of gene expression levels.

We first conduct a deterministic analysis by studying the ODE model associated with the simplified chromatin

modification circuit, i.e., (S.11), and determine how ε and ε' affect the value of $\bar{D}^A$ at the equilibrium for different fractions of CpGs methylated in the gene, i.e., $\bar{Y}_1$ (Fig. S.3A). When ε is large, the system consistently exhibits a unique stable steady state characterized by low $\bar{D}^A$ (Fig. S.3A). The value of $\bar{D}^A$ is smaller for higher $\bar{Y}_1$. As ε decreases, the steady-state value of D^A increases, particularly for low values of $\bar{Y}_1$, where $\bar{D}^A \approx 1$ (Fig. S.3A). Further reduction in ε results in the system becoming bistable for intermediate values of $\bar{Y}_1$ (Fig. S.3A). Changes in ε' do not significantly impact these trends, except for when ε is small. In such cases, smaller values of ε' reduce the range of $\bar{Y}_1$ for bistability and diminish the difference in the values of $\bar{D}^A$ between the two steady states (Fig. S.3A). We next study the impact of ε and ε' on the number of CpGs methylated at equilibrium for various initial levels of DNMT3A, represented by $\bar{W}_1$ as defined in SI Eq. (S.6) (Fig. S.3B). In general, $\bar{Y}_1$ increases with higher $\bar{W}_1$. However, for large values of ε, $\bar{Y}_1$ remains low over an extended range of $\bar{W}_1$ values. As ε decreases, $\bar{Y}_1$ reaches higher values. In the case of small ε, an increase in ε' results in a more ultrasensitive curve.

Overall, this analysis suggests that high fractions of nucleosomes with H3K4me3, and then a high level of gene expression, is achievable only when ε is sufficiently small. In this parameter regime, different ranges of DNMT3A would lead to either high or low gene expression levels only when ε' is sufficiently high (Fig. S.1D). To validate these findings, we use the Stochastic Simulation Algorithm (SSA) [43] to perform a computational study on the 4D+X model, that is, the model that incorporates the full chromatin modification circuit, whose reactions are listed in SI Tables S.1 and S.3 (Fig. S.1E and Fig. S.3C).

For different ranges of the initial amount of DNMT3A transfected ($\bar{W}_1$), a bimodal probability distribution of gene expression levels emerges when ε' is sufficiently large (Fig. S.3C, left-hand side plots). As ε' decreases, the stationary distribution becomes unimodal, with a unique peak that shifts towards lower gene expression levels for sufficiently high ranges of $\bar{W}_1$ (Fig. S.1E and Fig. S.3C, right-hand side plots).

We then conduct a similar computational analysis to assess the impact of ε and ε' on CpGs methylated number and gene expression level across various initial levels of TET1 enzyme ($\bar{T}$) (Fig. S.3D,E). The obtained results mirror those described in the previous analysis (Fig. S.3B,C).

S.5 Refined chromatin modification circuit model to replicate the bisulfite sequencing data from the monoclonal experiment (Fig. 4)

In the study conducted in the previous sections, we observed that, in absence of external stimuli and when α' and μ' are equal to zero, the chromatin modification circuit model, whose associated reactions are listed in Table S.1, predicts a "frozen" level of DNA methylation, i.e., $\dot{\bar{Y}}_1 = 0$ (SI Section S.3). However, this model does not

perfectly align with the experimental results obtained from bisulfite sequencing of the synthetic reporter system in eight different clones, each once associated with a distinct EBFP2 expression level (Fig. 4A, C, D, and E). In fact, for each clone, we do not observe a single value for CpGs methylated across the entire cell population. Instead, we observe a distribution with mean and standard deviation that remain approximately constant throughout the observed time points (a time interval approximately equal to 5 months). Notably, the distribution of methylated CpGs appears more spread for clones associated with an intermediate CpGs methylated levels.

In order to recapitulate this observed behavior, we have to modify the DNA methylation maintenance model. Specifically, considering the species D, $\mathrm{D}_1^{\mathrm{R}}$, and $\mathrm{D}_2^{\mathrm{R}}$ that correspond to unmodified nucleosome, nucleosome with DNA methylation, nucleosome with H3K9me3, we added to

$$\mathrm{D}_1^{\mathrm{R}} \xrightarrow{\delta'} \mathrm{D}, \tag{S.17}$$

in which δ' represents the net passive erasure rate constant obtained from the balance between the dilution and the DNMT1 maintenance process, the following reactions to create a more realistic model:

$$\mathrm{D} \xrightarrow{c_0} \mathrm{D}_1^{\mathrm{R}}, \;\; \mathrm{D} \xrightarrow{c \cdot D_2^R} \mathrm{D}_1^{\mathrm{R}}, \;\; \mathrm{D}_1^{\mathrm{R}} \xrightarrow{\tilde{\delta}' \cdot \left(\frac{1}{1+D_2^R/K}\right)} \mathrm{D}. \tag{S.18}$$

The first reaction represents the possibility that the DNA methylation maintenance enzyme DNMT1 can cause de novo DNA methylation, although at very low rate (low c_0) [46, 47]. The second reaction represents the fact that H3K9me3 helps recruit DNMT1 to the gene and then reinforces DNMT1-mediated maintenance [45]. Finally, we introduce the third reaction since H3K9me3 helps recruit DNMT1 and DNMT1 can, by mistake, establish DNA methylation on previously unmethylated sites.

The ODE for $\mathrm{D}_1^{\mathrm{R}}$ associated with reactions (S.17) and (S.18) can be written as

$$\dot{D}_1^R = (c_0 + cD_2^R)D - (\delta' + \tilde{\delta}'\frac{1}{1+D_2^R/K})D_1^R. \tag{S.19}$$

Then, the average level of DNA methylation remains approximately constant in time (i.e., $\dot{D}_1^R \approx 0$) if all the reaction rate constants are sufficiently small ($c_0, c, \delta', \tilde{\delta}' \ll 1$).

This result is confirmed by the computational study conducted by simulations the reactions of the refined chromatin modification circuit model that incorporates the DNA methylation maintenance model described above, whose reactions are listed in SI Table S.5, using SSA (SI Fig. S.6B). Additionally, this analysis shows that the reactions encapsulating the recruitment mechanism of DNMT1 by H3K9me3 (the second and the third in (S.18))

are crucial for obtaining broader distributions in correspondence of intermediate levels of CpGs methylated (SI Fig. S.6C).

S.6 4D+X model: reactions

S.6.1 Chromatin modification circuit

In this reaction model, it is assumed that the rate constants of the establishment, auto and cross-catalytic, and erasure processes of H3K9me3 (DNA methylation) do not change if the other repressive mark is present on the same modifiable unit. The chromatin modification circuit reaction model can then be written as in SI Table S.1.

$\mathbf{R}_j$	Reaction	Prop.Func.(a_j)	Param.	$\mathbf{R}_j$	Reaction	Prop.Func.(a_j)	Param.
1	$\mathrm{D} \xrightarrow{k^A_{W0}} \mathrm{D^A}$	$a_1 = k^A_{W0} n^D$	k^A_{W0}	21	$\mathrm{D} + \mathrm{D^R_2} \xrightarrow{k_M} \mathrm{D^R_2} + \mathrm{D^R_2}$	$a_{21} = \frac{k_M}{\Omega} n^D n^R_2$	$\frac{k_M}{\Omega}$
2	$\mathrm{D} \xrightarrow{k^A_W} \mathrm{D^A}$	$a_2 = k^A_W n^D$	k^A_W	22	$\mathrm{D} + \mathrm{D^R_{12}} \xrightarrow{k_M} \mathrm{D^R_2} + \mathrm{D^R_{12}}$	$a_{22} = \frac{k_M}{\Omega} n^D n^R_{12}$	$\frac{k_M}{\Omega}$
3	$\mathrm{D^A} \xrightarrow{\bar{k}^A_E} \mathrm{D}$	$a_3 = \bar{k}^A_E n^A$	$\bar{k}^A_E$	23	$\mathrm{D} + \mathrm{D^R_1} \xrightarrow{\bar{k}_M} \mathrm{D^R_2} + \mathrm{D^R_1}$	$a_{23} = \frac{\bar{k}_M}{\Omega} n^D n^R_1$	$\frac{\bar{k}_M}{\Omega}$
4	$\mathrm{D^A} \xrightarrow{\delta} \mathrm{D}$	$a_4 = \delta n^A$	δ	24	$\mathrm{D} + \mathrm{D^R_{12}} \xrightarrow{\bar{k}_M} \mathrm{D^R_2} + \mathrm{D^R_{12}}$	$a_{24} = \frac{\bar{k}_M}{\Omega} n^D n^R_{12}$	$\frac{\bar{k}_M}{\Omega}$
5	$\mathrm{D} + \mathrm{D^A} \xrightarrow{k^A_M} \mathrm{D^A} + \mathrm{D^A}$	$a_5 = \frac{k^A_M}{\Omega} n^D n^A$	$\frac{k^A_M}{\Omega}$	25	$\mathrm{D^R_2} + \mathrm{D^A} \xrightarrow{k^R_E} \mathrm{D} + \mathrm{D^A}$	$a_{25} = \frac{k^R_E}{\Omega} n^R_2 n^A$	$\frac{k^R_E}{\Omega}$
6	$\mathrm{D^A} + \mathrm{D^R_1} \xrightarrow{k^A_E} \mathrm{D} + \mathrm{D^R_1}$	$a_6 = \frac{k^A_E}{\Omega} n^A n^R_1$	$\frac{k^A_E}{\Omega}$	26	$\mathrm{D^R_1} \xrightarrow{k^2_{W0}} \mathrm{D^R_{12}}$	$a_{26} = k^2_{W0} n^R_1$	k^2_{W0}
7	$\mathrm{D^A} + \mathrm{D^R_{12}} \xrightarrow{k^A_E} \mathrm{D} + \mathrm{D^R_{12}}$	$a_7 = \frac{k^A_E}{\Omega} n^A n^R_{12}$	$\frac{k^A_E}{\Omega}$	27	$\mathrm{D^R_{12}} \xrightarrow{\bar{k}^R_E} \mathrm{D^R_1}$	$a_{27} = \bar{k}^R_E n^R_{12}$	$\bar{k}^R_E$
8	$\mathrm{D^A} + \mathrm{D^R_2} \xrightarrow{k^A_E} \mathrm{D} + \mathrm{D^R_2}$	$a_8 = \frac{k^A_E}{\Omega} n^A n^R_2$	$\frac{k^A_E}{\Omega}$	28	$\mathrm{D^R_{12}} \xrightarrow{\delta} \mathrm{D^R_1}$	$a_{28} = \delta n^R_{12}$	δ
9	$\mathrm{D^A} + \mathrm{D^R_{12}} \xrightarrow{k^A_E} \mathrm{D} + \mathrm{D^R_{12}}$	$a_9 = \frac{k^A_E}{\Omega} n^A n^R_{12}$	$\frac{k^A_E}{\Omega}$	29	$\mathrm{D^R_1} + \mathrm{D^R_2} \xrightarrow{k_M} \mathrm{D^R_{12}} + \mathrm{D^R_2}$	$a_{29} = \frac{k_M}{\Omega} n^R_1 n^R_2$	$\frac{k_M}{\Omega}$
10	$\mathrm{D} \xrightarrow{k^1_{W0}} \mathrm{D^R_1}$	$a_{10} = k^1_{W0} n^D$	k^1_{W0}	30	$\mathrm{D^R_1} + \mathrm{D^R_{12}} \xrightarrow{k_M} \mathrm{D^R_{12}} + \mathrm{D^R_{12}}$	$a_{30} = \frac{k_M}{\Omega} n^R_1 n^R_{12}$	$\frac{k_M}{\Omega}$
11	$\mathrm{D} \xrightarrow{k^1_W} \mathrm{D^R_1}$	$a_{11} = k^1_W n^D$	k^1_W	31	$\mathrm{D^R_1} + \mathrm{D^R_1} \xrightarrow{\bar{k}_M} \mathrm{D^R_{12}} + \mathrm{D^R_1}$	$a_{31} = \frac{\bar{k}_M}{\Omega} \frac{n^R_1(n^R_1-1)}{2}$	$\frac{\bar{k}_M}{\Omega}$
12	$\mathrm{D^R_1} \xrightarrow{k'_T} \mathrm{D}$	$a_{12} = k'_T n^R_1$	k'_T	32	$\mathrm{D^R_1} + \mathrm{D^R_{12}} \xrightarrow{\bar{k}_M} \mathrm{D^R_{12}} + \mathrm{D^R_{12}}$	$a_{32} = \frac{\bar{k}_M}{\Omega} n^R_1 n^R_{12}$	$\frac{\bar{k}_M}{\Omega}$
13	$\mathrm{D^R_1} \xrightarrow{\delta'} \mathrm{D}$	$a_{13} = \delta' n^R_1$	δ'	33	$\mathrm{D^R_{12}} + \mathrm{D^A} \xrightarrow{k^R_E} \mathrm{D^R_1} + \mathrm{D^A}$	$a_{33} = \frac{k^R_E}{\Omega} n^R_{12} n^A$	$\frac{k^R_E}{\Omega}$
14	$\mathrm{D} + \mathrm{D^R_2} \xrightarrow{k'_M} \mathrm{D^R_1} + \mathrm{D^R_2}$	$a_{14} = \frac{k'_M}{\Omega} n^D n^R_2$	$\frac{k'_M}{\Omega}$	34	$\mathrm{D^R_2} \xrightarrow{k^1_{W0}} \mathrm{D^R_{12}}$	$a_{34} = k^1_{W0} n^R_2$	k^1_{W0}
15	$\mathrm{D} + \mathrm{D^R_{12}} \xrightarrow{k'_M} \mathrm{D^R_1} + \mathrm{D^R_{12}}$	$a_{15} = \frac{k'_M}{\Omega} n^D n^R_{12}$	$\frac{k'_M}{\Omega}$	35	$\mathrm{D^R_{12}} \xrightarrow{k'_T} \mathrm{D^R_2}$	$a_{35} = k'_T n^R_{12}$	k'_T
16	$\mathrm{D^R_1} + \mathrm{D^A} \xrightarrow{k'^*_T} \mathrm{D} + \mathrm{D^A}$	$a_{16} = \frac{k'^*_T}{\Omega} n^R_1 n^A$	$\frac{k'^*_T}{\Omega}$	36	$\mathrm{D^R_{12}} \xrightarrow{\delta'} \mathrm{D^R_2}$	$a_{36} = \delta' n^R_{12}$	δ'
17	$\mathrm{D} \xrightarrow{k^2_{W0}} \mathrm{D^R_2}$	$a_{17} = k^2_{W0} n^D$	k^2_{W0}	37	$\mathrm{D^R_2} + \mathrm{D^R_2} \xrightarrow{k'_M} \mathrm{D^R_{12}} + \mathrm{D^R_2}$	$a_{37} = \frac{k'_M}{\Omega} \frac{n^R_2(n^R_2-1)}{2}$	$\frac{k'_M}{\Omega}$
18	$\mathrm{D} \xrightarrow{k^2_W} \mathrm{D^R_2}$	$a_{18} = k^2_W n^D$	k^2_W	38	$\mathrm{D^R_2} + \mathrm{D^R_{12}} \xrightarrow{k'_M} \mathrm{D^R_{12}} + \mathrm{D^R_{12}}$	$a_{38} = \frac{k'_M}{\Omega} n^R_2 n^R_{12}$	$\frac{k'_M}{\Omega}$
19	$\mathrm{D^R_2} \xrightarrow{\bar{k}^R_E} \mathrm{D}$	$a_{19} = \bar{k}^R_E n^R_2$	$\bar{k}^R_E$	39	$\mathrm{D^R_{12}} + \mathrm{D^A} \xrightarrow{k'^*_T} \mathrm{D^R_2} + \mathrm{D^A}$	$a_{39} = \frac{k'^*_T}{\Omega} n^R_{12} n^A$	$\frac{k'^*_T}{\Omega}$
20	$\mathrm{D^R_2} \xrightarrow{\delta} \mathrm{D}$	$a_{20} = \delta n^R_2$	δ				

Table S.1: Full chromatin modification circuit model: reactions

When DNA methylation is not included in the system, the only species included in the model are D, $\mathrm{D^A}$, and $\mathrm{D^R_2}$, and the reactions included in the model become only the ones listed in SI Table S.2.

R_j	Reaction	Prop.Func.(a_j)	Param.	R_j	Reaction	Prop.Func.(a_j)	Param.
1	$\mathrm{D} \xrightarrow{k^A_{W0}} \mathrm{D^A}$	$a_1 = k^A_{W0} n^D$	k^A_{W0}	7	$\mathrm{D} \xrightarrow{k^2_{W0}} \mathrm{D^R_2}$	$a_7 = k^2_{W0} n^D$	k^2_{W0}
2	$\mathrm{D} \xrightarrow{k^A_{W}} \mathrm{D^A}$	$a_2 = k^A_{W} n^D$	k^A_{W}	8	$\mathrm{D} \xrightarrow{k^2_{W}} \mathrm{D^R_2}$	$a_8 = k^2_{W} n^D$	k^2_{W}
3	$\mathrm{D^A} \xrightarrow{\bar{k}^A_E} \mathrm{D}$	$a_3 = \bar{k}^A_E n^A$	$\bar{k}^A_E$	9	$\mathrm{D^R_2} \xrightarrow{\bar{k}^R_E} \mathrm{D}$	$a_9 = \bar{k}^R_E n^R_2$	$\bar{k}^R_E$
4	$\mathrm{D^A} \xrightarrow{\delta} \mathrm{D}$	$a_4 = \delta n^A$	δ	10	$\mathrm{D^R_2} \xrightarrow{\delta} \mathrm{D}$	$a_{10} = \delta n^R_2$	δ
5	$\mathrm{D} + \mathrm{D^A} \xrightarrow{k^A_M} \mathrm{D^A} + \mathrm{D^A}$	$a_5 = \frac{k^A_M}{\Omega} n^D n^A$	$\frac{k^A_M}{\Omega}$	11	$\mathrm{D} + \mathrm{D^R_2} \xrightarrow{k_M} \mathrm{D^R_2} + \mathrm{D^R_2}$	$a_{11} = \frac{k_M}{\Omega} n^D n^R_2$	$\frac{k_M}{\Omega}$
6	$\mathrm{D^A} + \mathrm{D^R_2} \xrightarrow{k^A_E} \mathrm{D} + \mathrm{D^R_2}$	$a_6 = \frac{k^A_E}{\Omega} n^A n^R_2$	$\frac{k^A_E}{\Omega}$	12	$\mathrm{D^R_2} + \mathrm{D^A} \xrightarrow{k^R_E} \mathrm{D} + \mathrm{D^A}$	$a_{12} = \frac{k^R_E}{\Omega} n^R_2 n^A$	$\frac{k^R_E}{\Omega}$

Table S.2: Histone modification circuit model: reactions

S.6.2 Transcriptional regulation

By lumping together transcription and translation, we obtain the gene expression model whose reactions are listed in SI Table S.3. Here, m is the mRNA, X is the gene product, γ_m is the decay rate constant of m, γ is the decay rate constant of X, β^A_m, β_m are the transcription rate constants, with $\beta_m < \beta^A_m$, and β is the translation rate constant.

R_j	Reaction	Prop.Func.(a_j)	Param.	R_j	Reaction	Prop.Func.(a_j)	Param.
1	$\mathrm{D^A} \xrightarrow{\beta^A_m} \mathrm{D^A} + \mathrm{m}$	$a_1 = \beta^A_m n^A$	β^A_m	5	$\mathrm{D^R_{12}} \xrightarrow{\beta_m} \mathrm{D^R_{12}} + \mathrm{m}$	$a_5 = \beta_m n^R_{12}$	β_m
2	$\mathrm{D} \xrightarrow{\beta_m} \mathrm{D} + \mathrm{m}$	$a_2 = \beta_m n^D$	β_m	6	$\mathrm{m} \xrightarrow{\beta} \mathrm{m} + \mathrm{X}$	$a_6 = \beta n^m$	β
3	$\mathrm{D^R_1} \xrightarrow{\beta_m} \mathrm{D^R_1} + \mathrm{m}$	$a_3 = \beta_m n^R_1$	β_m	7	$\mathrm{m} \xrightarrow{\gamma_m} \emptyset$	$a_7 = \gamma_m n^m$	γ_m
4	$\mathrm{D^R_2} \xrightarrow{\beta_m} \mathrm{D^R_2} + \mathrm{m}$	$a_4 = \beta_m n^R_2$	β_m	8	$\mathrm{X} \xrightarrow{\gamma} \emptyset$	$a_8 = \gamma n^X$	γ

Table S.3: Gene expression model: reactions

When DNA methylation, and then species $\mathrm{D^R_1}$ and $\mathrm{D^R_{12}}$ are not included in the chromatin modification circuit, then the gene expression model can be simplified as in SI Table S.4.

R_j	Reaction	Prop.Func.(a_j)	Param.	R_j	Reaction	Prop.Func.(a_j)	Param.
1	$\mathrm{D^A} \xrightarrow{\beta^A_m} \mathrm{D^A} + \mathrm{m}$	$a_1 = \beta^A_m n^A$	β^A_m	4	$\mathrm{m} \xrightarrow{\beta} \mathrm{m} + \mathrm{X}$	$a_4 = \beta n^m$	β
2	$\mathrm{D} \xrightarrow{\beta_m} \mathrm{D} + \mathrm{m}$	$a_2 = \beta_m n^D$	β_m	5	$\mathrm{m} \xrightarrow{\gamma_m} \emptyset$	$a_5 = \gamma_m n^m$	γ_m
3	$\mathrm{D^R_2} \xrightarrow{\beta_m} \mathrm{D^R_2} + \mathrm{m}$	$a_3 = \beta_m n^R_2$	β_m	6	$\mathrm{X} \xrightarrow{\gamma} \emptyset$	$a_6 = \gamma n^X$	γ

Table S.4: Gene expression model when we remove species $\mathrm{D^R_1}$, $\mathrm{D^R_{12}}$: reactions

S.6.3 DNA methylation maintenance and refined chromatin modification circuit

To recapitulate the experimental results shown in Fig. 4F, modifications need to be made to the reaction system that models the DNA methylation maintenance process, as explained in SI Section S.5. The reaction model for the chromatin modification circuit can then be revised and expressed as detailed in Table S.5.

R_j	Reaction	Prop.Func.(a_j)	Param.	R_j	Reaction	Prop.Func.(a_j)	Param.
1	$\mathrm{D} \xrightarrow{k^A_{W0}} \mathrm{D^A}$	$a_1 = k^A_{W0} n^D$	k^A_{W0}	21	$\mathrm{D} + \mathrm{D^R_2} \xrightarrow{k_M} \mathrm{D^R_2} + \mathrm{D^R_2}$	$a_{21} = \frac{k_M}{\Omega} n^D n^R_2$	$\frac{k_M}{\Omega}$
2	$\mathrm{D} \xrightarrow{k^A_W} \mathrm{D^A}$	$a_2 = k^A_W n^D$	k^A_W	22	$\mathrm{D} + \mathrm{D^R_{12}} \xrightarrow{k_M} \mathrm{D^R_2} + \mathrm{D^R_{12}}$	$a_{22} = \frac{k_M}{\Omega} n^D n^R_{12}$	$\frac{k_M}{\Omega}$
3	$\mathrm{D^A} \xrightarrow{\bar{k}^A_E} \mathrm{D}$	$a_3 = \bar{k}^A_E n^A$	$\bar{k}^A_E$	23	$\mathrm{D} + \mathrm{D^R_1} \xrightarrow{\bar{k}_M} \mathrm{D^R_2} + \mathrm{D^R_1}$	$a_{23} = \frac{\bar{k}_M}{\Omega} n^D n^R_1$	$\frac{\bar{k}_M}{\Omega}$
4	$\mathrm{D^A} \xrightarrow{\delta} \mathrm{D}$	$a_4 = \delta n^A$	δ	24	$\mathrm{D} + \mathrm{D^R_{12}} \xrightarrow{\bar{k}_M} \mathrm{D^R_2} + \mathrm{D^R_{12}}$	$a_{24} = \frac{\bar{k}_M}{\Omega} n^D n^R_{12}$	$\frac{\bar{k}_M}{\Omega}$
5	$\mathrm{D} + \mathrm{D^A} \xrightarrow{k^A_M} \mathrm{D^A} + \mathrm{D^A}$	$a_5 = \frac{k^A_M}{\Omega} n^D n^A$	$\frac{k^A_M}{\Omega}$	25	$\mathrm{D^R_2} + \mathrm{D^A} \xrightarrow{k^R_E} \mathrm{D} + \mathrm{D^A}$	$a_{25} = \frac{k^R_E}{\Omega} n^R_2 n^A$	$\frac{k^R_E}{\Omega}$
6	$\mathrm{D^A} + \mathrm{D^R_1} \xrightarrow{k^A_E} \mathrm{D} + \mathrm{D^R_1}$	$a_6 = \frac{k^A_E}{\Omega} n^A n^R_1$	$\frac{k^A_E}{\Omega}$	26	$\mathrm{D^R_1} \xrightarrow{k^2_{W0}} \mathrm{D^R_{12}}$	$a_{26} = k^2_{W0} n^R_1$	k^2_{W0}
7	$\mathrm{D^A} + \mathrm{D^R_{12}} \xrightarrow{k^A_E} \mathrm{D} + \mathrm{D^R_{12}}$	$a_7 = \frac{k^A_E}{\Omega} n^A n^R_{12}$	$\frac{k^A_E}{\Omega}$	27	$\mathrm{D^R_{12}} \xrightarrow{\bar{k}^R_E} \mathrm{D^R_1}$	$a_{27} = \bar{k}^R_E n^R_{12}$	$\bar{k}^R_E$
8	$\mathrm{D^A} + \mathrm{D^R_2} \xrightarrow{k^A_E} \mathrm{D} + \mathrm{D^R_2}$	$a_8 = \frac{k^A_E}{\Omega} n^A n^R_2$	$\frac{k^A_E}{\Omega}$	28	$\mathrm{D^R_{12}} \xrightarrow{\delta} \mathrm{D^R_1}$	$a_{28} = \delta n^R_{12}$	δ
9	$\mathrm{D^A} + \mathrm{D^R_{12}} \xrightarrow{k^A_E} \mathrm{D} + \mathrm{D^R_{12}}$	$a_9 = \frac{k^A_E}{\Omega} n^A n^R_{12}$	$\frac{k^A_E}{\Omega}$	29	$\mathrm{D^R_1} + \mathrm{D^R_2} \xrightarrow{k_M} \mathrm{D^R_{12}} + \mathrm{D^R_2}$	$a_{29} = \frac{k_M}{\Omega} n^R_1 n^R_2$	$\frac{k_M}{\Omega}$
10	$\mathrm{D} \xrightarrow{k^1_{W0}} \mathrm{D^R_1}$	$a_{10} = k^1_{W0} n^D$	k^1_{W0}	30	$\mathrm{D^R_1} + \mathrm{D^R_{12}} \xrightarrow{k_M} \mathrm{D^R_{12}} + \mathrm{D^R_{12}}$	$a_{30} = \frac{k_M}{\Omega} n^R_1 n^R_{12}$	$\frac{k_M}{\Omega}$
11	$\mathrm{D} \xrightarrow{k^1_W} \mathrm{D^R_1}$	$a_{11} = k^1_W n^D$	k^1_W	31	$\mathrm{D^R_1} + \mathrm{D^R_1} \xrightarrow{\bar{k}_M} \mathrm{D^R_{12}} + \mathrm{D^R_1}$	$a_{31} = \frac{\bar{k}_M}{\Omega} \frac{n^R_1(n^R_1-1)}{2}$	$\frac{\bar{k}_M}{\Omega}$
12	$\mathrm{D^R_1} \xrightarrow{k'_T} \mathrm{D}$	$a_{12} = k'_T n^R_1$	k'_T	32	$\mathrm{D^R_1} + \mathrm{D^R_{12}} \xrightarrow{\bar{k}_M} \mathrm{D^R_{12}} + \mathrm{D^R_{12}}$	$a_{32} = \frac{\bar{k}_M}{\Omega} n^R_1 n^R_{12}$	$\frac{\bar{k}_M}{\Omega}$
13	$\mathrm{D^R_1} \xrightarrow{\delta'} \mathrm{D}$	$a_{13} = \delta' n^R_1$	δ'	33	$\mathrm{D^R_{12}} + \mathrm{D^A} \xrightarrow{k^R_E} \mathrm{D^R_1} + \mathrm{D^A}$	$a_{33} = \frac{k^R_E}{\Omega} n^R_{12} n^A$	$\frac{k^R_E}{\Omega}$
14	$\mathrm{D^R_1} \xrightarrow{\frac{\tilde{\delta}'}{1+(D^R_2+D^R_{12})/K}} \mathrm{D}$	$a_{14} = \frac{\tilde{\delta}'}{1+(D^R_2+D^R_{12})/K} n^R_1$	$\tilde{\delta}'$	34	$\mathrm{D^R_2} \xrightarrow{k^1_{W0}} \mathrm{D^R_{12}}$	$a_{34} = k^1_{W0} n^R_2$	k^1_{W0}
15	$\mathrm{D} \xrightarrow{c_0} \mathrm{D^R_1}$	$a_{15} = c_0 n^D$	c_0	35	$\mathrm{D^R_{12}} \xrightarrow{k'_T} \mathrm{D^R_2}$	$a_{35} = k'_T n^R_{12}$	k'_T
16	$\mathrm{D} + \mathrm{D^R_2} \xrightarrow{c} \mathrm{D^R_1} + \mathrm{D^R_2}$	$a_{16} = \frac{c}{\Omega} n^D n^R_2$	$\frac{c}{\Omega}$	36	$\mathrm{D^R_{12}} \xrightarrow{\delta'} \mathrm{D^R_2}$	$a_{36} = \delta' n^R_{12}$	δ'
17	$\mathrm{D} + \mathrm{D^R_{12}} \xrightarrow{c} \mathrm{D^R_1} + \mathrm{D^R_{12}}$	$a_{17} = \frac{c}{\Omega} n^D n^R_{12}$	$\frac{c}{\Omega}$	37	$\mathrm{D^R_{12}} \xrightarrow{\frac{\tilde{\delta}'}{1+(D^R_2+D^R_{12})/K}} \mathrm{D^R_2}$	$a_{14} = \frac{\tilde{\delta}'}{1+(D^R_2+D^R_{12})/K} n^R_{12}$	$\tilde{\delta}'$
18	$\mathrm{D} + \mathrm{D^R_2} \xrightarrow{k'_M} \mathrm{D^R_1} + \mathrm{D^R_2}$	$a_{18} = \frac{k'_M}{\Omega} n^D n^R_2$	$\frac{k'_M}{\Omega}$	38	$\mathrm{D^R_2} \xrightarrow{c_0} \mathrm{D^R_{12}}$	$a_{38} = c_0 n^R_2$	c_0
19	$\mathrm{D} + \mathrm{D^R_{12}} \xrightarrow{k'_M} \mathrm{D^R_1} + \mathrm{D^R_{12}}$	$a_{19} = \frac{k'_M}{\Omega} n^D n^R_{12}$	$\frac{k'_M}{\Omega}$	39	$\mathrm{D^R_2} + \mathrm{D^R_2} \xrightarrow{c} \mathrm{D^R_{12}} + \mathrm{D^R_2}$	$a_{39} = \frac{c}{\Omega} \frac{n^R_2(n^R_2-1)}{2}$	$\frac{c}{\Omega}$
20	$\mathrm{D^R_1} + \mathrm{D^A} \xrightarrow{k'^*_T} \mathrm{D} + \mathrm{D^A}$	$a_{20} = \frac{k'^*_T}{\Omega} n^R_1 n^A$	$\frac{k'^*_T}{\Omega}$	40	$\mathrm{D^R_2} + \mathrm{D^R_{12}} \xrightarrow{c} \mathrm{D^R_{12}} + \mathrm{D^R_{12}}$	$a_{40} = \frac{c}{\Omega} n^R_2 n^R_{12}$	$\frac{c}{\Omega}$
21	$\mathrm{D} \xrightarrow{k^2_{W0}} \mathrm{D^R_2}$	$a_{21} = k^2_{W0} n^D$	k^2_{W0}	41	$\mathrm{D^R_2} + \mathrm{D^R_2} \xrightarrow{k'_M} \mathrm{D^R_{12}} + \mathrm{D^R_2}$	$a_{41} = \frac{k'_M}{\Omega} \frac{n^R_2(n^R_2-1)}{2}$	$\frac{k'_M}{\Omega}$
22	$\mathrm{D} \xrightarrow{k^2_W} \mathrm{D^R_2}$	$a_{22} = k^2_W n^D$	k^2_W	42	$\mathrm{D^R_2} + \mathrm{D^R_{12}} \xrightarrow{k'_M} \mathrm{D^R_{12}} + \mathrm{D^R_{12}}$	$a_{42} = \frac{k'_M}{\Omega} n^R_2 n^R_{12}$	$\frac{k'_M}{\Omega}$
23	$\mathrm{D^R_2} \xrightarrow{\bar{k}^R_E} \mathrm{D}$	$a_{23} = \bar{k}^R_E n^R_2$	$\bar{k}^R_E$	43	$\mathrm{D^R_{12}} + \mathrm{D^A} \xrightarrow{k'^*_T} \mathrm{D^R_2} + \mathrm{D^A}$	$a_{43} = \frac{k'^*_T}{\Omega} n^R_{12} n^A$	$\frac{k'^*_T}{\Omega}$
24	$\mathrm{D^R_2} \xrightarrow{\delta} \mathrm{D}$	$a_{24} = \delta n^R_2$	δ				

Table S.5: Full chromatin modification circuit model incorporating the refined DNA methylation maintenance model described in SI Section S.5: reactions

S.7 Modification to the chromatin modification circuit model to include more than one CpG per nucleosome

In the original model of chromatin modification circuit, it is assumed that the basic unit is a nucleosome with DNA wrapped around can have only one modifiable CpG [23]. There are cases in which this assumption is not verified. However, it is possible to show that this assumption does not affect the qualitative results related to the effect of the parameters α' (normalized rate of DNA methylation establishment through repressive histone modifications) and μ' (ratio between the DNA methylation erasure rate and the activating histone modification erasure rate) on the probability distribution of gene expression levels.

To this end, let us assume that basic unit of the model, D, is the nucleosome with DNA wrapped around it with two modifiable CpGs. The conclusion obtaine din this section would not change if we consider the DNA

wrapped around the nucleosome having $n \in \mathbb{Z}^+$ modifiable CpGs. The basic unit of the model can then be modified with H3K4me3, $\mathrm{D^A}$, one DNA methylation, $\mathrm{D_1^R}$, H3K9me3, $\mathrm{D_2^R}$, one DNA methylation and H3K9me3, $\mathrm{D_{12}^R}$, two DNA methylations, $\mathrm{D_{11}^R}$, and two DNA methylation and H3K9me3, $\mathrm{D_{112}^R}$. Now, defining the number of $\mathrm{D^A}, \mathrm{D_1^R}, \mathrm{D_2^R}, \mathrm{D_{12}^R}, \mathrm{D_{11}^R}, \mathrm{D_{112}^R}, \mathrm{D}$ as n^A, n_1^R, n_2^R, n_{12}^R, $n_{D_{11}^R}$, n_{112}^R and n^D, let us derive the related ordinary differential equation (ODE) model in terms of the fractions $\bar{D}^A = n^A/\mathrm{D_{tot}}$, $\bar{D}_1^R = n_{D_1^R}/\mathrm{D_{tot}}$, $\bar{D}_2^R = n_{D_2^R}/\mathrm{D_{tot}}$, $\bar{D}_{12}^R = n_{D_{12}^R}/\mathrm{D_{tot}}$, $\bar{D}_{11}^R = n_{D_{11}^R}/\mathrm{D_{tot}}$, $\bar{D}_{112}^R = n_{D_{112}^R}/\mathrm{D_{tot}}$ and $\bar{D} = n_D/\mathrm{D_{tot}}$, with $\mathrm{D_{tot}}$ the total number of nucleosomes on a gene of interest. This can be done by assuming that $\mathrm{D_{tot}}$ is sufficiently large so that $\bar{D}^A$, $\bar{D}_1^R$, $\bar{D}_2^R$, $\bar{D}_{12}^R$ and $\bar{D}$ can be treated as real number. Now, considering the dimensionless parameters and normalized inputs introduced Section S.1 and the normalized time $\tau = tk_M^A D_{tot}$, the ODEs associated with the chromatin modification circuit are

$$
\begin{aligned}
\frac{d\bar{D}_1^R}{d\tau} &= (u_{10}^R + u_1^R + \alpha'(\bar{D}_2^R + \bar{D}_{12}^R + \bar{D}_{112}^R))\bar{D} + \mu(b\varepsilon + \varepsilon'\bar{D}^A)\bar{D}_{12}^R + \mu'(\beta\varepsilon + \varepsilon'\bar{D}^A)\bar{D}_{11}^R \\
&\quad - (u_{20}^R + \alpha(\bar{D}_2^R + \bar{D}_{12}^R + \bar{D}_{112}^R) + \bar{\alpha}(\bar{D}_1^R + \bar{D}_{12}^R + 2\bar{D}_{11}^R + 2\bar{D}_{112}^R))\bar{D}_1^R \\
&\quad - (u_{10}^R + u_1^R + \alpha'(\bar{D}_2^R + \bar{D}_{12}^R + \bar{D}_{112}^R) + \mu'(\beta\varepsilon + \varepsilon'\bar{D}^A))\bar{D}_1^R \\
\frac{d\bar{D}_{12}^R}{d\tau} &= (u_{10}^R + \alpha'(\bar{D}_2^R + \bar{D}_{12}^R + \bar{D}_{112}^R))\bar{D}_2^R \\
&\quad + (u_{20}^R + \alpha(\bar{D}_2^R + \bar{D}_{12}^R + \bar{D}_{112}^R) + \bar{\alpha}(\bar{D}_1^R + \bar{D}_{12}^R + 2\bar{D}_{11}^R + 2\bar{D}_{112}^R))\bar{D}_1^R + \mu'(\beta\varepsilon + \varepsilon'\bar{D}^A)\bar{D}_{112}^R \\
&\quad - (\mu'(\beta\varepsilon + \varepsilon'\bar{D}^A) + \mu(b\varepsilon + \varepsilon'\bar{D}^A) + u_{10}^R + u_1^R + \alpha'(\bar{D}_2^R + \bar{D}_{12}^R + \bar{D}_{112}^R))\bar{D}_{12}^R \\
\frac{d\bar{D}_{11}^R}{d\tau} &= (u_{10}^R + u_1^R + \alpha'(\bar{D}_2^R + \bar{D}_{12}^R + \bar{D}_{112}^R))\bar{D}_1^R + \mu(b\varepsilon + \varepsilon'\bar{D}^A)\bar{D}_{112}^R \\
&\quad - (u_{20}^R + \alpha(\bar{D}_2^R + \bar{D}_{12}^R + \bar{D}_{112}^R) + \bar{\alpha}(\bar{D}_1^R + \bar{D}_{12}^R + 2\bar{D}_{11}^R + 2\bar{D}_{112}^R) + \mu'(\beta\varepsilon + \varepsilon'\bar{D}^A))\bar{D}_1^R \\
\frac{d\bar{D}_{112}^R}{d\tau} &= (u_{20}^R + \alpha(\bar{D}_2^R + \bar{D}_{12}^R + \bar{D}_{112}^R) + \bar{\alpha}(\bar{D}_1^R + \bar{D}_{12}^R + 2\bar{D}_{11}^R + 2\bar{D}_{112}^R))\bar{D}_{11}^R \\
&\quad + (u_{10}^R + \alpha'(\bar{D}_2^R + \bar{D}_{12}^R + \bar{D}_{112}^R))\bar{D}_{12}^R \\
&\quad - (\mu'(\beta\varepsilon + \varepsilon'\bar{D}^A) + \mu(b\varepsilon + \varepsilon'\bar{D}^A))\bar{D}_{112}^R \\
\frac{d\bar{D}_2^R}{d\tau} &= (u_{20}^R + u_2^R + \alpha(\bar{D}_2^R + \bar{D}_{12}^R + \bar{D}_{112}^R) + \bar{\alpha}(\bar{D}_1^R + \bar{D}_{12}^R + 2\bar{D}_{11}^R + 2\bar{D}_{112}^R))\bar{D} + \mu'(\beta\varepsilon + \varepsilon'\bar{D}^A)\bar{D}_{12}^R \\
&\quad - (u_{10}^R + \alpha'(\bar{D}_2^R + \bar{D}_{12}^R + \bar{D}_{112}^R) + \mu(b\varepsilon + \varepsilon'\bar{D}^A))\bar{D}_2^R \\
\frac{d\bar{D}^A}{d\tau} &= (u_0^A + u^A + \bar{D}^A)\bar{D} - (\varepsilon + \varepsilon'(\bar{D}_2^R + \bar{D}_{12}^R + \bar{D}_{112}^R) + \varepsilon'(\bar{D}_1^R + \bar{D}_{12}^R + 2\bar{D}_{11}^R + 2\bar{D}_{112}^R))\bar{D}^A,
\end{aligned}
\tag{S.20}
$$

with $\bar{D} = 1 - \bar{D}_1^R - \bar{D}_{12}^R - \bar{D}_{11}^R - \bar{D}_{112}^R - \bar{D}_2^R - \bar{D}^A$.

As we did for the original ODE system (S.3), let us merge the rates linked to the enhancement of H3K9me3 establishment by $\bar{D}_{12}^R$, $\bar{D}_{11}^R$, and $\bar{D}_{112}^R$ into a single rate. We will assume that this rate is identical to the one

associated with the enhancement of H3K9me3 establishment by $\bar{D}_1^R$. Similarly, let us merge the rates linked to the recruited erasure of H3K4me3 by $\bar{D}_{12}^R$, $\bar{D}_{11}^R$, and $\bar{D}_{112}^R$ into a single rate and assume that this rate is identical to the one associated with the recruited erasure of H3K4me3 by $\bar{D}_1^R$. The ODE system (S.20) can then be rewritten as

$$\begin{aligned}
\frac{d\bar{D}_1^R}{d\tau} &= (u_{10}^R + u_1^R + \alpha'(\bar{D}_2^R + \bar{D}_{12}^R + \bar{D}_{112}^R))\bar{D} + \mu(b\varepsilon + \varepsilon'\bar{D}^A)\bar{D}_{12}^R + \mu'(\beta\varepsilon + \varepsilon'\bar{D}^A)\bar{D}_{11}^R \\
&\quad - (u_{20}^R + \alpha\bar{D}_2^R + \bar{\alpha}(\bar{D}_1^R + \bar{D}_{12}^R + \bar{D}_{11}^R + \bar{D}_{112}^R))\bar{D}_1^R \\
&\quad - (u_{10}^R + u_1^R + \alpha'(\bar{D}_2^R + \bar{D}_{12}^R + \bar{D}_{112}^R) + \mu'(\beta\varepsilon + \varepsilon'\bar{D}^A))\bar{D}_1^R \\
\frac{d\bar{D}_{12}^R}{d\tau} &= (u_{10}^R + \alpha'(\bar{D}_2^R + \bar{D}_{12}^R + \bar{D}_{112}^R))\bar{D}_2^R \\
&\quad + (u_{20}^R + \alpha\bar{D}_2^R + \bar{\alpha}(\bar{D}_1^R + \bar{D}_{12}^R + \bar{D}_{11}^R + \bar{D}_{112}^R))\bar{D}_1^R + \mu'(\beta\varepsilon + \varepsilon'\bar{D}^A)\bar{D}_{112}^R \\
&\quad - (\mu'(\beta\varepsilon + \varepsilon'\bar{D}^A) + \mu(b\varepsilon + \varepsilon'\bar{D}^A) + u_{10}^R + u_1^R + \alpha'(\bar{D}_2^R + \bar{D}_{12}^R + \bar{D}_{112}^R))\bar{D}_{12}^R \\
\frac{d\bar{D}_{11}^R}{d\tau} &= (u_{10}^R + u_1^R + \alpha'(\bar{D}_2^R + \bar{D}_{12}^R + \bar{D}_{112}^R))\bar{D}_1^R + \mu(b\varepsilon + \varepsilon'\bar{D}^A)\bar{D}_{112}^R \\
&\quad - (u_{20}^R + \alpha\bar{D}_2^R + \bar{\alpha}(\bar{D}_1^R + \bar{D}_{12}^R + \bar{D}_{11}^R + \bar{D}_{112}^R) + \mu'(\beta\varepsilon + \varepsilon'\bar{D}^A))\bar{D}_1^R \\
\frac{d\bar{D}_{112}^R}{d\tau} &= (u_{20}^R + \alpha\bar{D}_2^R + \bar{\alpha}(\bar{D}_1^R + \bar{D}_{12}^R + \bar{D}_{11}^R + \bar{D}_{112}^R))\bar{D}_{11}^R \\
&\quad + (u_{10}^R + \alpha'(\bar{D}_2^R + \bar{D}_{12}^R + \bar{D}_{112}^R))\bar{D}_{12}^R - (\mu'(\beta\varepsilon + \varepsilon'\bar{D}^A) + \mu(b\varepsilon + \varepsilon'\bar{D}^A))\bar{D}_{112}^R \\
\frac{d\bar{D}_2^R}{d\tau} &= (u_{20}^R + u_2^R + \alpha\bar{D}_2^R + \bar{\alpha}(\bar{D}_1^R + \bar{D}_{12}^R + \bar{D}_{11}^R + \bar{D}_{112}^R))\bar{D} + \mu'(\beta\varepsilon + \varepsilon'\bar{D}^A)\bar{D}_{12}^R \\
&\quad - (u_{10}^R + \alpha'(\bar{D}_2^R + \bar{D}_{12}^R + \bar{D}_{112}^R) + \mu(b\varepsilon + \varepsilon'\bar{D}^A))\bar{D}_2^R \\
\frac{d\bar{D}^A}{d\tau} &= (u_0^A + u^A + \bar{D}^A)\bar{D} - (\varepsilon + \varepsilon'(\bar{D}_2^R + \bar{D}_1^R + \bar{D}_{12}^R + \bar{D}_{11}^R + \bar{D}_{112}^R))\bar{D}^A,
\end{aligned} \tag{S.21}$$

Now, let us rewrite system (S.21) by assuming negligible basal *de novo* establishment ($u_{10}^R = u_{20}^R = u_0^A = 0$) and introducing the variable $\bar{Y}_1 = \bar{D}_1^R + \bar{D}_{12}^R$, that corresponds to the fraction of nucleosomes with one methylated CpG, and the variable $\bar{Y}_{1tot} = \bar{D}_1^R + \bar{D}_{12}^R + \bar{D}_{11}^R + \bar{D}_{112}^R$, that corresponds to the fraction of nucleosomes with at least one methylated CpG. We then obtain

$$\begin{aligned}
\frac{d\bar{D}_1^R}{d\tau} &= (u_1^R + \alpha'(\bar{D}_2^R + \bar{Y}_{1tot} - \bar{D}_1^R - \bar{D}_{11}^R))\bar{D} + \mu(b\varepsilon + \varepsilon'\bar{D}^A)(\bar{Y}_1 - \bar{D}_1^R) + \mu'(\beta\varepsilon + \varepsilon'\bar{D}^A)\bar{D}_{11}^R \\
&\quad - (\alpha\bar{D}_2^R + \bar{\alpha}\bar{Y}_{tot} + u_1^R + \alpha'(\bar{D}_2^R + \bar{Y}_{1tot} - \bar{D}_1^R - \bar{D}_{11}^R) + \mu'(\beta\varepsilon + \varepsilon'\bar{D}^A))\bar{D}_1^R \\
\frac{d\bar{D}_{11}^R}{d\tau} &= (u_1^R + \alpha'(\bar{D}_2^R + \bar{Y}_{1tot} - \bar{D}_1^R - \bar{D}_{11}^R))\bar{D}_1^R + \mu(b\varepsilon + \varepsilon'\bar{D}^A)(\bar{Y}_{1tot} - \bar{Y}_1 - \bar{D}_{11}^R)) \\
&\quad - (\alpha\bar{D}_2^R + \bar{\alpha}\bar{Y}_{1tot} + \mu'(\beta\varepsilon + \varepsilon'\bar{D}^A))\bar{D}_1^R
\end{aligned} \tag{S.22}$$

$$
\begin{aligned}
\frac{d\bar{Y}_1}{d\tau} &= u_1^R(\bar{D} - \bar{D}_1^R) + (\alpha'(\bar{D}_2^R + \bar{Y}_{1tot} - \bar{D}_1^R - \bar{D}_{11}^R))(\bar{D} + \bar{D}_2^R) \\
&\quad + \mu'(\beta\varepsilon + \varepsilon'\bar{D}^A)(\bar{Y}_{1tot} - \bar{Y}_1) - (\mu'(\beta\varepsilon + \varepsilon'\bar{D}^A) + \alpha'(\bar{D}_2^R + \bar{Y}_{1tot} - \bar{D}_1^R - \bar{D}_{11}^R))\bar{Y}_1 \\
\frac{d\bar{Y}_{1tot}}{d\tau} &= u_1^R\bar{D} + (\alpha'(\bar{D}_2^R + \bar{Y}_{1tot} - \bar{D}_1^R - \bar{D}_{11}^R))(\bar{D} + \bar{D}_2^R) - \mu'(\beta\varepsilon + \varepsilon'\bar{D}^A))\bar{Y}_1 \\
\frac{d\bar{D}_2^R}{d\tau} &= (u_2^R + \alpha\bar{D}_2^R + \bar{\alpha}\bar{Y}_{1tot})\bar{D} + \mu'(\beta\varepsilon + \varepsilon'\bar{D}^A)\bar{D}_{12}^R - (\alpha'(\bar{D}_2^R + \bar{D}_{12}^R + \bar{D}_{112}^R) + \mu(b\varepsilon + \varepsilon'\bar{D}^A))\bar{D}_2^R \\
\frac{d\bar{D}^A}{d\tau} &= (u^A + \bar{D}^A)\bar{D} - (\varepsilon + \varepsilon'(\bar{D}_2^R + \bar{Y}_{1tot}))\bar{D}^A,
\end{aligned}
$$

with $\bar{D} = 1 - \bar{Y}_{1tot} - \bar{D}_2^R - \bar{D}^A$. As we did for the ODE system associated with our original chromatin modification circuit in Section S.1, we can further simplify our model by assuming that the enhancement of DNA methylation establishment by H3K9me3 is negligible, i.e., $\alpha' = 0$. The ODE system (S.22) can then be rewritten as

$$
\begin{aligned}
\frac{d\bar{D}_1^R}{d\tau} &= (u_1^R)\bar{D} + \mu(b\varepsilon + \varepsilon'\bar{D}^A)(\bar{Y}_1 - \bar{D}_1^R) + \mu'(\beta\varepsilon + \varepsilon'\bar{D}^A)\bar{D}_{11}^R - (\alpha\bar{D}_2^R + \bar{\alpha}\bar{Y}_{tot} + u_1^R + \mu'(\beta\varepsilon + \varepsilon'\bar{D}^A))\bar{D}_1^R \\
\frac{d\bar{D}_{11}^R}{d\tau} &= (u_1^R)\bar{D}_1^R + \mu(b\varepsilon + \varepsilon'\bar{D}^A)(\bar{Y}_{1tot} - \bar{Y}_1 - \bar{D}_{11}^R)) - (\alpha\bar{D}_2^R + \bar{\alpha}\bar{Y}_{1tot} + \mu'(\beta\varepsilon + \varepsilon'\bar{D}^A))\bar{D}_1^R \\
\frac{d\bar{Y}_1}{d\tau} &= u_1^R(\bar{D} - \bar{D}_1^R) + \mu'(\beta\varepsilon + \varepsilon'\bar{D}^A)(\bar{Y}_{1tot} - \bar{Y}_1) - \mu'(\beta\varepsilon + \varepsilon'\bar{D}^A)\bar{Y}_1 \\
\frac{d\bar{Y}_{1tot}}{d\tau} &= u_1^R\bar{D} - \mu'(\beta\varepsilon + \varepsilon'\bar{D}^A))\bar{Y}_1 \\
\frac{d\bar{D}_2^R}{d\tau} &= (u_2^R + \alpha\bar{D}_2^R + \bar{\alpha}\bar{Y}_{1tot})\bar{D} + \mu'(\beta\varepsilon + \varepsilon'\bar{D}^A)\bar{D}_{12}^R - \mu(b\varepsilon + \varepsilon'\bar{D}^A)\bar{D}_2^R \\
\frac{d\bar{D}^A}{d\tau} &= (u^A + \bar{D}^A)\bar{D} - (\varepsilon + \varepsilon'(\bar{D}_2^R + \bar{Y}_{1tot}))\bar{D}^A,
\end{aligned}
\tag{S.23}
$$

with $\bar{D} = 1 - \bar{Y}_{1tot} - \bar{D}_2^R - \bar{D}^A$. Now, introducing in (S.23) the expressions for u_2^R, u_1^R, and μ' derived in Section

S.1.1 (Expressions (S.5), (S.7), and (S.9)), we obtain:

$$
\begin{aligned}
\frac{d\bar{D}_1^R}{d\tau} &= \tilde{u}_1^R \bar{W}_1 e^{-\varepsilon\tau}\bar{D} + \mu(b\varepsilon + \varepsilon'\bar{D}^A)(\bar{Y}_1 - \bar{D}_1^R) + (\mu_1' + \tilde{\mu}'\frac{\frac{DOX}{K_1}}{1+\frac{DOX}{K_1}}\bar{T}e^{-\varepsilon\tau})(\beta\varepsilon + \varepsilon'\bar{D}^A)\bar{D}_{11}^R \\
&\quad - (\alpha\bar{D}_2^R + \bar{\alpha}\bar{Y}_{tot} + \tilde{u}_1^R\bar{W}_1 e^{-\varepsilon\tau} + (\mu_1' + \tilde{\mu}'\frac{\frac{DOX}{K_1}}{1+\frac{DOX}{K_1}}\bar{T}e^{-\varepsilon\tau})(\beta\varepsilon + \varepsilon'\bar{D}^A))\bar{D}_1^R \\
\frac{d\bar{D}_{11}^R}{d\tau} &= \tilde{u}_1^R \bar{W}_1 e^{-\varepsilon\tau}\bar{D}_1^R + \mu(b\varepsilon + \varepsilon'\bar{D}^A)(\bar{Y}_{1tot} - \bar{Y}_1 - \bar{D}_{11}^R)) \\
&\quad - (\alpha\bar{D}_2^R + \bar{\alpha}\bar{Y}_{1tot} + (\mu_1' + \tilde{\mu}'\frac{\frac{DOX}{K_1}}{1+\frac{DOX}{K_1}}\bar{T}e^{-\varepsilon\tau})(\beta\varepsilon + \varepsilon'\bar{D}^A))\bar{D}_1^R \qquad \text{(S.24)} \\
\frac{d\bar{Y}_1}{d\tau} &= \tilde{u}_1^R \bar{W}_1 e^{-\varepsilon\tau}(\bar{D} - \bar{D}_1^R) + (\mu_1' + \tilde{\mu}'\frac{\frac{DOX}{K_1}}{1+\frac{DOX}{K_1}}\bar{T}e^{-\varepsilon\tau})(\beta\varepsilon + \varepsilon'\bar{D}^A)(\bar{Y}_{1tot} - \bar{Y}_1) \\
&\quad - (\mu_1' + \tilde{\mu}'\frac{\frac{DOX}{K_1}}{1+\frac{DOX}{K_1}}\bar{T}e^{-\varepsilon\tau})(\beta\varepsilon + \varepsilon'\bar{D}^A)\bar{Y}_1 \\
\frac{d\bar{Y}_{1tot}}{d\tau} &= \tilde{u}_1^R \bar{W}_1 e^{-\varepsilon\tau}\bar{D} - (\mu_1' + \tilde{\mu}'\frac{\frac{DOX}{K_1}}{1+\frac{DOX}{K_1}}\bar{T}e^{-\varepsilon\tau})(\beta\varepsilon + \varepsilon'\bar{D}^A))\bar{Y}_1 \\
\frac{d\bar{D}_2^R}{d\tau} &= (\tilde{u}_2^R\frac{1}{1+\frac{DAPG}{K_2}}\bar{W}_2 e^{-\varepsilon\tau} + \alpha\bar{D}_2^R + \bar{\alpha}\bar{Y}_{1tot})\bar{D} + \mu'(\beta\varepsilon + \varepsilon'\bar{D}^A)\bar{D}_{12}^R - \mu(b\varepsilon + \varepsilon'\bar{D}^A)\bar{D}_2^R \\
\frac{d\bar{D}^A}{d\tau} &= (u^A + \bar{D}^A)\bar{D} - (\varepsilon + \varepsilon'(\bar{D}_2^R + \bar{Y}_{1tot}))\bar{D}^A,
\end{aligned}
$$

with $\bar{D} = 1 - \bar{Y}_{1tot} - \bar{D}_2^R - \bar{D}^A$. Furthermore, if we consider the parameter regime in which the erasure rate of DNA methylation, without transfection of eTetR-TET1, is sufficiently low compared to histone modification

dynamics,i.e., $\mu_1' \to 0$, the system (S.24) can then be rewritten as follows:

$$
\begin{aligned}
\frac{d\bar{D}_1^R}{d\tau} &= \tilde{u}_1^R \bar{W}_1 e^{-\varepsilon\tau}\bar{D} + \mu(b\varepsilon + \varepsilon'\bar{D}^A)(\bar{Y}_1 - \bar{D}_1^R) + \tilde{\mu}'\frac{\frac{DOX}{K_1}}{1+\frac{DOX}{K_1}}\bar{T}e^{-\varepsilon\tau}(\beta\varepsilon + \varepsilon'\bar{D}^A)\bar{D}_{11}^R \\
&\quad - (\alpha\bar{D}_2^R + \bar{\alpha}\bar{Y}_{tot} + \tilde{u}_1^R\bar{W}_1 e^{-\varepsilon\tau} + \tilde{\mu}'\frac{\frac{DOX}{K_1}}{1+\frac{DOX}{K_1}}\bar{T}e^{-\varepsilon\tau}(\beta\varepsilon + \varepsilon'\bar{D}^A))\bar{D}_1^R \\
\frac{d\bar{D}_{11}^R}{d\tau} &= \tilde{u}_1^R \bar{W}_1 e^{-\varepsilon\tau}\bar{D}_1^R + \mu(b\varepsilon + \varepsilon'\bar{D}^A)(\bar{Y}_{1tot} - \bar{Y}_1 - \bar{D}_{11}^R)) \\
&\quad - (\alpha\bar{D}_2^R + \bar{\alpha}\bar{Y}_{1tot} + \tilde{\mu}'\frac{\frac{DOX}{K_1}}{1+\frac{DOX}{K_1}}\bar{T}e^{-\varepsilon\tau}(\beta\varepsilon + \varepsilon'\bar{D}^A))\bar{D}_1^R \\
\frac{d\bar{Y}_1}{d\tau} &= \tilde{u}_1^R \bar{W}_1 e^{-\varepsilon\tau}(\bar{D} - \bar{D}_1^R) + \tilde{\mu}'\frac{\frac{DOX}{K_1}}{1+\frac{DOX}{K_1}}\bar{T}e^{-\varepsilon\tau}(\beta\varepsilon + \varepsilon'\bar{D}^A)(\bar{Y}_{1tot} - \bar{Y}_1) \\
&\quad - \tilde{\mu}'\frac{\frac{DOX}{K_1}}{1+\frac{DOX}{K_1}}\bar{T}e^{-\varepsilon\tau}(\beta\varepsilon + \varepsilon'\bar{D}^A)\bar{Y}_1 \\
\frac{d\bar{Y}_{1tot}}{d\tau} &= \tilde{u}_1^R \bar{W}_1 e^{-\varepsilon\tau}\bar{D} - \tilde{\mu}'\frac{\frac{DOX}{K_1}}{1+\frac{DOX}{K_1}}\bar{T}e^{-\varepsilon\tau}(\beta\varepsilon + \varepsilon'\bar{D}^A))\bar{Y}_1 \\
\frac{d\bar{D}_2^R}{d\tau} &= (\tilde{u}_2^R\frac{1}{1+\frac{DAPG}{K_2}}\bar{W}_2 e^{-\varepsilon\tau} + \alpha\bar{D}_2^R + \bar{\alpha}\bar{Y}_{1tot})\bar{D} + \mu'(\beta\varepsilon + \varepsilon'\bar{D}^A)\bar{D}_{12}^R - \mu(b\varepsilon + \varepsilon'\bar{D}^A)\bar{D}_2^R \\
\frac{d\bar{D}^A}{d\tau} &= (u^A + \bar{D}^A)\bar{D} - (\varepsilon + \varepsilon'(\bar{D}_2^R + \bar{Y}_{1tot}))\bar{D}^A,
\end{aligned}
\tag{S.25}
$$

with $\bar{D} = 1 - \bar{Y}_1 - \bar{D}_2^R - \bar{D}^A$. From the fourth equation in (S.25), it is possible to notice that, following a temporary phase during which the externally transfected inputs decrease, $e^{-\varepsilon\tau} \approx 0$, and then $d\bar{Y}_{1tot}/d\tau \approx 0$. This implies that, once the transient phase concludes, $\bar{Y}_{1tot}$ stabilizes at a constant value and the behavior of the original model can be captured by a reduced 2D model described by the subsequent ODEs:

$$
\frac{d\bar{D}_2^R}{d\tau} = (\alpha\bar{D}_2^R + \bar{\alpha}\bar{Y}_{1tot})\bar{D} - \mu(b\varepsilon + \varepsilon'\bar{D}^A)\bar{D}_2^R, \quad \frac{d\bar{D}^A}{d\tau} = (u^A + \bar{D}^A)\bar{D} - (\varepsilon + \varepsilon'(\bar{D}_2^R + \bar{Y}_{1tot}))\bar{D}^A, \tag{S.26}
$$

with $\bar{D} = 1 - \bar{D}^A - \bar{D}_2^R - \bar{Y}_{1tot}$ and $\bar{Y}_{1tot} = constant$. It is evident that the ODE model (S.26) closely resembles the original model, in which we assume to have one CpG per nucleosome, i.e., (S.11), with the only distinction being the presence of $\bar{Y}_{1tot}$ instead of $\bar{Y}_1$. That is, in this revised model, the representation of the fraction of the number of CpGs methylated in the gene is denoted by $\bar{Y}_{1tot}$. Then, the introduction of the simplifying assumption, having one CpG per nucleosome, does not affect the qualitative results of the analysis that focuses on identifying the impact of the parameters α' (normalized rate of DNA methylation establishment through repressive histone modifications) and μ' (ratio between the DNA methylation erasure rate and the activating histone modification erasure rate) on the probability distribution of gene expression levels.

S.8 Supplementary Figures

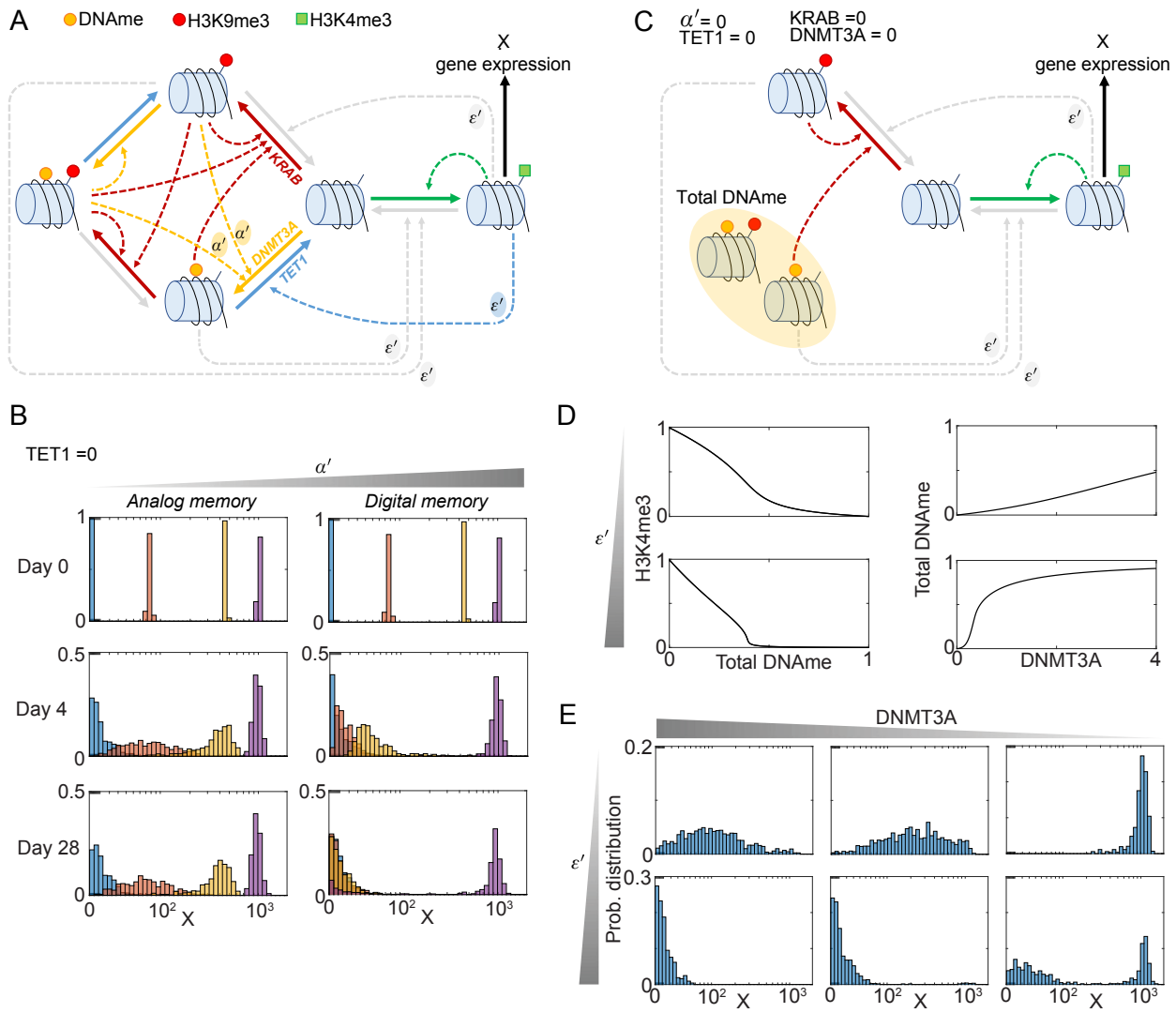

Fig. S.1. Continued on the following page.

Fig. S.1: **The dynamics of system including chromatin modification circuit and transcriptional regulation can be captured by a reduced model, under specific parameter regimes. A** Full chromatin modification circuit diagram. The species involved are unmodified nucleosome, nucleosome with H3K4me3, nucleosome with H3K9me3, nucleosome with DNAme, and nucleosome with bothr H3K9me3 and DNAme. We use solid arrows to represent the nucleosome modifications and gene expression. We use dashed arrows to represent the recruitment process and the consequent effect on establishment or erasing. For each arrow, we use red for processes involved in the H3K9me3 establishment, orange for processes involved in the DNAme establishment, green for processes involved in the H3K4me3 establishment, light blue for processes involved in the DNAme erasure, gray for processes involved in the erasure of histone modificationsa, and balck for gene expression. In order to simplify the diagram without compromising the essential interactions among modifications, we removed some non-critical dashed arrows (refer to Fig. 1 in [23] for the complete diagram). **B** Probability distributions of the system represented by reactions listed in SI Tables S.1 and S.3. The distributions are obtained computationally using SSA [43] and we indicate with X the gene expression level (logicle scale). In particular, we determine how α' affects the probability distribution of the system when $\mu' = 0$. The parameter values used for these simulations are listed in SI Section S.9. In particular, we consider $\alpha' = 0, 0.1$ and four initial conditions (H3K9me3 and DNAme, DNAme only, H3K9me3 only, H3K4me3)= (n_{12}^R,n_1^R,n_2^R,n^A): (14,0,1,0) (blue), (6,0,8,1) (red), (4,0,5,6) (yellow), and (1,0,1,13) (purple). For each case, the initial value of X at time $t = 0$ was set to its steady state. For all the simulations we set $\alpha = \bar{\alpha} = 1$, $\varepsilon = 0.08$, $\varepsilon' = 25$, $\mu = 0.1$, $b = \beta = 1$. See SI Fig. S.2 for how different values of α' and μ' influence the probability distribution of the system. **C** Simplified chromatin modification circuit diagram obtained when $\alpha' = 0$, TET1 = 0 (i.e., $\mu' = 0$), KRAB = 0 (i.e., $u_1^R = 0$), and DNMT3A = 0 (i.e., $u_2^R = 0$). **D** Left-hand side plots: dose-response curve for the (Total DNAme,H3K4me3) pair, i.e, $(\bar{Y}_1, \bar{D}^A)$, for different values of ε' obtained from simulations of system (S.11) with (Total DNAme,H3K9me3,H3K4me3) $= (\bar{Y}_1, \bar{D}_2^R, \bar{D}^A) = (k, 0, 1-k)$ as initial conditions, with $0 \leq k \leq 1$. Right hand-side plots: dose-response curve for the (DNMT3A,Total DNAme) pair, i.e, $(\bar{W}_1, \bar{Y}_1)$, for different values of ε' obtained from simulations of system (S.16) with (Total DNAme,H3K9me3,H3K4me3) $= (\bar{Y}_1, \bar{D}_2^R, \bar{D}^A) = (0, 0, 1)$ as initial conditions. The parameter values used for these simulations are listed in SI Section S.9. In particular, we consider $\varepsilon = 0.1$ and $\varepsilon' = 1, 25$ (See SI Fig. S.3 for how different values of ε and ε' influence the deterministic behavior of the system). Here, the DNMT3A dynamics is modeled as a pulse that exponentially decreases over time. The value on the x-axis corresponds to the DNMT3A value at time 0. **E** Probability distributions of the system after t = 28 days, obtained as described in panel B. The parameter values used for these simulations are listed in SI Section S.9. In particular, we consider $\varepsilon = 0.13$, $\varepsilon' = 1.5, 25$, DNMT3A $= \bar{W}_1 = [0, 0.4], [2.4, 2.8], [3.4, 3.8]$ and (H3K9me3 and DNAme, DNAme only, H3K9me3 only, H3K4me3) = (n_{12}^R,n_1^R,n_2^R,n^A) = $(0, 0, 0, \mathrm{D_{tot}})$ as initial condition (see SI Fig. S.3 for how different values of ε and ε' influence the probability distribution of the system). In our model, α' is the normalized rate of DNA methylation establishment through repressive histone modifications, μ' is ratio between the DNA methylation erasure rate and the activating histone modification erasure rate, and ε (ε') is the parameter that scales the ratio between the basal (recruited) erasure rate and the auto-catalysis rate of each modification. For panels B and E, we consider $\mathrm{D_{tot}} = 15$ and we consider $N = 1000$ samples to realize each distribution.

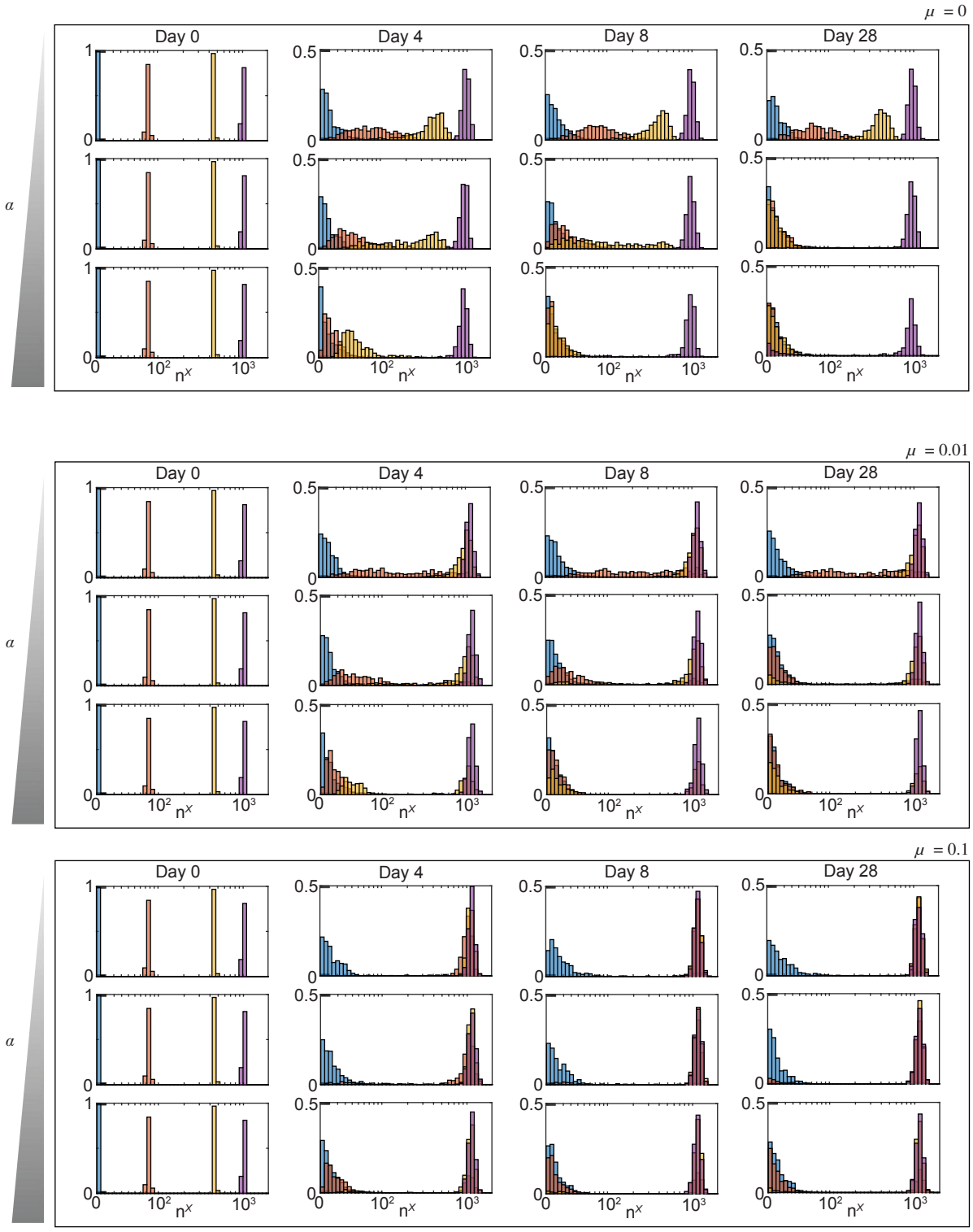

Fig. S.2. Continued on the following page.

Fig. S.2: **Achieving analog memory is only possible when $\alpha' = 0$ and $\mu' = 0$.** Probability distributions of the system represented by reactions listed in SI Tables S.1 and S.3. The distributions are obtained computationally using SSA [43] and we indicate with n^X the gene expression level (logicle scale). In particular, we determine how α' and μ' affect the probability distribution of the system. The parameter values used for these simulations are listed in SI Section S.9. In particular, we consider $\alpha' = 0, 0.01, 0.1$ and $\mu' = 0, 0.01, 0.1$ and four initial conditions: (n_{12}^R,n_1^R,n_2^R,n^A) = (14,0,1,0) (blue), (n_{12}^R,n_1^R,n_2^R,n^A) = (6,0,8,1) (red), (n_{12}^R,n_1^R,n_2^R,n^A) = (4,0,5,6) (yellow), (n_{12}^R,n_1^R,n_2^R,n^A) = (1,0,1,13) (purple). For each case, the initial values of n^X of n^m at time $t = 0$ were set to their steady states. For all the simulations we set $\alpha = \bar{\alpha} = 1$, $\varepsilon = 0.08$, $\varepsilon' = 25$, $\mu = 0.1$, $b = \beta = 1$. In our model, α' is the normalized rate of DNA methylation establishment through repressive histone modifications and μ' is ratio between the DNA methylation erasure rate and the activating histone modification erasure rate. For all simulations, we consider $\mathrm{D_{tot}} = 15$ and we consider $N = 1000$ samples to realize each distribution.

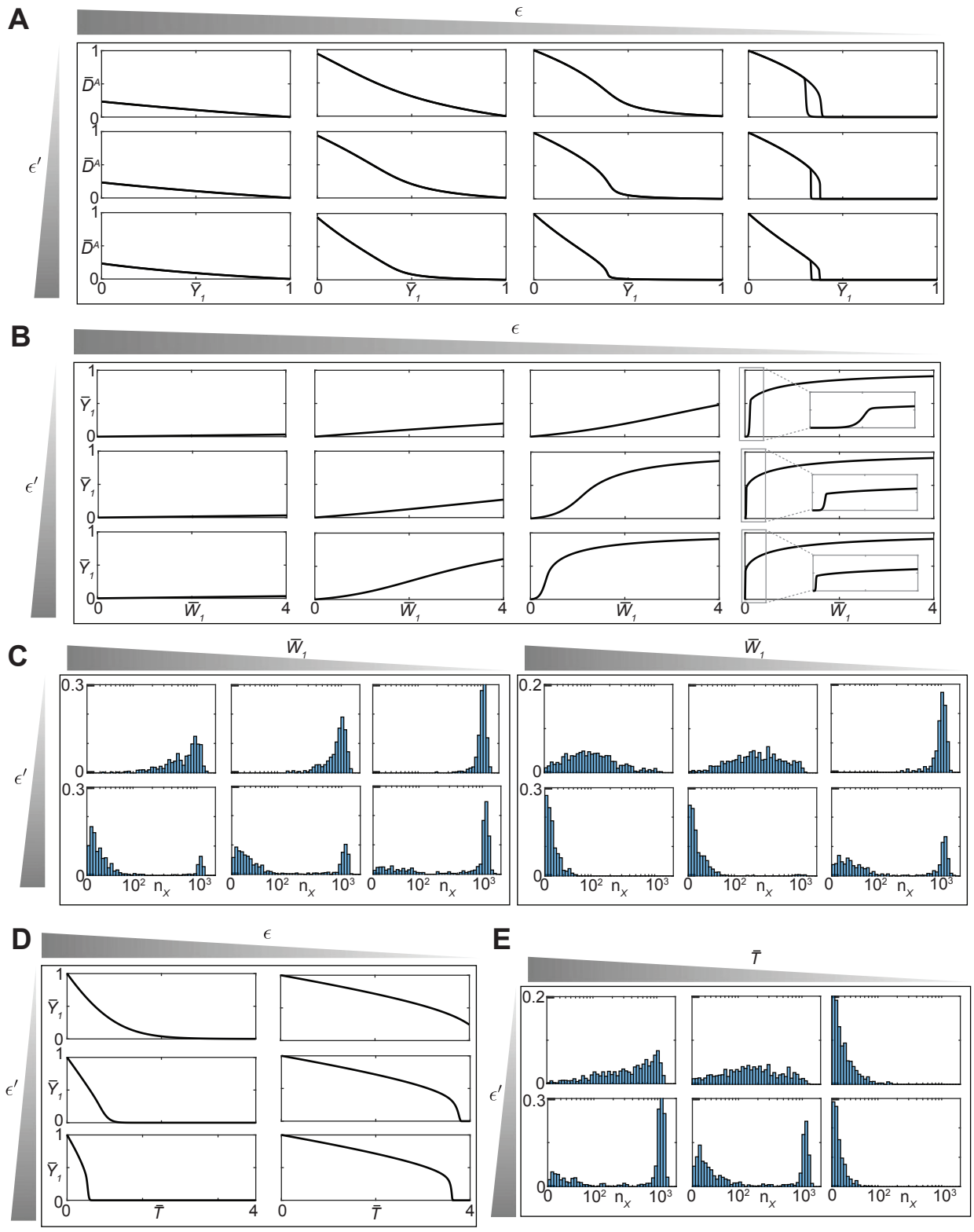

Fig. S.3. Continued on the following page.

Fig. S.3: **The parameters ε and ε' affect the shape of the probability distribution for gene expression levels. A** Input/output steady state characteristics for the $(\bar{Y}_1, \bar{D}^A)$ pair for different values of ε and ε' obtained from simulations of system (S.11) with $(\bar{Y}_1, \bar{D}_2^R, \bar{D}^A) = (k, 0, 1-k)$ as initial conditions, with $0 \leq k \leq 1$. The parameter values used for these simulations are listed in SI Section S.9. In particular, $\varepsilon = 0.0001, 0.1, 1, 50$ and $\varepsilon' = 1, 5, 25$. **B** dose-response curve for the $(\bar{W}_1, \bar{Y}_1)$ pair for different values of ε and ε' obtained from simulations of system (S.16) with $(\bar{Y}_1, \bar{D}_2^R, \bar{D}^A) = (0, 0, 1)$ as initial conditions. The parameter values used for these simulations are listed in SI Section S.9. In particular, $\varepsilon = 0.0001, 0.1, 1, 50$ and $\varepsilon' = 1, 5, 25$. **C** Probability distributions of the system represented by reactions listed in SI Tables S.1 and S.3 after t = 28 days. The distributions are obtained computationally using SSA [43] and we indicate with n^X the gene expression level (logicle scale). The parameter values used for these simulations are listed in SI Section S.9. In particular, in the left-hand side panel we consider $\varepsilon' = 1.5, 25$, $\bar{W}_1 = [0, 0.7], [0.5, 1.2], [1, 1.7]$ and (n_{12}^R,n_1^R,n_2^R,n^A) = $(0, 0, 0, \mathrm{D_{tot}})$ as initial conditions. The initial values of n^X of n^m at time $t = 0$ were set to their steady states. In the right-hand side panel we consider $\bar{W}_1 = [0, 0.4], [2.4, 2.8], [3.4, 3.8]$ and all the other parameter values as the ones used for the simulations in the left-hand side panel. For all the simulations we set $\alpha = \bar{\alpha} = 1$, $\varepsilon = 0.13$, $\mu = 0.1$, $b = \beta = 1$, and we consider $\mathrm{D_{tot}} = 15$ and $N = 1000$ samples to realize each distribution. **D** Dose-response curve for the $(\bar{Y}_1, \bar{T})$ pair for different values of ε and ε' obtained from simulations of system (S.16) with $(\bar{Y}_1, \bar{D}_2^R, \bar{D}^A) = (1, 0, 0)$ as initial conditions. The parameter values used for these simulations are listed in SI Section S.9. In particular, $\varepsilon = 0.0001, 0.1$ and $\varepsilon' = 1, 5, 25$. **E** Probability distributions of the system represented by reactions listed in SI Tables S.1 and S.3 after t = 28 days. The distributions are obtained computationally using SSA [43] and we indicate with n^X the gene expression level (logicle scale). The parameter values used for these simulations are listed in SI Section S.9. In particular, we consider $\varepsilon' = 1.5, 25$, $\bar{T} = [0, 0.05], [0.24, 0.28], [0.36, 0.4]$ and (n_{12}^R,n_1^R,n_2^R,n^A) = $(\mathrm{D_{tot}}, 0, 0, 0)$ as initial conditions. The initial values of n^X of n^m at time $t = 0$ were set to their steady states. For all the simulations we set $\alpha = \bar{\alpha} = 1$, $\varepsilon = 0.13$, $\mu = 0.1$, $b = \beta = 1$, and we consider $\mathrm{D_{tot}} = 15$ and $N = 1000$ samples to realize each distribution. In our model, ε (ε') is the parameter that scales the ratio between the basal (recruited) erasure rate and the auto-catalysis rate of each modification, and $\bar{W}_1$ and $\bar{T}$ represent the normalized amounts of DNMT3A and TET1 at time 0, which exponentially decrease over time.

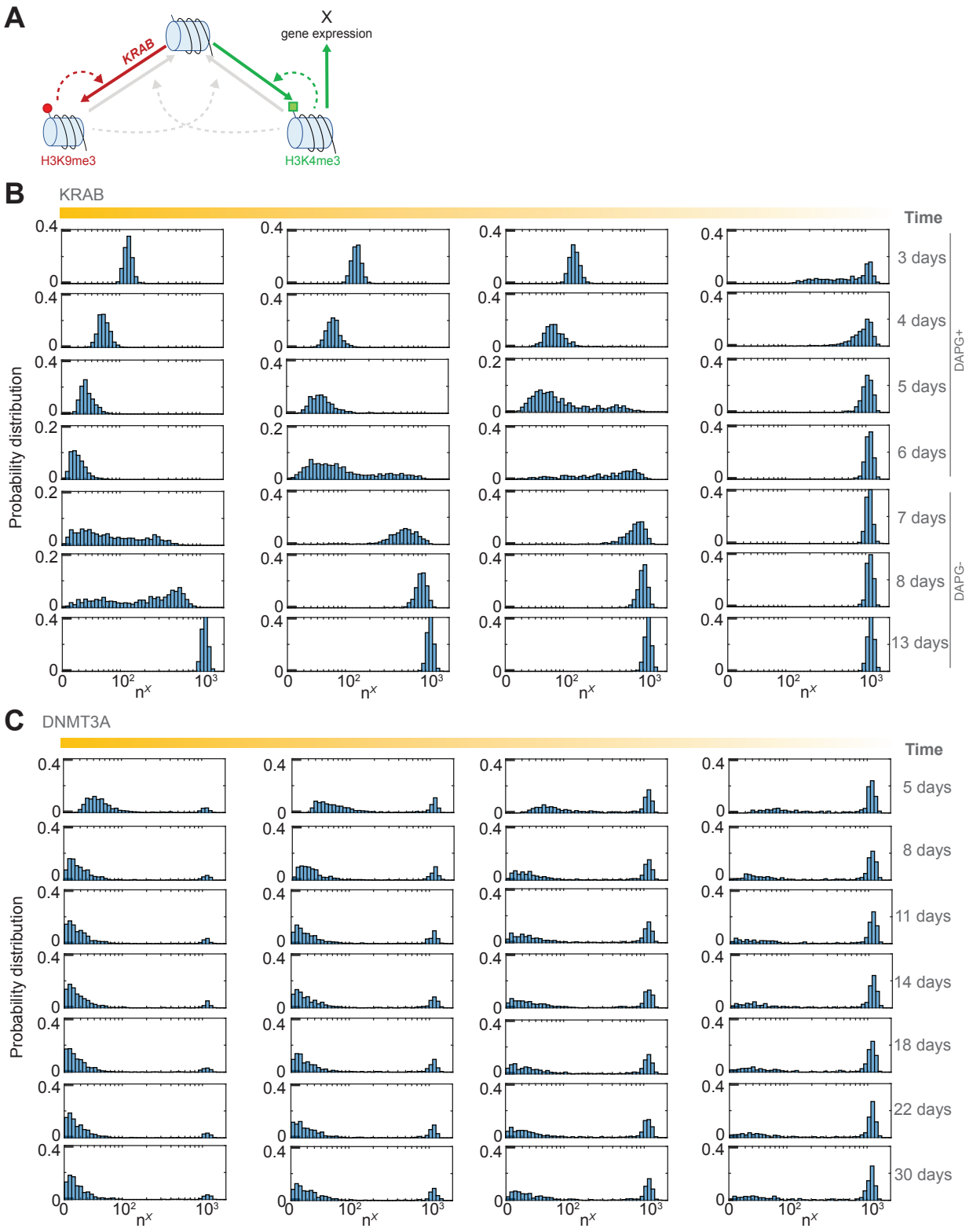

Fig. S.4. Continued on the following page.

Fig. S.4: **Simulations recapitulating the effect of transient transfection of DNMT3A and KRAB on the gene expression probability distribution. A** Diagram of the simplified chromatin modification circuit, including H3K9me3 and H3K4me3 only. We use solid arrows to represent the nucleosome modifications and gene expression. We use dashed arrows to represent the recruitment process and the consequent effect on establishment or erasing. For each arrow, we use red for processes involved in the H3K9me3 establishment, green for processes involved in the H3K4me3 establishment, and gray for processes involved in the erasure of histone modifications. **B** Probability distributions of the system represented in panel A, whose reactions are listed in SI Tables S.2 and S.4. The distributions are obtained computationally using SSA [43] and we indicate with n^X the gene expression level (logicle scale). The parameter values used for these simulations are listed in SI Section S.9. In particular, we consider $KRAB = \bar{W}_2 = [1.5, 7.5], [20, 100], [45, 225], [4000, 20000]$, and ($n_2^R$,$n^A$) = $(0, \mathrm{D_{tot}})$ as initial conditions. The initial values of n^X of n^m at time $t = 0$ were set to their steady states. **C** Probability distributions of the system represented in Fig. S.1A, whose reactions are listed in SI Tables S.1 and S.3. The distributions are obtained computationally using SSA [43] and we indicate with n^X the gene expression level (logicle scale). The parameter values used for these simulations are listed in SI Section S.9. In particular, we consider $DNMT3A = \bar{W}_1 = [0.2, 0.7]$, $[0.35, 1.23]$, $[0.6, 2.1]$, $[0.9, 3.1]$, $KRAB = 0$, and (n_{12}^R,n_1^R,n_2^R,n^A) = $(0, 0, 0, \mathrm{D_{tot}})$ as initial conditions. The initial values of n^X of n^m at time $t = 0$ were set to their steady states. For all the simulations we set $\alpha = 1$, $\varepsilon = 0.13$, $\varepsilon' = 25$, $\mu = 0.1$, $b = 1$, we model the dynamics of KRAB and DNMT3A as pulses that exponentially decrease over time, and we consider $\mathrm{D_{tot}} = 15$ and $N = 1000$ samples to realize each distribution.

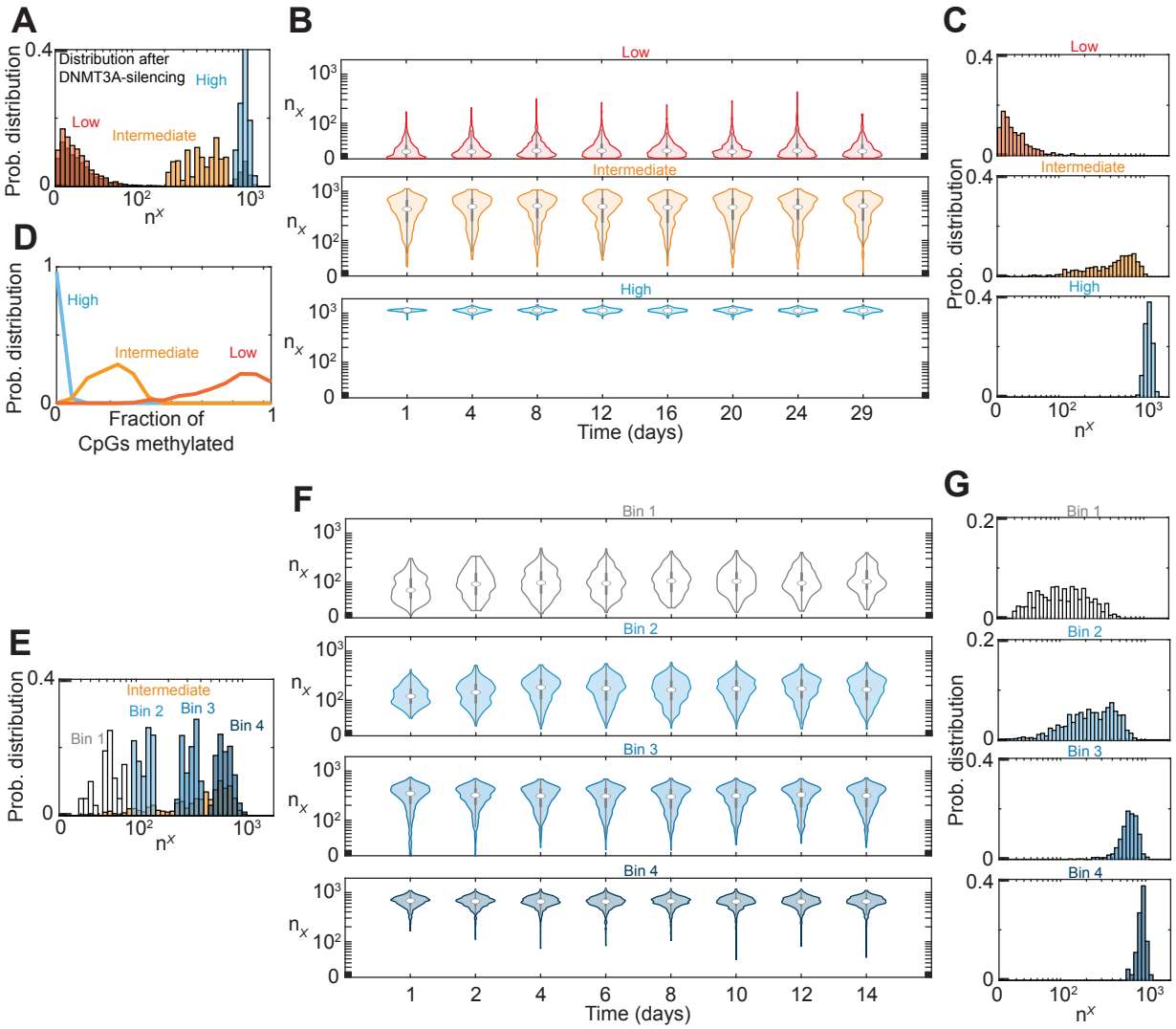

Fig. S.5. Continued on the following page.

Fig. S.5: **Simulations recapitulating the experimental results shown in Fig. 3, showing that intermediate gene expression levels are stable and exhibit intermediate DNA methylation levels. A** Probability distributions of the system represented in Fig. S.1A, whose reactions are listed in SI Tables S.1 and S.3. The distributions are obtained computationally using SSA [43] and we indicate with n^X the gene expression level (logicle scale). The black distribution represents the probability distribution of the system at day 30 after DNMT3A-silecing. The parameter values used for these simulations are listed in SI Section S.9. In particular, we consider $DNMT3A = \bar{W}_1 = [0.6, 2.1]$, $KRAB = 0$, and (n^R_{12},n^R_1,n^R_2,n^A) = $(0, 0, 0, \mathrm{D_{tot}})$ as initial conditions. The initial values of n^X of n^m at time $t = 0$ were set to their steady states. The low (red), intermediate (orange), and high (blue) distributions are obtained by subdividing the black distribution with respect to the following intervals of n^X:[0,100], [200,800], [900,10000]. **B** Probability distributions of the system represented in Fig. S.1A obtained as described in panel A. The parameter values used for these simulations are listed in SI Section S.9. In particular, for each case, we consider $DNMT3A = 0$, $KRAB = 0$, and, as initial conditions, points from the red, orange, and blue distributions shown in panel A, respectively. **C** Probability distributions of the system at day 29 from panel B. **D** Probability distribution of the fraction of CpGs methylated, i.e., $(n^R_1 + n^R_{12})/\mathrm{D_{tot}}$, at day 29 from panel B. **E** Probability distributions of the system represented in Fig. S.1A, whose reactions are listed in SI Tables S.1 and S.3. The distributions are obtained computationally using SSA [43] and we indicate with n^X the gene expression level (logicle scale). The orange distribution is the one obtained and described in panel C. The other ones are obtained by subdividing the orange distribution with respect to the following intervals of n^X: [0,80] (Bin 1), [90,150] (Bin 2), [250,400] Bin 3, [500,10000] (Bin 4). **F** Probability distributions of the system represented in Fig. S.1A obtained as described in panel A. The parameter values used for these simulations are listed in SI Section S.9. In particular, for each case, we consider $DNMT3A = 0$, $KRAB = 0$, and, as initial conditions, points from the "Bin 1", "Bin 2", "Bin 3", and "Bin 4" distributions shown in panel E, respectively. **G** Probability distributions of the system at day 14 from panel F.

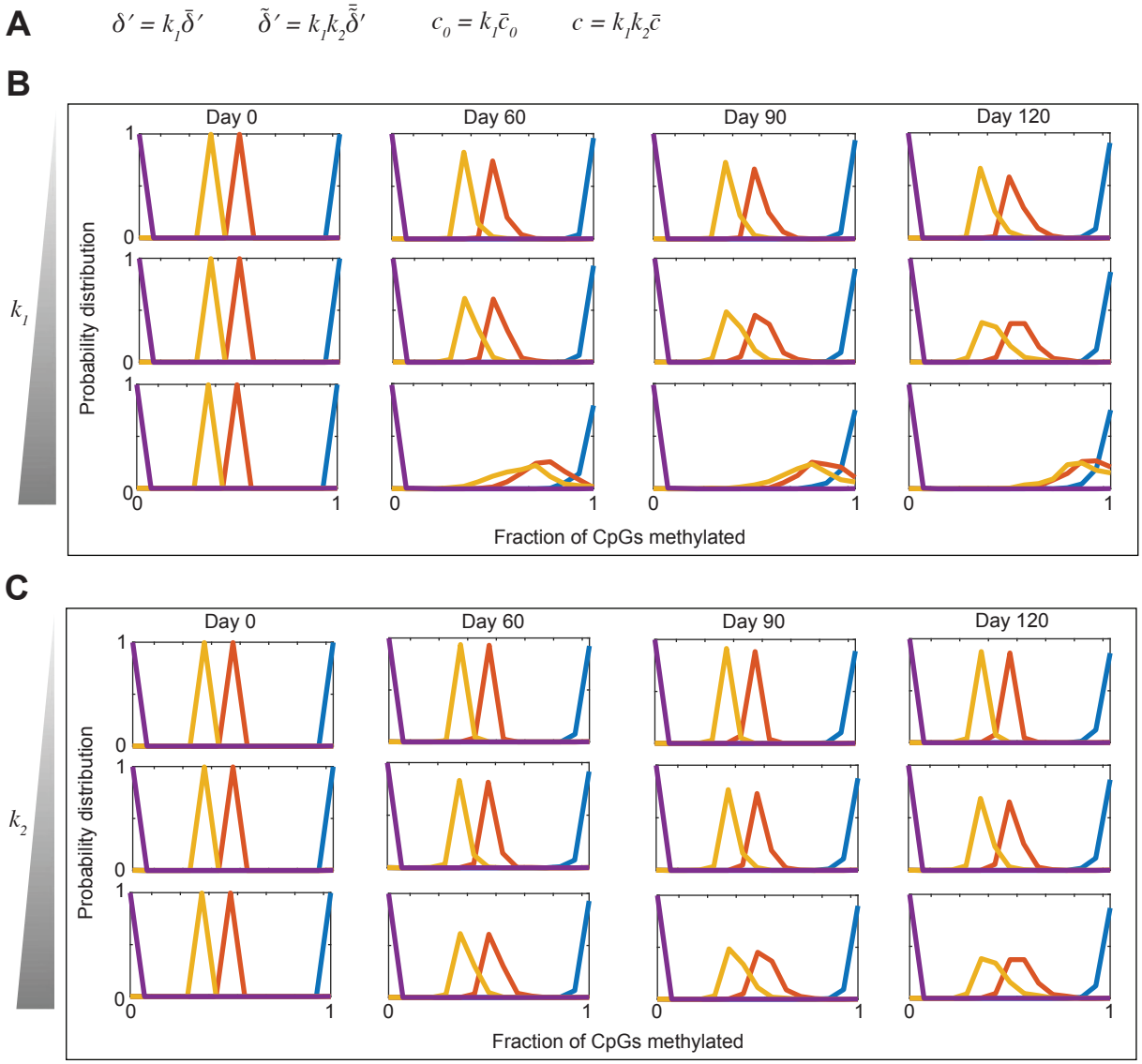

Fig. S.6. Continued on the following page.

Fig. S.6: **Stochastic analysis of the refined DNA methylation maintenance model. A** Introduction of parameters k_1 and k_2: k_1 scales all the rate constants associated with the reactions involved in the DNA methylation maintenance process, i.e., (S.17) and (S.18). Meanwhile, k_2 scales the rate constants associated with the reactions representing the effect of DNMT1 recruitment by H3K9me3 on the maintenance process, i.e., the second and third reactions in (S.18). **B** Probability distributions of the system represented by reactions listed in SI Tables S.5 and S.3. The distributions are obtained computationally using SSA [43] and, on the x we have the fraction of CpGs methylated. In particular, we determine how k_1 affects the probability distribution of the system. The parameter values used for these simulations are listed in SI Section S.9. In particular, we consider $k_1 = 0.00005, 0.0001, 0.001$ and $k_2 = 1$ and four initial fractions of CpGs methylated (0.93,0.4,0.27,0). Specifically, as initial conditions, we set (n^R_{12},n^R_1,n^R_2,n^A) = (14,0,0,1) (blue), (n^R_{12},n^R_1,n^R_2,n^A) = (6,0,0,9) (red), (n^R_{12},n^R_1,n^R_2,n^A) = (4,0,0,11) (yellow), (n^R_{12},n^R_1,n^R_2,n^A) = (0,0,0,15) (purple). For each case, The initial values of n^X of n^m at time $t = 0$ were set to their steady states. For all the simulations we set $\alpha = \bar{\alpha} = 1$, $\varepsilon = 0.13$, $\varepsilon' = 25$, $\mu = 0.1$, $b = \beta = 1$. **C** Probability distributions of the system represented by reactions listed in SI Tables S.5 and S.3. The distributions are obtained computationally using SSA [43] and, on the x we have the fraction of CpGs methylated. In particular, we determine how k_2 affects the probability distribution of the system. The parameter values used for these simulations are listed in SI Section S.9. In particular, we consider $k_1 = 0.0001$ and $k_2 = 0.1, 0.3, 1$ and the same initial conditions and parameter values used for panel B. For all simulations, we consider $\mathrm{D_{tot}} = 15$ and we consider $N = 1000$ samples to realize each distribution.

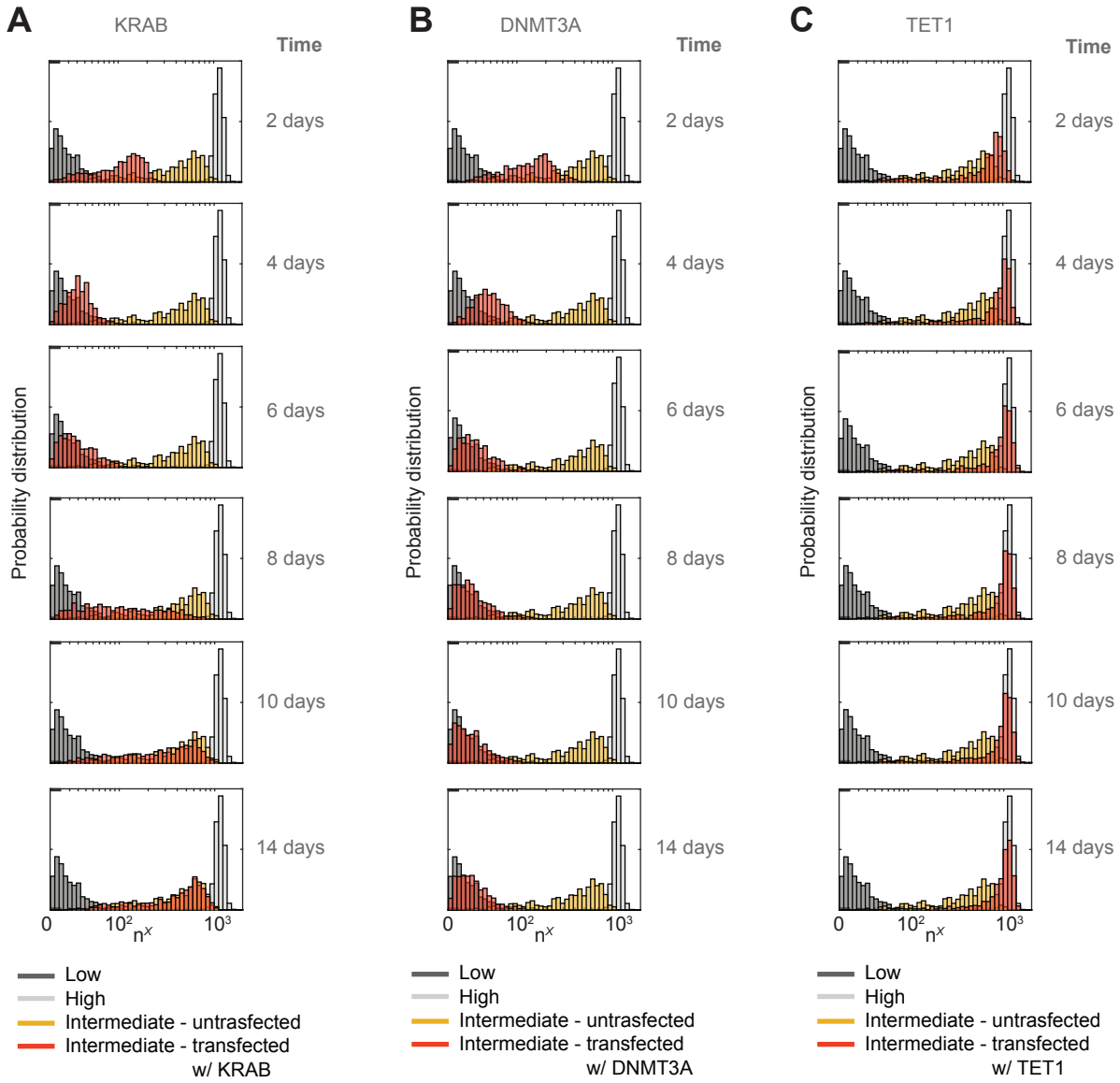

Fig. S.7. Continued on the following page.

Fig. S.7: **Simulations recapitulating the effect of DNMT3A, TET1, and KRAB on the gene expression probability distribution, starting from an intermediate level of gene expression. A** Probability distributions of the system represented in panel A, whose reactions are listed in SI Tables S.2 and S.4. The distributions are obtained computationally using SSA [43] and we indicate with n^X the gene expression level (logicle scale). The parameter values used for these simulations are listed in SI Section S.9. In particular, we consider $KRAB = \bar{W}_2 = [50, 250]$, $DNMT3A = \bar{W}_1 = 0$, $TET1 = \bar{T} = 0$. As initial conditions, we consider values of (n^R_{12},n^R_1,n^R_2,n^A,n^X,n^m) from the simulations associated with the orange distribution in SI Fig. S.5C. **B** Probability distributions obtained as described in panel A. The parameter values used for these simulations are listed in SI Section S.9. In particular, we consider $DNMT3A = \bar{W}_1 = [0.2, 0.7]$, $KRAB = \bar{W}_2 = 0$, and $TET1 = \bar{T} = 0$. **C** Probability distributions obtained as described in panel A. The parameter values used for these simulations are listed in SI Section S.9. In particular, we consider $DNMT3A = \bar{W}_1 = 0$, $KRAB = \bar{W}_2 = 0$, and $TET1 = \bar{T} = [0.004, 0.014]$. For all the simulations we set $\alpha = \bar{\alpha} = 1$, $\varepsilon = 0.13$, $\varepsilon' = 25$, $\mu = 0.1$, $b = 1$, we model the dynamics of KRAB, DNMT3A, and TET1 as pulses that exponentially decrease over time, and we consider $\mathrm{D_{tot}} = 15$ and $N = 1000$ samples to realize each distribution.

S.9 Values of parameters used in generating figures in the main paper and SI

S.9.1 Parameter values used to realize the plots in Fig. 2H - top panel

$\alpha = 1$, $\bar{\alpha} = 1$, $\mu = 0.1$, $b = 1$, $\varepsilon = 0.1$, $\varepsilon' = 25$, $u^A = 15$. As initial conditions, we set $(\bar{Y}_1, \bar{D}_2^R, \bar{D}^A) = (k, 0, 1-k)$, with $0 \leq k \leq 1$.

S.9.2 Parameter values used to realize the plots in Fig. 2H - bottom panel

$\tilde{u}_2^R = 0$, $\tilde{\mu}' = 0$, $\beta = 1$, $\tilde{u}_1^R = 1$, $\bar{W}_1 = [0, 4]$ $\alpha = 1$, $\bar{\alpha} = 1$, $\mu = 0.1$, $b = 1$, $\varepsilon = 0.1$, $\varepsilon' = 25$, $u^A = 15$. As initial conditions, we set $(\bar{Y}_1, \bar{D}_2^R, \bar{D}^A) = (0, 0, 1)$.

S.9.3 Parameter values used to realize the plots in Fig. 2I

$k_{W0}^A = 0$, $k_W^A = 7.8075$ h^{-1}, $\bar{k}_E^A = 0.0118$ h^{-1}, $\delta = 0.0291$ h^{-1}, $\frac{k_M^A}{\Omega} = 0.0347$ h^{-1}, $\frac{k_E^A}{\Omega} = 0.8675$ h^{-1}, $k_{W0}^1 = 0$, $k_W^1 = 0$, $k_T' = 0$, $\delta' = 0$, $\frac{k_M'}{\Omega} = 0$, $\frac{k_T'^*}{\Omega} = 0$, $k_{W0}^2 = 0$, $k_W^2 = 0$, $\bar{k}_E^R = 0.0012$ h^{-1}, $\frac{k_M}{\Omega} = 0.0347$ h^{-1}, $\frac{\bar{k}_M}{\Omega} = 0.0347$ h^{-1}, $\frac{k_E^R}{\Omega} = 0.0868$ h^{-1}, $\beta_m = 0.2556$ h^{-1}, $\beta_m^A = 0.0021$ h^{-1}, $\beta = 2.52$ h^{-1}, $\gamma_m = 0.24$ h^{-1}, $\gamma = 0.0349$ h^{-1}. We consider four initial conditions: (n_{12}^R,n_1^R,n_2^R,n^A) = (14,0,1,0) (blue), (n_{12}^R,n_1^R,n_2^R,n^A) = (6,0,8,1) (red), (n_{12}^R,n_1^R,n_2^R,n^A) = (4,0,5,6) (yellow), (n_{12}^R,n_1^R,n_2^R,n^A) = (1,0,1,13) (purple). For each case, the initial values of n^X of n^m at time $t = 0$ were set to their steady states.

S.9.4 Parameter values used to realize the plots in Fig. 2J

$k_{W0}^A = 0$, $k_W^A = 7.8075$ h^{-1}, $\bar{k}_E^A = 0.0315$ h^{-1}, $\delta = 0.035$ h^{-1}, $\frac{k_M^A}{\Omega} = 0.0347$ h^{-1}, $\frac{k_E^A}{\Omega} = 0.8675$ h^{-1}, $k_{W0}^1 = 0$, $k_W^1 \in [0, 0.3643]e^{-\delta t}, [0.2602, 0.6246]e^{-\delta t}, [0.5205, 0.8848]e^{-\delta t}$ h^{-1}, $k_T' = 0$, $\delta' = 0$, $\frac{k_M'}{\Omega} = 0$, $\frac{k_T'^*}{\Omega} = 0$, $k_{W0}^2 = 0$, $k_W^2 = 0$, $\bar{k}_E^R = 0.0032$ h^{-1}, $\frac{k_M}{\Omega} = 0.0347$ h^{-1}, $\frac{\bar{k}_M}{\Omega} = 0.0347$ h^{-1}, $\frac{k_E^R}{\Omega} = 0.0868$ h^{-1}, $\beta_m = 0.2556$ h^{-1}, $\beta_m^A = 0.0021$ h^{-1}, $\beta = 2.52$ h^{-1}, $\gamma_m = 0.24$ h^{-1}, $\gamma = 0.035$ h^{-1}. As initial condition, we consider (n_{12}^R,n_1^R,n_2^R,n^A) = (0,0,0,15) and the initial values of n^X of n^m at time $t = 0$ were set to their steady states.

S.9.5 Parameter values used to realize the plots in Fig. 4G and I

$k_{W0}^A = 0$, $k_W^A = 7.8075$ h^{-1}, $\bar{k}_E^A = 0.0176$ h^{-1}, $\delta = 0.035$ h^{-1}, $\frac{k_M^A}{\Omega} = 0.0347$ h^{-1}, $\frac{k_E^A}{\Omega} = 0.8675$ h^{-1}, $k_{W0}^1 = 0$, $k_W^1 = 0$, $c = 1.11 \cdot 10^{-6}$ h^{-1}, $c_0 = 8.37 \cdot 10^{-5}$ h^{-1}, $\delta' = 2.09 \cdot 10^{-5}$ h^{-1}, $\tilde{\delta}' = 4.15 \cdot 10^{-5}$ h^{-1}, $K = 1$, $\frac{k_M'}{\Omega} = 0$,

$\frac{k_T'^*}{\Omega} = 0$ h^{-1}, $k_{W0}^2 = 0$, $k_W^2 = 0$, $\bar{k}_E^R = 0.0018$ h^{-1}, $\frac{k_M}{\Omega} = 0.0347$ h^{-1}, $\frac{\bar{k}_M}{\Omega} = 0.0347$ h^{-1}, $\frac{k_E^R}{\Omega} = 0.0868$ h^{-1}, $\beta_m = 0.2556$ h^{-1}, $\beta_m^A = 0.0021$ h^{-1}, $\beta = 2.52$ h^{-1}, $\gamma_m = 0.24$ h^{-1}, $\gamma = 0.0349$ h^{-1}. We consider eight initial conditions: (n_{12}^R,n_1^R,n_2^R,n^A) = (13,0,0,2) (Bin 1), (12,0,0,3) (Bin 2), (8,0,0,7) (Bin 3), (6,0,0,9) (Bin 4), (5,0,0,10) (Bin 5), (4,0,0,11) (Bin 6), (1,0,0,14) (Bin 7), (0,0,0,15) (Bin 8). For each case, the initial values of n^X of n^m at time $t = 0$ were set to their steady states.

S.9.6 Parameter values used to realize the plots in SI Fig. S.1B

$k_{W0}^A = 0$, $k_W^A = 7.8075$ h^{-1}, $\bar{k}_E^A = 0.0118$ h^{-1}, $\delta = 0.0291$ h^{-1}, $\frac{k_M^A}{\Omega} = 0.0347$ h^{-1}, $\frac{k_E^A}{\Omega} = 0.8675$ h^{-1}, $k_{W0}^1 = 0$, $k_W^1 = 0$, $k_T' = 0$, $\delta' = 0$, $\frac{k_M'}{\Omega} = 0, 0.00347$ h^{-1}, $\frac{k_T'^*}{\Omega} = 0$, $k_{W0}^2 = 0$, $k_W^2 = 0$, $\bar{k}_E^R = 0.0012$ h^{-1}, $\frac{k_M}{\Omega} = 0.0347$ h^{-1}, $\frac{\bar{k}_M}{\Omega} = 0.0347$ h^{-1}, $\frac{k_E^R}{\Omega} = 0.0868$ h^{-1}, $\beta_m = 0.2556$ h^{-1}, $\beta_m^A = 0.0021$ h^{-1}, $\beta = 2.52$ h^{-1}, $\gamma_m = 0.24$ h^{-1}, $\gamma = 0.0349$ h^{-1}. We consider four initial conditions: (n_{12}^R,n_1^R,n_2^R,n^A) = (14,0,1,0) (blue), (n_{12}^R,n_1^R,n_2^R,n^A) = (6,0,8,1) (red), (n_{12}^R,n_1^R,n_2^R,n^A) = (4,0,5,6) (yellow), (n_{12}^R,n_1^R,n_2^R,n^A) = (1,0,1,13) (purple). For each case, the initial values of n^X of n^m at time $t = 0$ were set to their steady states.

S.9.7 Parameter values used to realize the plots in SI Fig. S.1D - left hand-side panel

$\alpha = 1$, $\bar{\alpha} = 1$, $\mu = 0.1$, $b = 1$, $\varepsilon = 0.1$, $\varepsilon' = 1, 25$, $u^A = 15$. As initial conditions, we set $(\bar{Y}_1, \bar{D}_2^R, \bar{D}^A) = (k, 0, 1-k)$, with $0 \leq k \leq 1$.

S.9.8 Parameter values used to realize the plots in SI Fig. S.1D - right hand-side panel

$\tilde{u}_2^R = 0$, $\tilde{\mu}' = 0$, $\beta = 1$, $\tilde{u}_1^R = 1$, $\bar{W}_1 = [0, 4]$ $\alpha = 1$, $\bar{\alpha} = 1$, $\mu = 0.1$, $b = 1$, $\varepsilon = 0.1$, $\varepsilon' = 1, 25$, $u^A = 15$. As initial conditions, we set $(\bar{Y}_1, \bar{D}_2^R, \bar{D}^A) = (0, 0, 1)$.

S.9.9 Parameter values used to realize the plots in SI Fig. S.1E

$k_{W0}^A = 0$, $k_W^A = 7.8075$ h^{-1}, $\bar{k}_E^A = 0.0315$ h^{-1}, $\delta = 0.035$ h^{-1}, $\frac{k_M^A}{\Omega} = 0.0347$ h^{-1}, $\frac{k_E^A}{\Omega} = 0.0520, 0.8675$ h^{-1}, $k_{W0}^1 = 0$, $k_W^1 \in [0, 0.3643]e^{-\delta t}, [0.2602, 0.6246]e^{-\delta t}, [0.5205, 0.8848]e^{-\delta t}$ h^{-1} (left hand-side panel) and $k_W^1 \in [0, 0.3643]e^{-\delta t}, [0.2602, 0.6246]e^{-\delta t}, [0.5205, 0.8848]e^{-\delta t}$ h^{-1} (right hand-side panel), $k_T' = 0$, $\delta' = 0$, $\frac{k_M'}{\Omega} = 0$, $\frac{k_T'^*}{\Omega} = 0$, $k_{W0}^2 = 0$, $k_W^2 = 0$, $\bar{k}_E^R = 0.0032$ h^{-1}, $\frac{k_M}{\Omega} = 0.0347$ h^{-1}, $\frac{\bar{k}_M}{\Omega} = 0.0347$ h^{-1}, $\frac{k_E^R}{\Omega} = 0.0052, 0.0868$ h^{-1}, $\beta_m = 0.2556$ h^{-1}, $\beta_m^A = 0.0021$ h^{-1}, $\beta = 2.52$ h^{-1}, $\gamma_m = 0.24$ h^{-1}, $\gamma = 0.035$ h^{-1}. As initial condition, we

consider (n_{12}^R,n_1^R,n_2^R,n^A) = (0,0,0,15) and the initial values of n^X of n^m at time $t = 0$ were set to their steady states.

S.9.10 Parameter values used to realize the plots in SI Fig. S.2

$k_{W0}^A = 0$, $k_W^A = 7.8075$ h^{-1}, $\bar{k}_E^A = 0.0118$ h^{-1}, $\delta = 0.0291$ h^{-1}, $\frac{k_M^A}{\Omega} = 0.0347$ h^{-1}, $\frac{k_E^A}{\Omega} = 0.8675$ h^{-1}, $k_{W0}^1 = 0$, $k_W^1 = 0$, $k_T' = 0, 0.00012, 0.0012$ h^{-1}, $\delta' = 0$, $\frac{k_M'}{\Omega} = 0, 3.47 \cdot 10^{-4}, 3.47 \cdot 10^{-3}$ h^{-1}, $\frac{k_T'^*}{\Omega} = 0, 0.0087, 0.087$ h^{-1}, $k_{W0}^2 = 0$, $k_W^2 = 0$, $\bar{k}_E^R = 0.0012$ h^{-1}, $\frac{k_M}{\Omega} = 0.0347$ h^{-1}, $\frac{\bar{k}_M}{\Omega} = 0.0347$ h^{-1}, $\frac{k_E^R}{\Omega} = 0.0868$ h^{-1}, $\beta_m = 0.2556$ h^{-1}, $\beta_m^A = 0.0021$ h^{-1}, $\beta = 2.52$ h^{-1}, $\gamma_m = 0.24$ h^{-1}, $\gamma = 0.0349$ h^{-1}. We consider four initial conditions: (n_{12}^R,n_1^R,n_2^R,n^A) = (14,0,1,0) (blue), (n_{12}^R,n_1^R,n_2^R,n^A) = (6,0,8,1) (red), (n_{12}^R,n_1^R,n_2^R,n^A) = (4,0,5,6) (yellow), (n_{12}^R,n_1^R,n_2^R,n^A) = (1,0,1,13) (purple). For each case, the initial values of n^X of n^m at time $t = 0$ were set to their steady states.

S.9.11 Parameter values used to realize the plots in SI Fig. S.3A

$\alpha = 1$, $\bar{\alpha} = 1$, $\mu = 0.1$, $b = 1$, $\varepsilon = 0.0001, 0.1, 1, 50$, $\varepsilon' = 1, 5, 25$, $u^A = 15$. As initial conditions, we set $(\bar{Y}_1, \bar{D}_2^R, \bar{D}^A) = (k, 0, 1-k)$, with $0 \leq k \leq 1$.

S.9.12 Parameter values used to realize the plots in SI Fig. S.3B

$\tilde{u}_2^R = 0$, $\tilde{\mu}' = 0$, $\beta = 1$, $\tilde{u}_1^R = 1$, $\bar{W}_1 = [0, 4]$ $\alpha = 1$, $\bar{\alpha} = 1$, $\mu = 0.1$, $b = 1$, $\varepsilon = 0.0001, 0.1, 1, 50$, $\varepsilon' = 1, 5, 25$, $u^A = 15$. As initial conditions, we set $(\bar{Y}_1, \bar{D}_2^R, \bar{D}^A) = (0, 0, 1)$.

S.9.13 Parameter values used to realize the plots in SI Fig. S.3C

$k_{W0}^A = 0$, $k_W^A = 7.8075$ h^{-1}, $\bar{k}_E^A = 0.0315$ h^{-1}, $\delta = 0.035$ h^{-1}, $\frac{k_M^A}{\Omega} = 0.0347$ h^{-1}, $\frac{k_E^A}{\Omega} = 0.0520, 0.8675$ h^{-1}, $k_{W0}^1 = 0$, $k_W^1 \in [0, 0.3643]e^{-\delta t}, [0.2602, 0.6246]e^{-\delta t}, [0.5205, 0.8848]e^{-\delta t}$ h^{-1} (left hand-side panel) and $k_W^1 \in [0, 0.2082]e^{-\delta t}, [1.2492, 1.4574]e^{-\delta t}, [1.7697, 1.9779]e^{-\delta t}$ h^{-1} (right hand-side panel), $k_T' = 0$, $\delta' = 0$, $\frac{k_M'}{\Omega} = 0$, $\frac{k_T'^*}{\Omega} = 0$, $k_{W0}^2 = 0$, $k_W^2 = 0$, $\bar{k}_E^R = 0.0032$ h^{-1}, $\frac{k_M}{\Omega} = 0.0347$ h^{-1}, $\frac{\bar{k}_M}{\Omega} = 0.0347$ h^{-1}, $\frac{k_E^R}{\Omega} = 0.0052, 0.0868$ h^{-1}, $\beta_m = 0.2556$ h^{-1}, $\beta_m^A = 0.0021$ h^{-1}, $\beta = 2.52$ h^{-1}, $\gamma_m = 0.24$ h^{-1}, $\gamma = 0.035$ h^{-1}. As initial condition, we consider (n_{12}^R,n_1^R,n_2^R,n^A) = (0,0,0,15) and the initial values of n^X of n^m at time $t = 0$ were set to their steady states.

S.9.14 Parameter values used to realize the plots in SI Fig. S.3D

$\tilde{u}_2^R = 0$, $\tilde{\mu}' = 1$, $\beta = 1$, $\tilde{u}_1^R = 0$, $\bar{T} = [0, 4]$ $\alpha = 1$, $\bar{\alpha} = 1$, $\mu = 0.1$, $b = 1$, $\varepsilon = 0.0001, 0.1, 1, 50$, $\varepsilon' = 1, 5, 25$, $u^A = 15$. As initial conditions, we set $(\bar{Y}_1, \bar{D}_2^R, \bar{D}^A) = (1, 0, 0)$.

S.9.15 Parameter values used to realize the plots in SI Fig. S.3E

$k_{W0}^A = 0$, $k_W^A = 7.8075$ h^{-1}, $\bar{k}_E^A = 0.0315$ h^{-1}, $\delta = 0.035$ h^{-1}, $\frac{k_M^A}{\Omega} = 0.0347$ h^{-1}, $\frac{k_E^A}{\Omega} = 0.0520, 0.8675$ h^{-1}, $k_{W0}^1 = 0$, $k_W^1 = 0$, $k_T' \in [0, 0.0016]e^{-\delta t}, [0.0076, 0.0088]e^{-\delta t}, [0.0113, 0.0126]e^{-\delta t}$ h^{-1}, $\delta' = 0$, $\frac{k_M'}{\Omega} = 0$, $\frac{k_T'^*}{\Omega} \in [0, 0.0434]e^{-\delta t}, [0.2082, 0.2429]e^{-\delta t}, [0.3123, 0.3470]e^{-\delta t}$ h^{-1}, $k_{W0}^2 = 0$, $k_W^2 = 0$, $\bar{k}_E^R = 0.0032$ h^{-1}, $\frac{k_M}{\Omega} = 0.0347$ h^{-1}, $\frac{\bar{k}_M}{\Omega} = 0.0347$ h^{-1}, $\frac{k_E^R}{\Omega} = 0.0052, 0.0868$ h^{-1}, $\beta_m = 0.2556$ h^{-1}, $\beta_m^A = 0.0021$ h^{-1}, $\beta = 2.52$ h^{-1}, $\gamma_m = 0.24$ h^{-1}, $\gamma = 0.035$ h^{-1}. As initial condition, we consider (n_{12}^R,n_1^R,n_2^R,n^A) = (15,0,0,0) and the initial values of n^X of n^m at time $t = 0$ were set to their steady states.

S.9.16 Parameter values used to realize the plots in SI Fig. S.4B

$k_{W0}^A = 0$, $k_W^A = 7.8075$ h^{-1}, $\bar{k}_E^A = 0.0176$ h^{-1}, $\delta = 0.035$ h^{-1}, $\frac{k_M^A}{\Omega} = 0.0347$ h^{-1}, $\frac{k_E^A}{\Omega} = 0.8675$ h^{-1}, $k_{W0}^2 = 0$, $k_W^2 \in [0.78, 3.90]e^{-\delta t}, [10.41, 52.05]e^{-\delta t}, [23.42, 117.11]e^{-\delta t}, [2082, 10410]e^{-\delta t}$ h^{-1}, $\bar{k}_E^R = 0.0018$ h^{-1}, $\frac{k_M}{\Omega} = 0.0347$ h^{-1}, $\frac{\bar{k}_M}{\Omega} = 0.0347$ h^{-1}, $\frac{k_E^R}{\Omega} = 0.0868$ h^{-1}, $\beta_m = 0.2556$ h^{-1}, $\beta_m^A = 0.0021$ h^{-1}, $\beta = 2.52$ h^{-1}, $\gamma_m = 0.24$ h^{-1}, $\gamma = 0.035$ h^{-1}. As initial condition, we consider (n_2^R,n^A) = (0,15) and the initial values of n^X of n^m at time $t = 0$ were set to their steady states.

S.9.17 Parameter values used to realize the plots in SI Fig. S.4C

$k_{W0}^A = 0$, $k_W^A = 7.8075$ h^{-1}, $\bar{k}_E^A = 0.0176$ h^{-1}, $\delta = 0.035$ h^{-1}, $\frac{k_M^A}{\Omega} = 0.0347$ h^{-1}, $\frac{k_E^A}{\Omega} = 0.8675$ h^{-1}, $k_{W0}^1 = 0$, $k_W^1 \in [0.10, 0.36]e^{-\delta t}, [0.18, 0.64]e^{-\delta t}, [0.31, 1.09]e^{-\delta t}, [0.47, 1.61]e^{-\delta t}$ h^{-1}, $k_T' = 0$, $\delta' = 0$, $\frac{k_M'}{\Omega} = 0$, $\frac{k_T'^*}{\Omega} = 0$, $k_{W0}^2 = 0$, $k_W^2 = 0$ $\bar{k}_E^R = 0.0018$ h^{-1}, $\frac{k_M}{\Omega} = 0.0347$ h^{-1}, $\frac{\bar{k}_M}{\Omega} = 0.0347$ h^{-1}, $\frac{k_E^R}{\Omega} = 0.0868$ h^{-1}, $\beta_m = 0.2556$ h^{-1}, $\beta_m^A = 0.0021$ h^{-1}, $\beta = 2.52$ h^{-1}, $\gamma_m = 0.24$ h^{-1}, $\gamma = 0.035$ h^{-1}. As initial condition, we consider (n_{12}^R,n_1^R,n_2^R,n^A) = (0,0,0,15) and the initial values of n^X of n^m at time $t = 0$ were set to their steady states.

S.9.18 Parameter values used to realize the plots in SI Fig. S.5A

$k^A_{W0} = 0$, $k^A_W = 7.8075$ h^{-1}, $\bar{k}^A_E = 0.0176$ h^{-1}, $\delta = 0.035$ h^{-1}, $\frac{k^A_M}{\Omega} = 0.0347$ h^{-1}, $\frac{k^A_E}{\Omega} = 0.8675$ h^{-1}, $k^1_{W0} = 0$, $k^1_W \in [0.31, 1.09]e^{-\delta t}$ h^{-1}, $k'_T = 0$, $\delta' = 0$, $\frac{k'_M}{\Omega} = 0$, $\frac{k'^*_T}{\Omega} = 0$, $k^2_{W0} = 0$, $k^2_W = 0$ $\bar{k}^R_E = 0.0018$ h^{-1}, $\frac{k_M}{\Omega} = 0.0347$ h^{-1}, $\frac{\bar{k}_M}{\Omega} = 0.0347$ h^{-1}, $\frac{k^R_E}{\Omega} = 0.0868$ h^{-1}, $\beta_m = 0.2556$ h^{-1}, $\beta^A_m = 0.0021$ h^{-1}, $\beta = 2.52$ h^{-1}, $\gamma_m = 0.24$ h^{-1}, $\gamma = 0.035$ h^{-1}. As initial condition, we consider (n^R_{12},n^R_1,n^R_2,n^A) = (0,0,0,15) and the initial values of n^X of n^m at time $t = 0$ were set to their steady states. The distribution shown is after 30 days.

S.9.19 Parameter values used to realize the plots in SI Fig. S.5B

$k^A_{W0} = 0$, $k^A_W = 7.8075$ h^{-1}, $\bar{k}^A_E = 0.0176$ h^{-1}, $\delta = 0.035$ h^{-1}, $\frac{k^A_M}{\Omega} = 0.0347$ h^{-1}, $\frac{k^A_E}{\Omega} = 0.8675$ h^{-1}, $k^1_{W0} = 0$, $k^1_W 0$, $k'_T = 0$, $\delta' = 0$, $\frac{k'_M}{\Omega} = 0$, $\frac{k'^*_T}{\Omega} = 0$, $k^2_{W0} = 0$, $k^2_W = 0$ $\bar{k}^R_E = 0.0018$ h^{-1}, $\frac{k_M}{\Omega} = 0.0347$ h^{-1}, $\frac{\bar{k}_M}{\Omega} = 0.0347$ h^{-1}, $\frac{k^R_E}{\Omega} = 0.0868$ h^{-1}, $\beta_m = 0.2556$ h^{-1}, $\beta^A_m = 0.0021$ h^{-1}, $\beta = 2.52$ h^{-1}, $\gamma_m = 0.24$ h^{-1}, $\gamma = 0.035$ h^{-1}. As initial condition, we consider values of (n^R_{12},n^R_1,n^R_2,n^A,n^X,n^m) from the simulations shown in SI Fig. S.5A and divide them with respect to their value of n^X, following the following intervals: $[0, 100]$ (red), $[200, 800]$ (orange), $[900, 10000]$ (blue).

S.9.20 Parameter values used to realize the plots in SI Fig. S.5F

$k^A_{W0} = 0$, $k^A_W = 7.8075$ h^{-1}, $\bar{k}^A_E = 0.0176$ h^{-1}, $\delta = 0.035$ h^{-1}, $\frac{k^A_M}{\Omega} = 0.0347$ h^{-1}, $\frac{k^A_E}{\Omega} = 0.8675$ h^{-1}, $k^1_{W0} = 0$, $k^1_W 0$, $k'_T = 0$, $\delta' = 0$, $\frac{k'_M}{\Omega} = 0$, $\frac{k'^*_T}{\Omega} = 0$, $k^2_{W0} = 0$, $k^2_W = 0$ $\bar{k}^R_E = 0.0018$ h^{-1}, $\frac{k_M}{\Omega} = 0.0347$ h^{-1}, $\frac{\bar{k}_M}{\Omega} = 0.0347$ h^{-1}, $\frac{k^R_E}{\Omega} = 0.0868$ h^{-1}, $\beta_m = 0.2556$ h^{-1}, $\beta^A_m = 0.0021$ h^{-1}, $\beta = 2.52$ h^{-1}, $\gamma_m = 0.24$ h^{-1}, $\gamma = 0.035$ h^{-1}. As initial condition, we consider values of (n^R_{12},n^R_1,n^R_2,n^A,n^X,n^m) from the simulations associated with the orange distribution in SI Fig. S.5C and divide them with respect to their value of n^X, following the following intervals: $[0, 80]$ (Bin 1), $[90, 150]$ (Bin 2), $[250, 400]$ Bin 3, $[500, 10000]$ (Bin 4).

S.9.21 Parameter values used to realize the plots in SI Fig. S.5B

$k^A_{W0} = 0$, $k^A_W = 7.8075$ h^{-1}, $\bar{k}^A_E = 0.0176$ h^{-1}, $\delta = 0.035$ h^{-1}, $\frac{k^A_M}{\Omega} = 0.0347$ h^{-1}, $\frac{k^A_E}{\Omega} = 0.8675$ h^{-1}, $k^1_{W0} = 0$, $k^1_W = 0$, $c = 1.74 \cdot 10^{-6}$, $3.47 \cdot 10^{-6}$, $3.47 \cdot 10^{-5}$ h^{-1}, $c_0 = 1.74 \cdot 10^{-6}$, $3.47 \cdot 10^{-6}$, $3.47 \cdot 10^{-5}$ h^{-1}, $\delta' = 1.74 \cdot 10^{-6}$, $3.47 \cdot 10^{-6}$, $3.47 \cdot 10^{-5}$ h^{-1}, $\tilde{\delta}' = 1.74 \cdot 10^{-6}$, $3.47 \cdot 10^{-6}$, $3.47 \cdot 10^{-5}$ h^{-1}, $K = 1$, $\frac{k'_M}{\Omega} = 0$, $\frac{k'^*_T}{\Omega} =$ h^{-1}, $k^2_{W0} = 0$, $k^2_W = 0$, $\bar{k}^R_E = 0.0018$ h^{-1}, $\frac{k_M}{\Omega} = 0.0347$ h^{-1}, $\frac{\bar{k}_M}{\Omega} = 0.0347$ h^{-1}, $\frac{k^R_E}{\Omega} = 0.0868$ h^{-1}, $\beta_m = 0.2556$ h^{-1}, $\beta^A_m = 0.0021$ h^{-1}, $\beta = 2.52$ h^{-1}, $\gamma_m = 0.24$ h^{-1}, $\gamma = 0.0349$ h^{-1}. We consider four initial

conditions: (n_{12}^R,n_1^R,n_2^R,n^A) = (14,0,0,1) (blue), (n_{12}^R,n_1^R,n_2^R,n^A) = (6,0,0,9) (red), (n_{12}^R,n_1^R,n_2^R,n^A) = (4,0,0,11) (yellow), (n_{12}^R,n_1^R,n_2^R,n^A) = (0,0,0,15) (purple). For each case, the initial values of n^X of n^m at time $t = 0$ were set to their steady states.

S.9.22 Parameter values used to realize the plots in SI Fig. S.6C

$k_{W0}^A = 0$, $k_W^A = 7.8075$ h^{-1}, $\bar{k}_E^A = 0.0176$ h^{-1}, $\delta = 0.035$ h^{-1}, $\frac{k_M^A}{\Omega} = 0.0347$ h^{-1}, $\frac{k_E^A}{\Omega} = 0.8675$ h^{-1}, $k_{W0}^1 = 0$, $k_W^1 = 0$, $c = 3.47 \cdot 10^{-7}$, $1.04 \cdot 10^{-6}$, $3.47 \cdot 10^{-6}$ h^{-1}, $c_0 = 3.47 \cdot 10^{-6}$ h^{-1}, $\delta' = 3.47 \cdot 10^{-6}$ h^{-1}, $\tilde{\delta}' = 3.47 \cdot 10^{-7}$, $1.04 \cdot 10^{-6}$, $3.47 \cdot 10^{-6}$ h^{-1}, $K = 1$, $\frac{k_M'}{\Omega} = 0$, $\frac{k_T'^*}{\Omega} =$ h^{-1}, $k_{W0}^2 = 0$, $k_W^2 = 0$, $\bar{k}_E^R = 0.0018$ h^{-1}, $\frac{k_M}{\Omega} = 0.0347$ h^{-1}, $\frac{\bar{k}_M}{\Omega} = 0.0347$ h^{-1}, $\frac{k_E^R}{\Omega} = 0.0868$ h^{-1}, $\beta_m = 0.2556$ h^{-1}, $\beta_m^A = 0.0021$ h^{-1}, $\beta = 2.52$ h^{-1}, $\gamma_m = 0.24$ h^{-1}, $\gamma = 0.0349$ h^{-1}. We consider four initial conditions: (n_{12}^R,n_1^R,n_2^R,n^A) = (14,0,0,1) (blue), (n_{12}^R,n_1^R,n_2^R,n^A) = (6,0,0,9) (red), (n_{12}^R,n_1^R,n_2^R,n^A) = (4,0,0,11) (yellow), (n_{12}^R,n_1^R,n_2^R,n^A) = (0,0,0,15) (purple). For each case, the initial values of n^X of n^m at time $t = 0$ were set to their steady states.

S.9.23 Parameter values used to realize the plots in SI Fig. S.7A

$k_{W0}^A = 0$, $k_W^A = 7.8075$ h^{-1}, $\bar{k}_E^A = 0.0176$ h^{-1}, $\delta = 0.035$ h^{-1}, $\frac{k_M^A}{\Omega} = 0.0347$ h^{-1}, $\frac{k_E^A}{\Omega} = 0.8675$ h^{-1}, $k_{W0}^1 = 0$, $k_W^1 = 0$, $k_T' = 0$, $\delta' = 0$, $\frac{k_M'}{\Omega} = 0$, $\frac{k_T'^*}{\Omega} = 0$, $k_{W0}^2 = 0$, $k_W^2 \in [26.02130.13]e^{-\delta t}$ h^{-1}, $\bar{k}_E^R = 0.0018$ h^{-1}, $\frac{k_M}{\Omega} = 0.0347$ h^{-1}, $\frac{\bar{k}_M}{\Omega} = 0.0347$ h^{-1}, $\frac{k_E^R}{\Omega} = 0.0868$ h^{-1}, $\beta_m = 0.2556$ h^{-1}, $\beta_m^A = 0.0021$ h^{-1}, $\beta = 2.52$ h^{-1}, $\gamma_m = 0.24$ h^{-1}, $\gamma = 0.035$ h^{-1}. As initial condition, we consider values of (n_{12}^R,n_1^R,n_2^R,n^A,n^X,n^m) from the simulations associated with the orange distribution in SI Fig. S.5C.

S.9.24 Parameter values used to realize the plots in SI Fig. S.7B

$k_{W0}^A = 0$, $k_W^A = 7.8075$ h^{-1}, $\bar{k}_E^A = 0.0176$ h^{-1}, $\delta = 0.035$ h^{-1}, $\frac{k_M^A}{\Omega} = 0.0347$ h^{-1}, $\frac{k_E^A}{\Omega} = 0.8675$ h^{-1}, $k_{W0}^1 = 0$, $k_W^1 \in [0.1041, 0.36]e^{-\delta t}$ h^{-1}, $k_T' = 0$, $\delta' = 0$, $\frac{k_M'}{\Omega} = 0$, $\frac{k_T'^*}{\Omega} = 0$, $k_{W0}^2 = 0$, $k_W^2 = 0$, $\bar{k}_E^R = 0.0018$ h^{-1}, $\frac{k_M}{\Omega} = 0.0347$ h^{-1}, $\frac{\bar{k}_M}{\Omega} = 0.0347$ h^{-1}, $\frac{k_E^R}{\Omega} = 0.0868$ h^{-1}, $\beta_m = 0.2556$ h^{-1}, $\beta_m^A = 0.0021$ h^{-1}, $\beta = 2.52$ h^{-1}, $\gamma_m = 0.24$ h^{-1}, $\gamma = 0.035$ h^{-1}. As initial condition, we consider values of (n_{12}^R,n_1^R,n_2^R,n^A,n^X,n^m) from the simulations associated with the orange distribution in SI Fig. S.5C.

S.9.25 Parameter values used to realize the plots in SI Fig. S.7C

$k_{W0}^{A} = 0$, $k_{W}^{A} = 7.8075$ h^{-1}, $\bar{k}_{E}^{A} = 0.0176$ h^{-1}, $\delta = 0.035$ h^{-1}, $\frac{k_{M}^{A}}{\Omega} = 0.0347$ h^{-1}, $\frac{k_{E}^{A}}{\Omega} = 0.8675$ h^{-1}, $k_{W0}^{1} = 0$, $k_{W}^{1} = 0$, $k_{T}' \in [0.7 \cdot 10^{-4}, 0.24 \cdot 10^{-3}]e^{-\delta t}$ h^{-1}, $\delta' = 0$, $\frac{k_{M}'}{\Omega} = 0$, $\frac{k_{T}'^{*}}{\Omega} in[3.5 \cdot 10^{-3}, 1.2 \cdot 10^{-2}]e^{-\delta t}$ h^{-1}, $k_{W0}^{2} = 0$, $k_{W}^{2} = 0$, $\bar{k}_{E}^{R} = 0.0018$ h^{-1}, $\frac{k_{M}}{\Omega} = 0.0347$ h^{-1}, $\frac{\bar{k}_{M}}{\Omega} = 0.0347$ h^{-1}, $\frac{k_{E}^{R}}{\Omega} = 0.0868$ h^{-1}, $\beta_{m} = 0.2556$ h^{-1}, $\beta_{m}^{A} = 0.0021$ h^{-1}, $\beta = 2.52$ h^{-1}, $\gamma_{m} = 0.24$ h^{-1}, $\gamma = 0.035$ h^{-1}. As initial condition, we consider values of (n_{12}^{R},n_{1}^{R},n_{2}^{R},n^{A},n^{X},n^{m}) from the simulations associated with the orange distribution in SI Fig. S.5C.